AEC RESEARCH AND DEVELOPMENT REPORT

ORNL-2837
C-86 - Nuclear Rocket
and Ram Jet Engines

AN EXPERIMENTAL STUDY OF VORTEX FLOW FOR APPLICATION TO GAS-PHASE FISSION HEATING

J. J. Keyes, Jr.
R. E. Dial

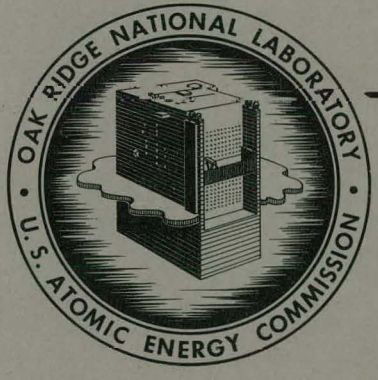

OAK RIDGE NATIONAL LABORATORY
operated by
UNION CARBIDE CORPORATION
for the
U.S. ATOMIC ENERGY COMMISSION

DISCLAIMER

ORNL-2837

Contract No. W-7405-eng-26

REACTOR EXPERIMENTAL ENGINEERING DIVISION

AN EXPERIMENTAL STUDY OF VORTEX FLOW FOR APPLICATION TO GAS-PHASE FISSION HEATING

J. J. Keyes, Jr.

R. E. Dial

DATE ISSUED

JUN 13 1960

OAK RIDGE NATIONAL LABORATORY
Oak Ridge, Tennessee
operated by
UNION CARBIDE CORPORATION
for the
U.S. ATOMIC ENERGY COMMISSION

THIS PAGE

WAS INTENTIONALLY

LEFT BLANK

ABSTRACT

An experimental investigation into the gas dynamics of a jet-driven vortex tube for application of a cavity nuclear reactor to rocket propulsion has shown that viscous retardation of the vortex motion is severe, owing to a high level of turbulence near the periphery. Based on the experience gained in this study, it is estimated that the achievement of vortex strengths sufficient for practical application will require the use of small diameter tubes with appreciable expenditure of power for recirculation of the gas. The effect of the high degree of turbulence on the separation process near the periphery remains to be determined.

The independent variables which were found to influence the vortex strength significantly for a given gas and temperature condition are the tube diameter, the mass flow rate per unit tube length, the injection velocity, and the wall pressure.

Estimates of the degree of turbulence in vortex flow have been made from data on the variation in tangential velocity with radius. Virtual (total) viscosities near the periphery ranged from 30 to 700 times the molecular viscosity for tangential Reynolds numbers of from 4×10^4 to 2×10^6.

Measurements of the position of the mole-fraction peak for separation of helium and a heavy vapor agreed with the theory for laminar flow. This suggests that near the center of the vortex tube where the peak developed the radial density gradient was sufficiently strong to suppress turbulence.

It is concluded that the vortex reactor concept appears promising for application to nuclear rocket propulsion provided a satisfactory method can be devised for recirculation of the large excess mass flow required to maintain the vortex strength, and if turbulence does not appreciably limit the separation process. A separation experiment at elevated temperature appears to be the next logical step in the research program.

NOMENCLATURE

A	$\mathcal{m}/2\pi\mu^*$, dimensionless
D	molecular diffusivity, ft^2/sec
g_c	gravitational constant, 32.17 $lb_m \cdot ft/(sec)^2 \cdot lb_f$
ℓ	tube length, ft
M	tangential Mach number, dimensionless
m	molecular weight, lb_m/lb mole
$\mathcal{m}$	mass flow rate per unit of tube length, $lb_m/sec \cdot ft$
N_{Re}	Reynolds number, dimensionless
P^*	effective jet input power, $\gamma\ \mathcal{m}_i\ M_j^2/2$ $(lb_m/sec \cdot ft)$
p	static pressure, psia
R	gas constant, 1545 $ft \cdot lb_f/lb$ mole $\cdot °R$
R_B	bleed ratio, dimensionless
r	radius, ft
T	absolute static temperature, °R
v	velocity, ft/sec
x	mole fraction of heavy component, dimensionless
γ	heat capacity ratio, c_p/c_v
μ	absolute (molecular) viscosity, $lb_m/ft \cdot sec$
μ^*	virtual (total) viscosity, $lb_m/ft \cdot sec$
ρ	density, lb_m/ft^3

NOMENCLATURE (continued)

Subscripts

a	jet entry position
e	exit
i	inlet
j	jet
m	peak mole fraction
o	upstream of nozzle
p	periphery
r	radial
t	tangential
1	light gas
2	heavy gas

Superscripts

ϵ	exponent in $M = M_p / r'^{\epsilon}$
'	denotes value divided by the value at the tube periphery

CONTENTS

AN EXPERIMENTAL STUDY OF VORTEX FLOW FOR APPLICATION TO GAS-PHASE FISSION HEATING

J. J. Keyes, Jr. R. E. Dial

SUMMARY

The feasibility of utilizing a vortex field to contain a fissioning gas which is supplying heat to a rocket propellant depends strongly upon the magnitude of the tangential velocities which can be generated at low mass flow rates (1). If the flow field is laminar, viscous shear drag would not be expected to retard the vortex motion appreciably; however, if the flow field is turbulent, viscous retardation becomes highly significant. The experiments described in this report, which are a continuation of preliminary work previously published (3), were performed to determine the nature of the flow in jet-driven vortex tubes under conditions dynamically similar to those necessary for operation of a vortex-cavity reactor.

When it was found experimentally that turbulence seriously limits the vortex strength attainable at low mass flow rates and power inputs, attempts were made to laminarize the flow field by application of such well-known techniques as uniform boundary-layer bleed and wall cooling. No significant effect of bleed on vortex strength (tangential peripheral Mach number) was observed for bleed ratios (ratio of bleed mass flow to exit mass flow) up to 3.0. It was possible, however, by injecting the gas into the tube at sufficiently low Reynolds and Mach numbers (continuous slit injection) and by bleeding uniformly through a porous wall to effect a reduction in exit mass

flow by a factor of four with less than 25% decrease in local vorticity. Some increase in vortex strength was measured with extreme wall cooling, indicating reduction in turbulent wall shear. Laminarization was not achieved, however.

Another promising technique which was employed for removal of the excess mass flow involved bleeding axially through an annular ring of orifice holes at the end of the vortex tube. In one experiment, a reduction in exit mass flow by a factor of 7.5 was effected with 15% decrease in local vorticity.

A sizable portion of the experimental effort was devoted to a systematic study of the effects on turbulent vortex strength of certain key variables. These include primarily:

1. tube diameter,
2. mass flow rate per unit tube length,
3. jet injection velocity,
4. wall pressure.

For example, decrease in tube diameter from 2.0 to 0.64 in. produced an increase in vortex strength of up to a factor of two. Vortex strength also increased with increasing mass flow rate. Experiments on the effect of injection velocity showed that stronger vortices were generated for subsonic than for supersonic injection, for the same input power. In one run with a 0.64-in.-ID tube, a peripheral tangential Mach number, M_p, of 0.49 was attained using nitrogen gas at a tube wall pressure of 83 psia; the jet Mach number was 0.9 and the mass flow rate 0.083 lb/sec·ft. The analysis of Kerrebrock and Meghreblian (1) indicates that values of M_p of at least 0.5 will be required for vortex reactor application.

A quantity which was found to correlate the combined effect of mass flow rate and injection velocity is the effective jet input power, which is proportional to the product of mass flow per unit tube length and the square of the jet Mach number. The data indicate that vortex strength increases with this parameter to the 0.42 power.

The tangential Reynolds number, based on the tube diameter and tangential velocity near the tube periphery, was found to be a valid similitude parameter. It is concluded that to achieve high tangential Mach numbers at Reynolds numbers of practical interest for vortex-cavity reactor application will require appreciable recirculation, unless some means can be found for effective suppression of turbulence. Recirculation techniques are discussed in ref 2.

In order to determine the degree of turbulence in vortex flow, estimates of virtual viscosity have been made from the experimentally determined variation in tangential velocity with radius. It was found that the virtual viscosities near the periphery ranged from 30 to 700 times the molecular viscosity for Reynolds numbers of from 4×10^4 to 2×10^6. Since Reynolds numbers in excess of 1×10^6 are possible in the actual application, it is apparent that turbulent shear drag will be the principle factor limiting the attainment of high vortex strength.

A final phase of the experimental program involved measurements of the separation profile of a heavy fluorocarbon vapor in helium, utilizing a direct sampling technique and thermal conductivity gas analysis. Axial bleed-off was employed to reduce the exit mass flow to a value permitted by the rate of diffusion of light through heavy gas. It was found that the measured concentration peak position agreed reasonably well with theory based on a laminar analysis (1, 3), indicating that turbulence must be effectively suppressed by

the large density gradient in the central region of the tube where the peaks developed. This study leaves unanswered the question of the effect of turbulence near the periphery on the position and intensity of the separation peak at larger radii.

INTRODUCTION

The possibility of developing a high-performance nuclear rocket engine utilizing direct energy exchange between a low molecular weight propellant and a fissioning gas or plasma was considered by Kerrebrock, Meghreblian, and Lafyatis in refs 1 and 2. It is generally concluded that some means for preventing loss of fissionable material during operation is required in order (a) to keep the mean molecular weight of the exhaust gas low and thus to keep the velocity and specific impulse high and (b) to maintain criticality without excessive expenditure of fuel. As is pointed out in these references, a possible method of containment involves use of a centrifugal field to counter the tendency for the fuel to be swept out with the propellant. By proper balance between these opposing forces, it should in principle be possible to hold the fissionable material as a concentrated gaseous "cloud" away from the wall of the containing vessel so that very high temperatures could be reached in the gas without exceeding allowable wall temperatures.

Figure 1 is a conceptual sketch of a single vortex tube, as presented in ref 1. A low molecular weight gas is introduced tangentially, producing the vortex motion. The light gas flows spirally inward, diffusing through the cloud of heavy fissionable gas and absorbing the fission heat. The analysis presented by Kerrebrock and Meghreblian (1) indicated the feasibility of the vortex containment scheme for laminar flow. In a later report (2),

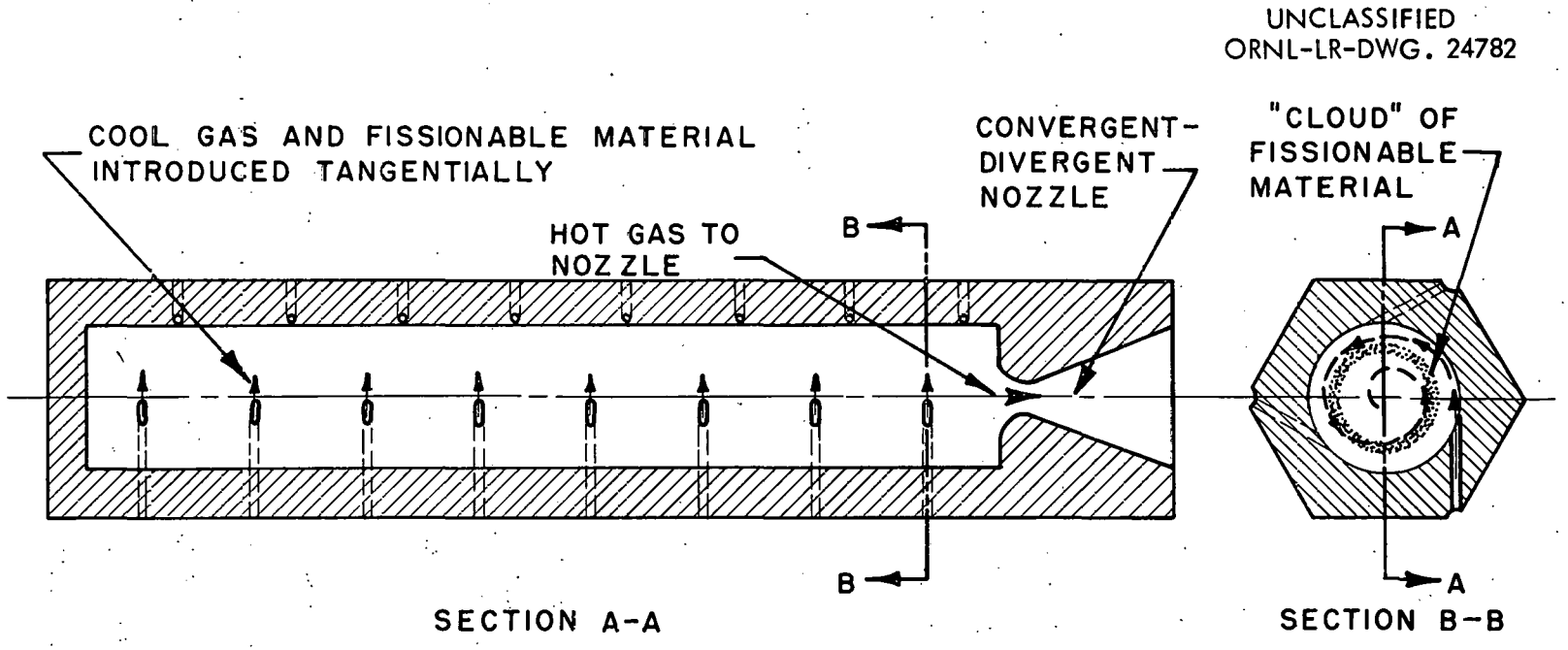

SPECIALIZATION OF THE VORTEX TUBE FOR ROCKET PROPULSION.

Fig. 1. A Unit Vortex Cell with Integral Nozzle.

the possibility of maintaining laminar flow by application of uniform wall suction was considered. No attempt was made to estimate the effects of turbulence on the vortex flow or on the separation process.

In order to fulfill criticality requirements in gaseous cavity reactors, it is necessary that the density ratio of fissionable material to propellant be large in the cloud region and that the propellant pressure be high, as shown in ref 2. The significance of these facts is that high tangential velocities have to be achieved under conditions of high gas density; consequently, the characteristic Reynolds number for the flow will be large and turbulence likely. Furthermore, the diffusional velocity of propellant through the cloud limits the exit mass flow rate to a very low value. There is obviously a limit also on the amount of energy which can be expended in maintaining the vortex. These factors impose severe limitations on the operation of gaseous vortex-cavity reactors.

An experimental program was consequently initiated to ascertain the nature of the flow in a gaseous vortex operating at room temperature under conditions estimated to be dynamically similar to those corresponding to high temperature operation. The first question which had to be answered experimentally was whether vortices of adequate strength could be generated with the low mass flow rates (of the order of 0.01 lb/sec·ft) which can be tolerated by the diffusion process. A preliminary report (3) on the initial phase of the study has been published, in which it was concluded that, due to turbulence, the retardation of the vortex motion in a simple, single-pass tube (Fig. 1)* is so severe as to prevent formation of vortices of sufficient strength for vortex reactor application.

*i.e., no bleed-off and recirculation of propellant.

Since it was confirmed experimentally that the flow field in a simple vortex tube would be turbulent, the next part of the experimental program, described in detail in this report, consisted of a series of experiments in which an attempt was made to produce laminar vortices. Methods of stabilizing the shear layer on the concave wall which were investigated include boundary-layer bleed-off through a uniformly porous wall as suggested by Kerrebrock (2), injection of a heavy gas uniformly through a porous wall, and wall cooling. These techniques have been used successfully for boundary-layer control on flat plates and on airfoils.

Another series of experiments was conducted to determine the effect of bleeding off a fraction of the total flow axially, at radial positions between the tube center and wall, so that the exit radial flow is held to an allowable rate, based on diffusion considerations. The flow bled off would, of course, represent a recirculating side-stream.

Measurements of the effects on vortex strength of mass flow rate, injection velocity, tube geometry, and pressure are described in this report. Estimates of eddy viscosity from the experimental velocity data are presented.

Preliminary attempts, described in ref 3, to ascertain the radial concentration distribution of a heavy gas were at best qualitative. Quantitative measurements of the radial distribution of C_8F_{16} in helium using improved techniques are described in this report.

As has been indicated, the organization of the experimental program was such as to survey the effects of many variables. The principle criterion used in evaluating a particular variable is its effect on the magnitude of the peripheral tangential Mach number, M_p (also referred to herein as the vortex strength), and on the variation in tangential Mach number, M, with

radius. Use of Mach number is convenient since a simple relationship exists between the tangential Mach number at the point of maximum mole fraction of heavy component, the mass flow rate, and properties of the gaseous mixture. Experiments were conducted near room temperature for simplicity. The similitude parameters considered to be of principle importance in vortex flow, as defined by Kerrebrock and others, are:

1. radial Reynolds number, $r\, v_r\, \rho/\mu = \dot{m}/2\, \pi\, \mu$,
2. tangential Reynolds number, $2\, r\, v_t\, \rho/\mu$,
3. inlet jet Mach number, M_j.

Note that the radial Reynolds number is independent of radius when temperature effects are neglected; the tangential Reynolds number decreases with radius.

In summary, the objectives of the initial experimental program were to determine the nature of flow in a gaseous vortex and to delineate the important variables and their effects on vortex strength. It is hoped that the results presented here will be useful in guiding the course of future analytical and experimental work.

LITERATURE REVIEW

It is to be expected that the majority of references in this field have to do with "Ranque-Hilsch tube" theory and performance, in which the concern is primarily that of explaining the observed temperature effects. Furthermore, such tubes operate with mass flow rates much larger than can be tolerated in vortex reactor application and, as measured by Eckert and Hartnett (4), the radial velocity distribution is closer to solid-body rotation

than it is to the potential vortex desired in this work. This fact suggests a high degree of turbulence and indeed Eckert, and later Deissler and Perlmutter (5), have indicated that the degree of energy transfer observed in vortex tubes can best be explained on the basis of large eddy viscosity.

The influence of viscosity on the velocity distribution in laminar vortex flow is shown by Einstein and Li (6), Pengelley (7), and Deissler to be governed by the radial Reynolds number, which can be expressed as

$$N_{Re_r} = \mathcal{M}/2\pi\mu$$

where $\mathcal{M}$ is the mass flow rate per unit tube length and μ is the absolute molecular viscosity. This is also in agreement with the theory of Kerrebrock and Meghreblian. When the flow is turbulent, Kassner and Knoernschild (8), Einstein, and Deissler have shown that it is reasonable to replace the molecular viscosity with an apparent or virtual viscosity, μ^*, which is assumed independent of radius. Rietema and Kragenbrink (9) derive a similar expression for the effect of turbulent viscosity.

Data on vortex flow of water as reviewed by Wilson (10) indicates that μ^* may be many times greater than μ even at relatively low tangential velocities. Shepherd and Lapple (11, 12) measured velocity distributions in cyclone separators and found that the exponent ϵ in the equation,

$$v_t = \frac{\text{const}}{r^{\epsilon}}$$

relating the tangential velocity to the radius, varied from 0.5 to 0.7. This deviation from potential vortex flow, $\epsilon = 1$, can best be explained in terms of a relatively high virtual viscosity.

It is known that flow along a concave surface becomes unstable at lower Reynolds numbers than does plane flow, or flow along a convex surface. This

was pointed out by Taylor (13) in considering rotation of concentric cylinders, and also by Goertler (14). The nature of the instability is such as to generate secondary vortices whose axes are parallel to the surface in the direction of curvature. Yeh (15) measured the velocity distribution and turbulent intensity in swirling flow in an annulus and found that the velocity gradient is steeper and the turbulent intensity greater at the concave wall than at the convex wall. Thus, shear stress is greater on the concave wall.

The explanation of the effect of curvature on stability in rotating flow lies in a consideration of the influence of centrifugal force on a fluid particle displaced from its equilibrium position, as discussed by Schlichting (16). A similar effect of bouyant forces on stability occurs when the fluid density varies in the radial direction. A stabilizing effect is produced if the density decreases in a direction opposite to the direction of the centrifugal field; i.e., density must decrease with decrease in radius for stability. The rapid decrease in density in a potential gaseous vortex may tend to produce a stabilizing effect, especially with strong internal heat addition as in a reactor (1). Experiments on the effect of a density gradient in the boundary layer are described in a later section.

Thus from a brief literature survey, it was concluded that the vortex flow field in the vicinity of the containing tube wall would in all probability be turbulent, but that the effect of the density decrease may tend to stabilize the flow in the inner regions. No conclusions as to the magnitude of the effect of turbulence on the vortex strength under conditions suitable for reactor application could be reached from the available literature. Thus, the experimental program described herein was undertaken to provide the necessary quantitative data.

ANALYSIS

I. Gas Dynamics

It is informative to list the independent variables likely to influence the tangential velocity and its radial gradient in a vortex tube, based on sources of information already reviewed:

A. Geometrical Variables

1. Radius, r
2. Length, ℓ
3. Radius at point of nozzle entry, r_a
4. Diameter of nozzle; hydraulic diameter of slit
5. Spacing and orientation of injection nozzles
6. Radius of exit nozzle or orifice, r_e

B. Flow Variables

1. Inlet mass flow per unit tube length, m_i
2. Exit mass flow per unit tube length, m_e
3. Injection jet velocity, v_j
4. Injection jet temperature, T_j

C. System Variables

1. Static pressure, p
2. Static temperature and temperature gradient, T, $\frac{\partial T}{\partial r}$
3. Properties of the working fluid:

   viscosity, μ; density, ρ; heat capacity ratio, γ;

   molecular weight, m_1

These variables are conveniently grouped into dimensionless ratios:

$N_{Re_r} = \mathcal{M}/2\,\pi\,\mu$ (radial Reynolds number)

$N_{Re_t} = 2\,r\,v_t\,\rho/\mu$ (tangential Reynolds number)

$M_j = v_j \Big/ \sqrt{\frac{\gamma\, g_c\, RT}{m_1}}$ (jet Mach number)

$r' = r/r_p$ (dimensionless radius)

$p' = p/p_p$ (dimensionless pressure)

$\ell/2\,r_p$ (length-to-diameter ratio)

$T' = T_w/T_p$ (ratio of adiabatic wall temperature to temperature of gas at radius of jet entry — used when wall heat transfer occurs)

A very important quantity derivable from the mass flow rate and jet velocity is the power input per unit tube length, which is given as follows:

$$(\text{Power})_i = \frac{\mathcal{M}_i\, v_j^2}{2\, g_c} \text{ ft·lb}_f/\text{sec·ft}$$

Dividing by the square of the sonic velocity:

$$\frac{(\text{Power})_i}{\gamma\, g_c \dfrac{RT_j}{m_1}} = \frac{\mathcal{M}_i\, M_j^2}{2\, g_c}$$

$$\therefore \quad \frac{(\text{Power})_i}{\dfrac{RT_j}{m_1}} = \frac{\gamma\, \mathcal{M}_i\, M_j^2}{2} = P^* \cong \mathcal{M}_i \ln (p_o/p_p)^* \qquad (1)$$

where $(p_o/p_p)^*$ is the pressure ratio across an inlet nozzle, neglecting friction;** the approximation in Eq. 1 is valid to within 10% for $M_j \leq 1$,

** $(p_o/p_p)^* = \left[1 + \left(\frac{\gamma - 1}{2}\right) M_j^2\right]^{\frac{\gamma}{\gamma - 1}}$

$\gamma \leq 1.4$. The quantity P^* is referred to herein as "effective jet input power", but must be multiplied by RT_j/m_1 to obtain the true amount of power input.

The dependent variable is the tangential Mach number, M, as a function of radius. In some correlations the ratio M_p/M_j is used, which represents the effectiveness of conversion of the inlet jet velocity to tangential velocity at the tube periphery. The experimental program was directed toward evaluating the effect of the independent variables on M.

Variation in tangential Mach number with radius is determined from a radial momentum balance for circular flow:

$$M^2 = \frac{r'}{\gamma p'} \frac{dp'}{dr'} \quad . \tag{2}$$

This equation is a simplified form of a more general expression which takes into account variation of radial and axial velocities with radius. It is readily shown that the radial velocity contribution is negligible for all conditions of this work. It is also concluded that the axial velocity effect is small, as discussed on page 60. Thus from Eq. 2, the value of M can be calculated directly from the distribution of static pressure with radius by graphical differentiation. The pressure distribution is determined experimentally by means of static taps drilled in the closed-off end of the tube. The peripheral Mach number, M_p, is estimated by extrapolation of a plot of M (or M/M_j) versus r' to $r' = r'_a$; thus, M_p can be interpreted as the Mach number at the radius of jet entry.

An alternative method of data analysis which does not require graphical differentiation assumes that the variation of M with radius can be expressed in the form:

$$M = \frac{M_p}{r'^{\epsilon}} \qquad \text{where } -1 \leq \epsilon \leq 1 \qquad (3)$$

Substitution of Eq. 3 in Eq. 2 and integrating gives the following relationship between p' and r':

$$1 - p'^{\frac{\gamma - 1}{\gamma}} = \frac{\gamma - 1}{2 \epsilon} M_p^2 \left(\frac{1}{r'^{2\epsilon}} - 1 \right) \qquad (4)$$

Thus from the measured pressure ratios, values of M_p and ϵ can be determined by curve fitting techniques. This method was used in the first experimental report (3); however, a more thorough mapping of radial pressure distribution has since indicated that Eq. 3 is not necessarily valid. Figures 40 and 41 of the Appendix compare the two methods of data analysis for 2.0-in.-dia and 0.6-in.-dia tubes. Agreement of the M_p values is good for the 2.0-in. tubes, but the analytical method appears to underestimate significantly M_p for the 0.6-in.-dia tubes. For the ϵ values, little agreement between the two methods is evident; the analytical method predicts consistently lower values of ϵ for the 2.0-in. tubes, and higher values for the 0.6-in. tubes, as compared with the graphical slope method. The latter method, although not too precise, is in principle correct and was used in analysis of all data presented in this report.

As has been discussed, the effect of turbulence may be described by substituting the virtual viscosity μ^* for μ in the term $\dot{m}/2\pi\mu$ which appears in the solution of the Navier-Stokes equations for laminar flow:

$$\text{Let} \qquad A = \dot{m}/2\pi\mu^* \qquad (5)$$

Einstein and Li (6) give the solution for a two-dimensional incompressible vortex in the following form:

$$r' \, v_t/v_{t,p} = \frac{\left[A - 2(1 - e^{-A/2})\right]\left[1 - r'^{-(A-2)}\right]}{A\left(1 - e^{-A/2} \, r_e'^{(A-2)}\right) - 2(1 - e^{-A/2})} + r'^{-(A-2)} \quad , \qquad (6)$$

for $r' > r_e'$, $A \neq 2$; v_t is the tangential velocity. It is assumed that μ^* is constant in the derivation of Eq. 6, and that the gas leaves uniformly through the exit hole. Figure 42 (Appendix) is a plot of Eq. 6 for $r' = 0.5$ and for various values of the dimensionless exit radius, r_e'. From the experimental ratio of tangential velocities at two radii, a value of A is determined from which μ^* is found from Eq. 5. The assumption of incompressibility is, of course, a weakness in applying the theory to a gaseous vortex. Near the wall, however, where velocities are appreciably subsonic and the radial pressure and temperature gradients are relatively small, it is assumed that the error in neglecting density variations is not significant.

II. Separation

The following equation, based on the analysis presented in ref 1, relates the tangential Mach number at the radius of maximum mole-fraction of heavy component, M_m, to the exit mole-fraction of heavy component, x_e, the peak mole-fraction of heavy component, x_m, the exit mass flow rate of light component, $\mathcal{M}_{1e}$, the ratio of molecular weights m_2/m_1, and the molecular diffusivity-density product at the point of maximum mole-fraction, $(\rho D_{12})_m$,

$$M_m^2 = \frac{\mathcal{M}_{1e}\,(1 - x_e/x_m)}{2\,\pi\,(\rho D_{12})_m\,(m_2/m_1 - 1)\,\gamma} \quad . \qquad (7)$$

This equation is derived for laminar flow and assumes further that the mole-fraction of heavy component is small.

THE EXPERIMENTAL INVESTIGATION

I. Apparatus

The preliminary experimental work on solid-wall tubes without bleed-off is covered in a previous report (3) and will be reviewed briefly here for the sake of continuity. Figure 2 is a sketch of the 2-in.-dia Plexiglas vortex tube employed in the initial work. Twelve feed nozzles were located in the wall of the block so as to form a broken spiral of entrance jets spaced 1-in. axially with 90-deg rotation between adjacent nozzles and continuing the length of the block. The inside surfaces of the nozzles were honed flush with the inside diameter of the tube as shown in the detail. Gas was exhausted at one end through an adjustable annular orifice of 0.280-in. outside diameter. Two such tubes were run, as described in Table I. The radial static pressure distribution was obtained by means of thirteen pressure taps drilled in the closed-off end of the tube, as seen at the left in Fig. 2. Helium or nitrogen gas was supplied through pressure regulators and appropriate metering devices to each of the four supply headers at pressures up to 600 psig. The pressure in the vortex tube was regulated by the exit valve up to a maximum of 150 psig. Differential pressures were read on suitable manometers and Bourdon gages.

When it became evident from preliminary experiments that the flow would be turbulent, the suggestion was made (2) that experiments be conducted with uniform bleed applied to the boundary layer as a possible means of stabilization.* The first porous wall model, designated "vortex tube assembly No. 3", is shown in Fig. 3 and describe in Table I. The wall of the tube was made of uniformly porous metal,** 2-in. inside diameter by 0.25-in. wall thickness

*Equivalent to boundary-layer suction.

**Sintered Ni, approximately 2-micron pore size, trade name "Cormet", product of Corning Glass Company, Corning, New York.

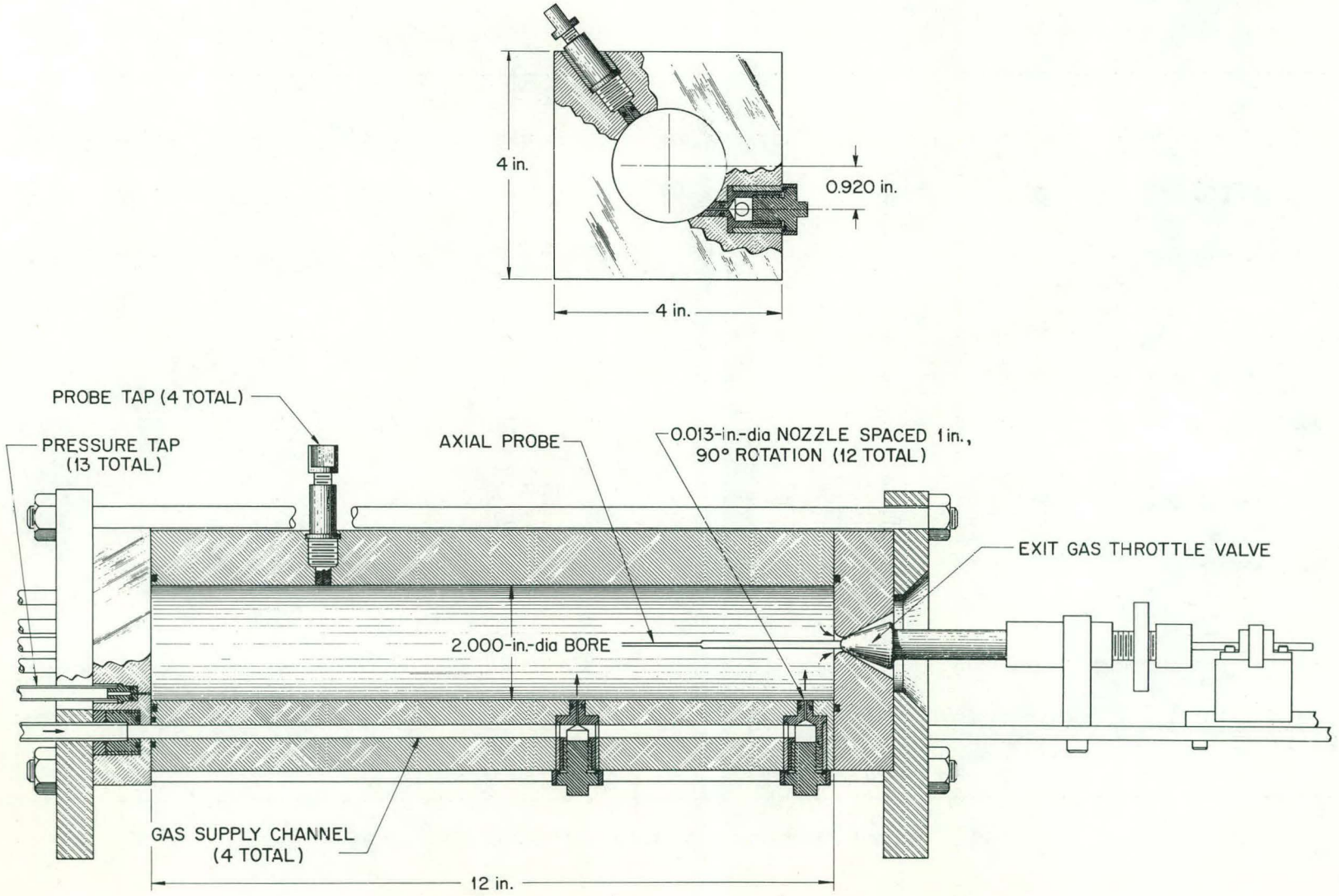

Fig. 2. Sketch of Experimental Vortex Tube.

Table I. Description of Experimental Vortex Tubes

Tube No.	Insert	Fig. ref	Tube ID, 2 r_p (in.)	Tube Length (in.)	Tube Wall Description	Injection Geometry			Exit Orifice Radius / Tube Radius (r_e')
						Description	Dia or Width (in.)	Radial Position (r_a')	
1		2	2.00	12.0	Plexiglas	12 Nozzles	0.0135	0.92	0.140
2		2	2.00	12.0	Plexiglas	12 Nozzles	0.0100	0.84	0.140
3		3,8	2.00	12.0	Porous Ni (Cormet)	12 Nozzles	0.0135, 0.0330	0.92	0.0625 – 0.250
3	A	8	1.00	12.0	Plexiglas	12 – 164 Nozzles	0.020	0.90	0.280 – 0.500
3	B	8	0.63	3.25, 6.0, 12.0	Brass	11 – 54 Nozzles	0.020	0.90, 0.95	0.308 – 0.525
4	A	9	2.00	12.0	Porous Ni (Cormet)	12-in.-long Slit	0.002	1.00	0.140
4	B	10,11	2.00	12.0	"	"	0.002	0.92	0.140
5		12,13	0.64	3.5	Brass	12 Nozzles	0.028	0.88	0.308 – 0.362

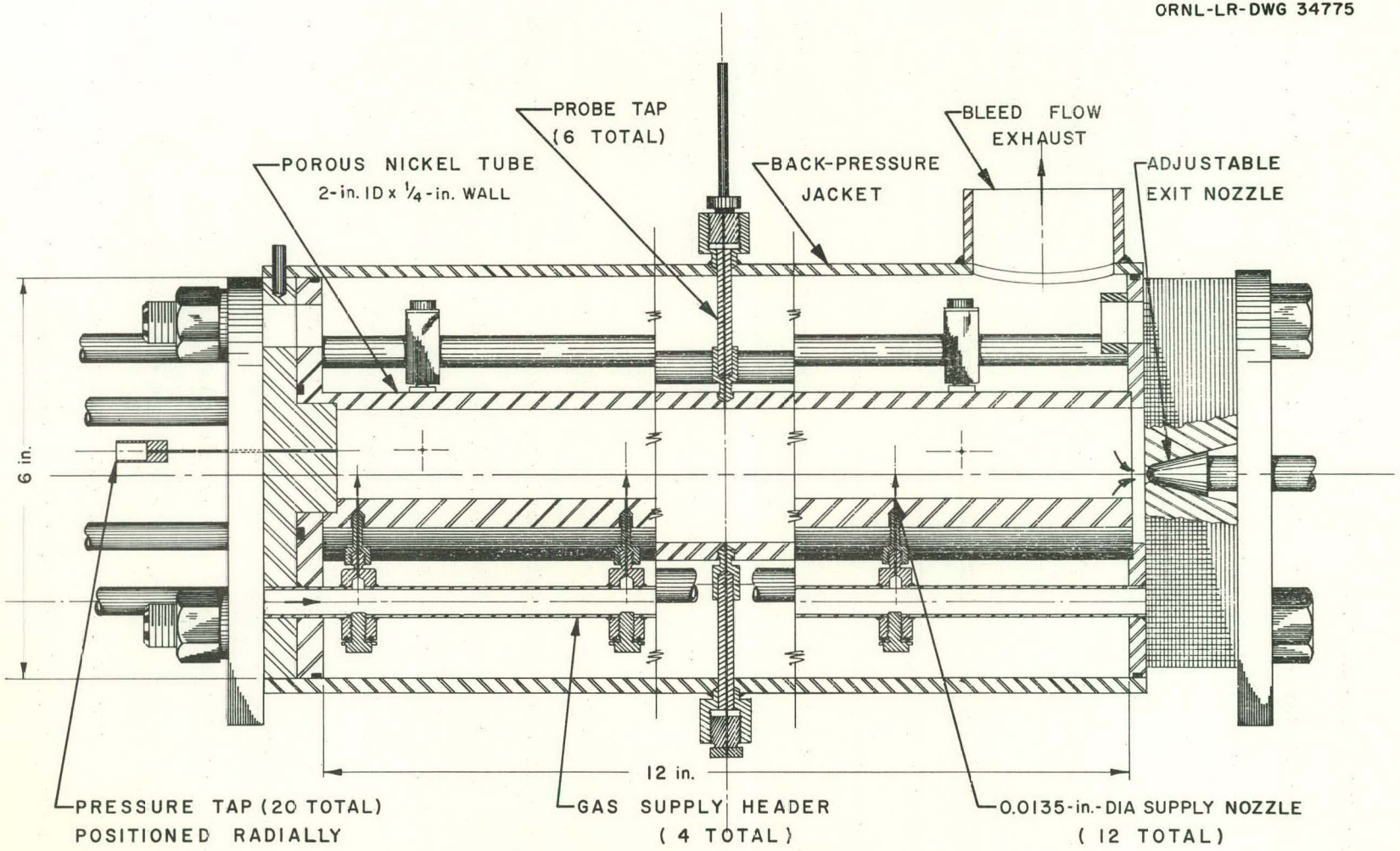

Fig. 3. Porous Wall Vortex Tube Assembly No. 3.

and of sufficient permeability to allow up to 75% of the inlet mass flow to be bled-off through the wall. The tube length was 12 in. The porous material was estimated to have 50 to 75 μin. finish on the inside diameter, with some waviness in the form of circumferential ripples. Attempts to improve the surface finish by machining caused severe plugging. Permeability characteristics of the porous tubes are shown graphically in Fig. 43 (Appendix).

Gas was introduced into the tube by means of twelve nozzles arranged along the tube length in identical manner to that employed in the plastic model. The nozzle inside diameter was varied from 0.0135 in. to 0.033 in. in order to vary the inlet mass flow rate; the length of the nozzle was about 1/4 in., and the radius of entry of the jet emerging from the nozzle was 0.92 in. The nozzles were fed in groups of three by four headers which penetrated the annular space around the porous tube. The tube-heater assembly was enclosed in a 6-in.-dia jacket which was provided with a pipe connection through which gas could be discharged to atmosphere, or injected. "O-ring" seals were used between the jacket and end flanges of the porous tube to enable quick disassembly and interchangeability of tube-header assemblies. Gas which was not withdrawn through the wall was exhausted through an adjustable conical exit nozzle, 0.280-in. diameter, which was contained in a removable plastic plate. In some of the runs, the adjustable nozzle was replaced by thick orifices, ranging in diameter from 1/8 to 1/2 in.

Six tubes, which penetrate the annular space radially and which communicate with the inside wall of the 2-in. porous tube, were included for the dual purpose of measuring the wall static pressure and providing positions through which probes could be inserted. The radial static pressure distribution was obtained by means of twenty pressure taps, 0.020-in. inside diameter,

drilled in a flange insert which provided the end closure, as shown at the left in Fig. 3. Figure 4 illustrates the layout and radial position of the twenty pressure taps.

Figure 5 is a diagram of the flow and instrument system used to supply metered flow of nitrogen or helium gas, at controlled pressures up to 600 psig, to the vortex tube. Assembly No. 3 is illustrated, but the same system was also used for runs employing subsequent assemblies. Provision was included for controlling and metering the flows to the individual supply headers and the total inlet flow. The Foxboro Corporation orifice-differential pressure transmitter flow indicating devices employed are accurate to within ±1%. All absolute pressures were measured with laboratory-type test gages with accuracy better than ±1/2%. Differential pressures were measured by means of 100-in. mercury and water manometers connected directly to the twenty pressure taps. For pressure differences greater than 50 psi, a Bourdon-type ("Heise") gage, 0 to 150 psig, was used, accurate to ±1/4%. This gage was also used for measuring the pressure at the inside wall of the vortex tube. Bleed flow through the porous wall was measured by calibrated rotameters (±1%) discharging to atmosphere.

Provision for separation studies was included by introducing a heavy gaseous component into the vortex tube. This was done by diverting a small sidestream (1 scfm or so) of helium through a bubbler tank containing a relatively volatile liquid, in this study the fluorocarbon C_8F_{16}. The gas thus saturated at a temperature a little below room temperature could be introduced uniformly through the porous wall of the tube to mix with the gas introduced by way of the feed nozzles.

POS	RADIAL DISTANCE FROM CENTER	r'
1	.000	0
2	.041	.042
3	.060	.061
4	.100	.1025
5	.139	.1425
6	.160	.164
7	.200	.205
8	.240	.246
9	.280	.287
10	.320	.328
11	.385	.395
12	.450	.461
13	.515	.528
14	.580	.595
15	.645	.661
16	.716	.734
17	.787	.807
18	.859	.880
19	.929	.953
20	.975	1.000

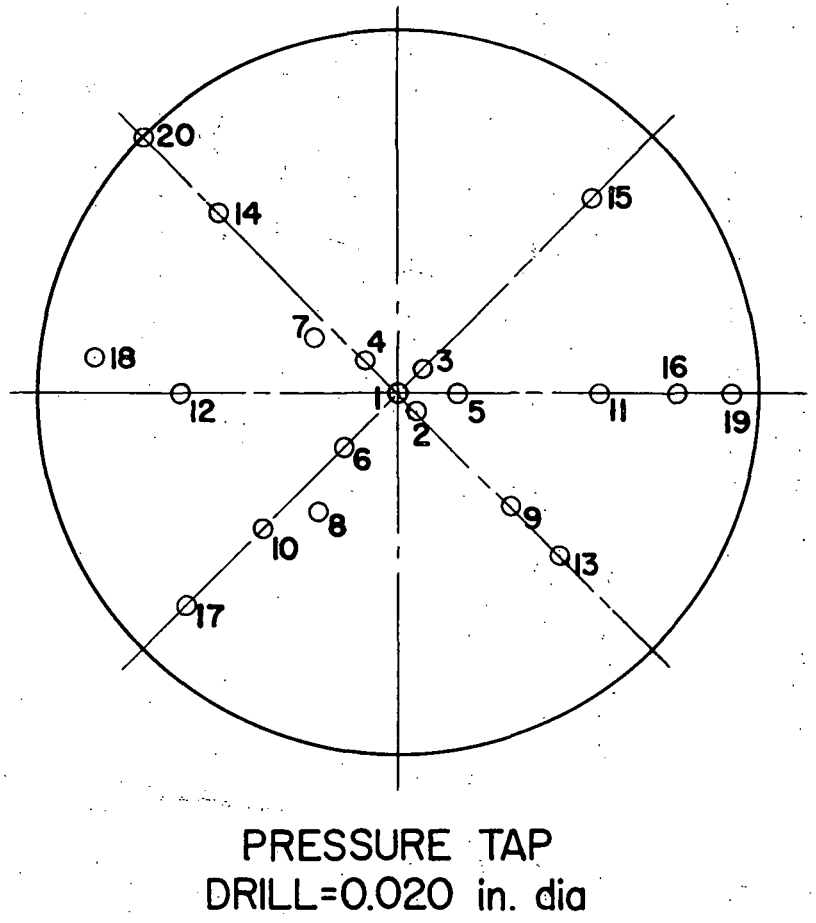

Fig. 4. Face of Pressure Tap End Plate for 2 in. dia Tubes No. 3 and 4.

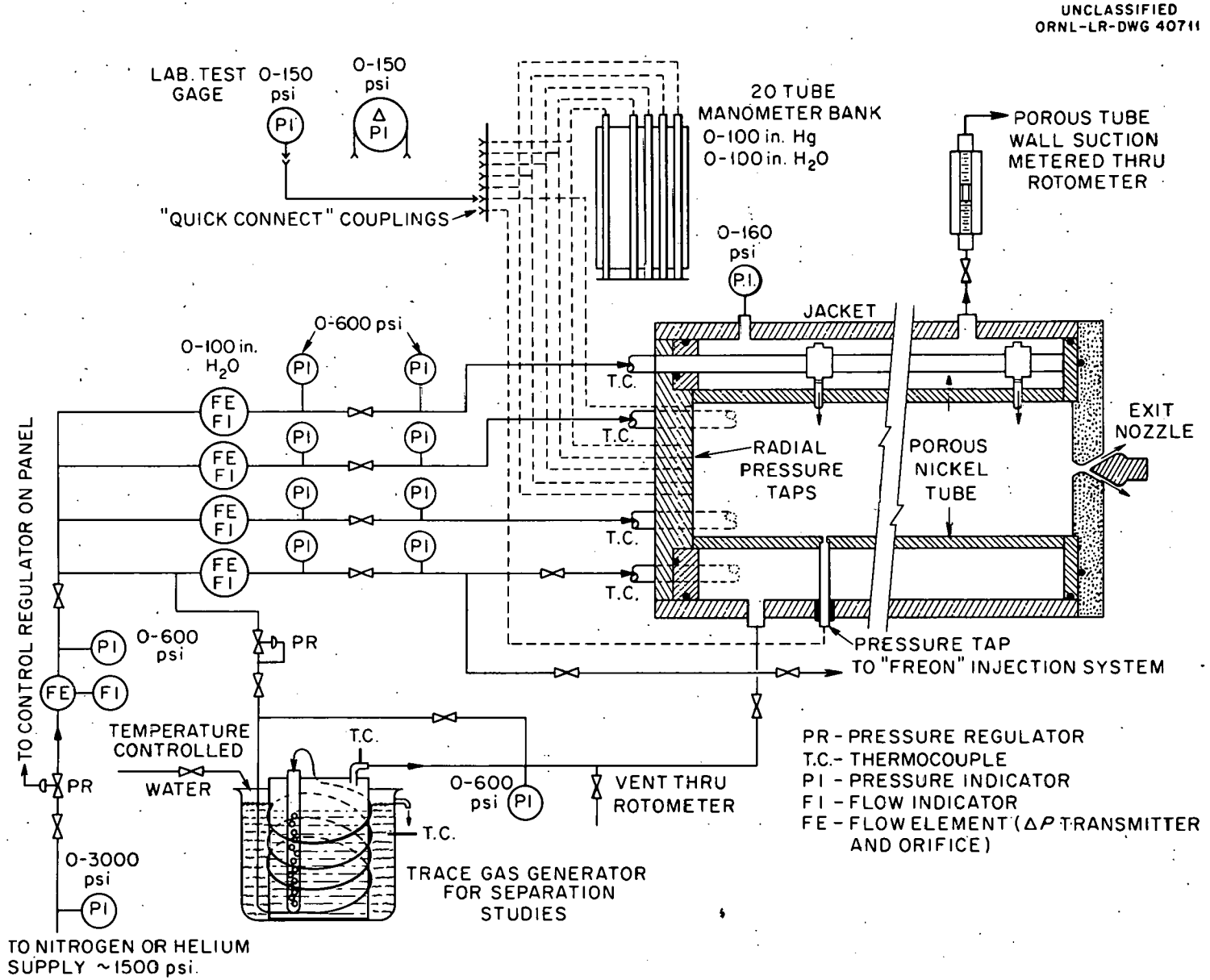

Fig. 5. Flow and Instrument Diagram Showing Vortex Tube Assembly No. 3.

Figure 6 is a photograph of the instrument and control panel showing the operating position of the vortex tube assembly at the center of and behind the panel. Figure 7 is a closer view of the assembly with the radial pressure taps at the left. Three of the four supply headers are also visible.

Vortex tube No. 3 is shown in the upper portion of Fig. 8. Also shown are insert tubes A and B used to study the effects of decreasing tube diameter. These inserts, 1-in.-ID plastic and 0.63-in.-ID brass, were made with 2-in.-OD flanges on each end and appropriate "O-ring" gaskets for end seals, so that they could be slipped into the 2-in.-ID tube without modification of the latter. The injection nozzles consisted of a series of holes drilled directly in the insert wall. The location, size, and number of nozzles is given in Table I. The tubes were carefully polished to a mirror finish on the inside diameter subsequent to drilling, and the 0.63-in. brass tube was nickel-chrome plated to give a hard, smooth surface.

In order to investigate the effect of subsonic, near laminar injection on the ability of wall suction to stabilize the flow in a vortex, an additional 2-in.-dia porous-wall tube was fabricated, which is designated tube No. 4. The design of this tube featured a removable wall insert piece which provided for a continuous injection slit along the length of the tube. Two such inserts were studied. Wall insert slit A, shown schematically in Fig. 9 installed in tube No. 4, was designed to provide a tangential slit of about 0.002-in. width between the wall of the 2-in. porous tube and a small lip projecting into the tube about 0.040 in. The lip was contoured to blend smoothly with the inside diameter of the tube at the tube-insert boundry, as indicated in the cross-sectional view. The purpose of this design was to enable the gas to be injected into the boundry layer on the inside tube wall in as nearly laminar

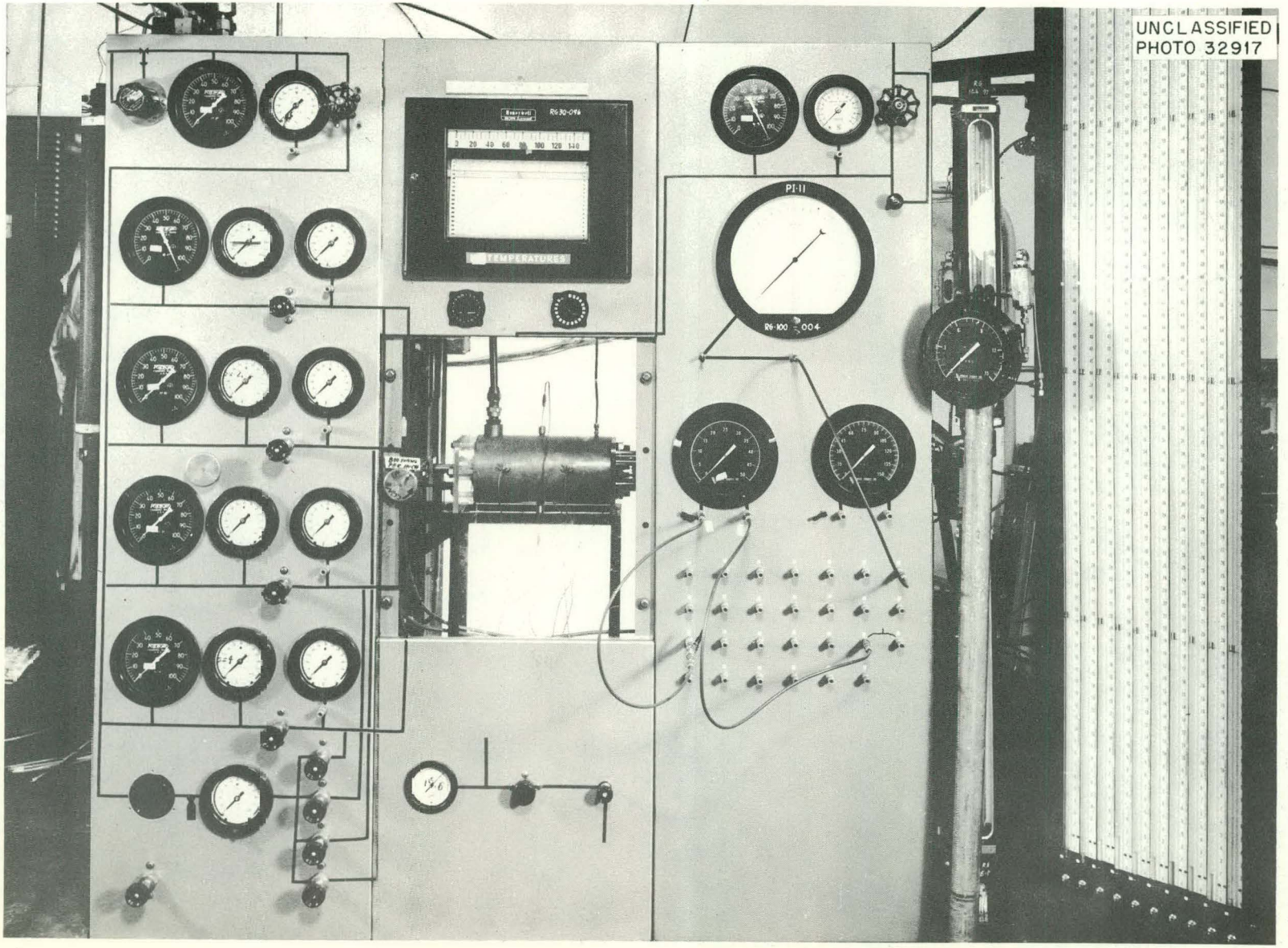

Fig. 6. Instrument and Control Panel (Vortex Tube Assembly No. 3 Shown at Center).

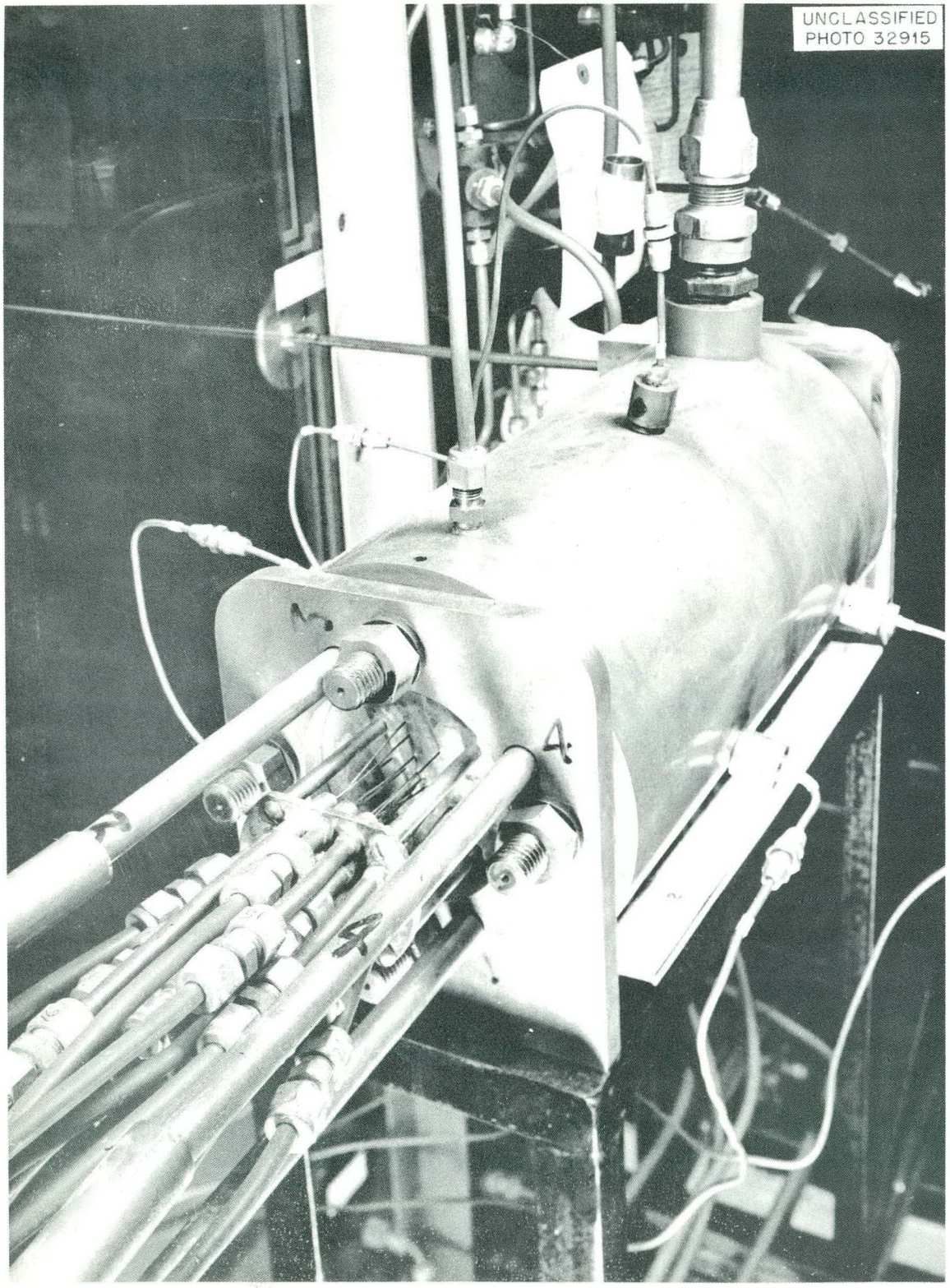

Fig. 7. Vortex Tube Assembly No. 3.

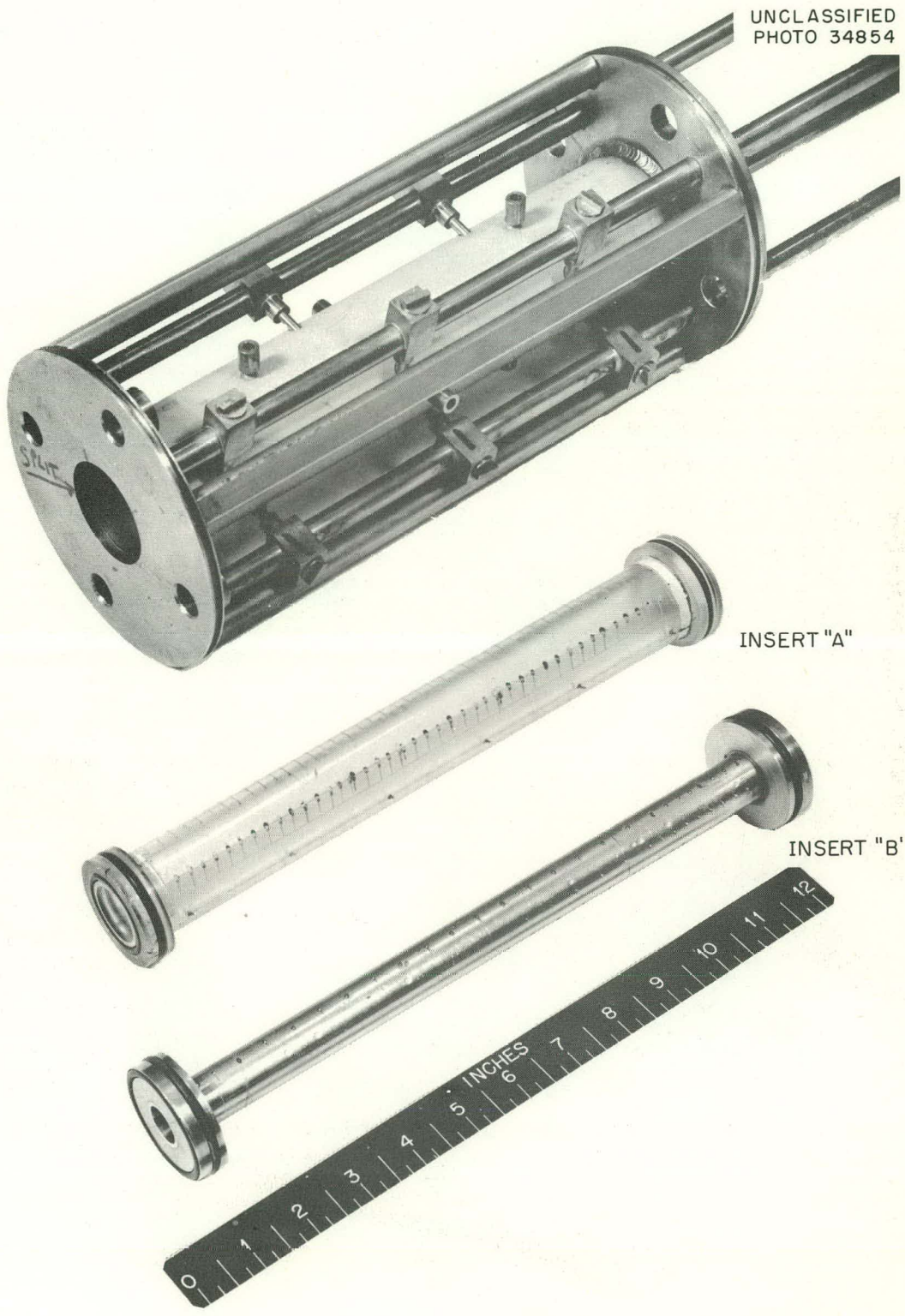

Fig. 8. Vortex Tube No. 3 and Inserts.

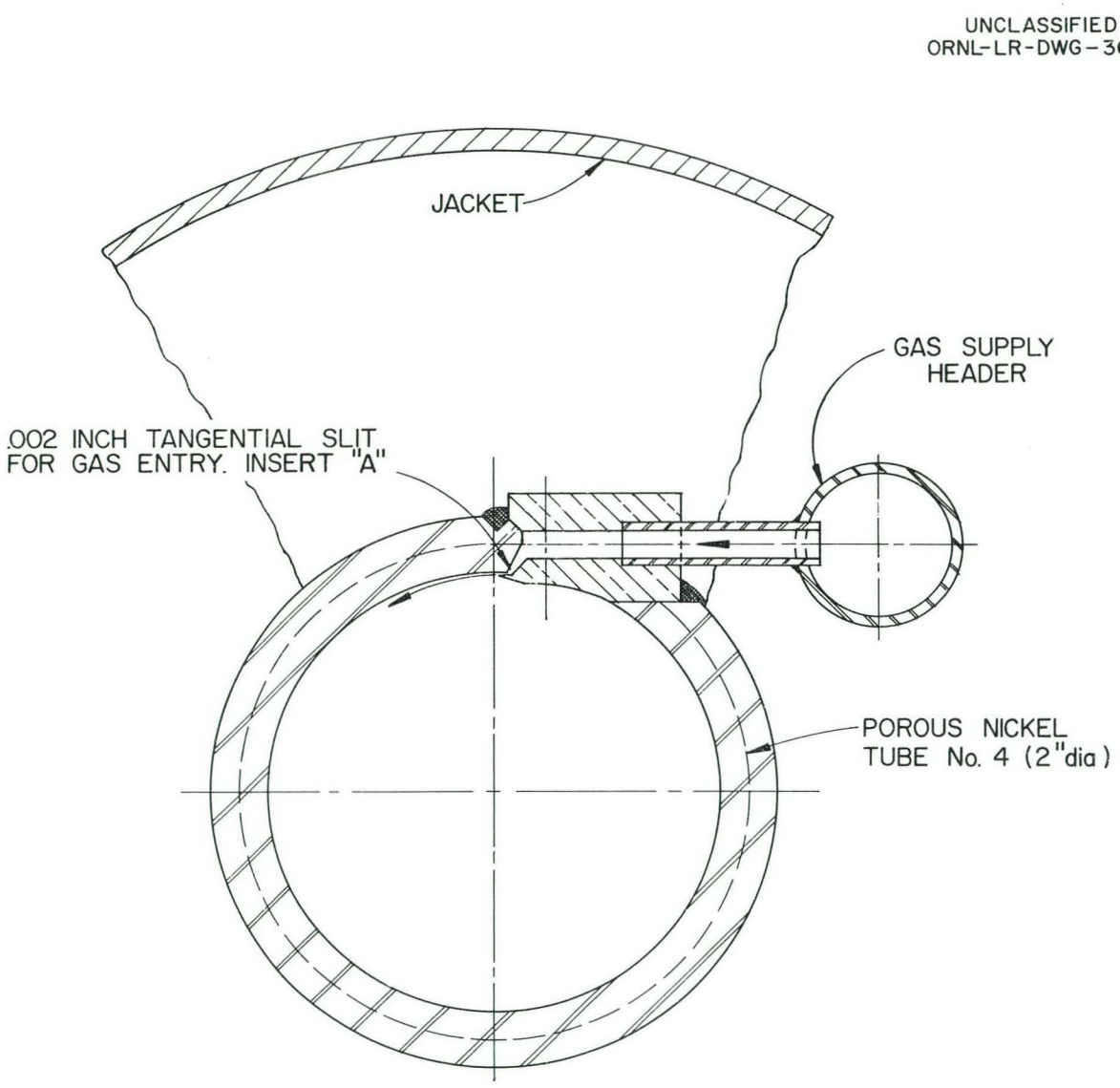

Fig. 9. Cross-Sectional Diagram at Vortex Tube No. 4 – Wall Insert Slit A.

fashion as possible and at $M_j \leq 1.0$. In this manner it was hoped to circumvent the type of disturbance introduced by the highly turbulent, supersonic jets employed in tube Nos. 1, 2, and 3 impinging obliquely on the boundary layer.

Due to difficulty in fabrication and assembly, the boundary layer injection slit was not of uniform width, resulting in large injection flow asymmetries. Thus, some regions of the entering flow were probably highly turbulent. In order to insure a more uniform aperature and to eliminate the lip which projected into the boundary layer and which could be a source of turbulence, wall insert slit B, shown in cross section in Fig. 10, was fabricated by grinding a 0.002-in. step in one face of the insert. A thin strip of metal formed the smooth side of the slit. In this way, the width was held to within ±0.0002 in. The slit entered at a radial position of 0.92, and blended smoothly with the tube radius. The injection Reynolds number was 2,000, based on the equivalent diameter of the slit, for nitrogen flow of 10 scfm. Figure 11 is a photograph of tube No. 4-B.

Vortex tube No. 5 was designed to study the effect of a favorable temperature gradient in the boundary layer, by removing heat through the tube wall to a coolant. Figure 12 is a schematic diagram of the brass tube, which was 0.64-in. inside diameter and 3.5 in. in internal length, with 1/8-in.-wall thickness. The vortex was generated by means of twelve 0.020-in.-dia nozzles drilled in the tube wall so as to enter at a radial position r_a' of 0.90. The tube was polished to a mirror finish on the inside diameter and nickel-chrome plated. The nozzles were fed by twelve 1/4-in.-dia tubes brazed to the tube outside diameter and joined to two 5/8-in.-dia supply headers. The radial pressure distribution was obtained by means of 18 taps

UNCLASSIFIED
ORNL-LR-DWG-40840

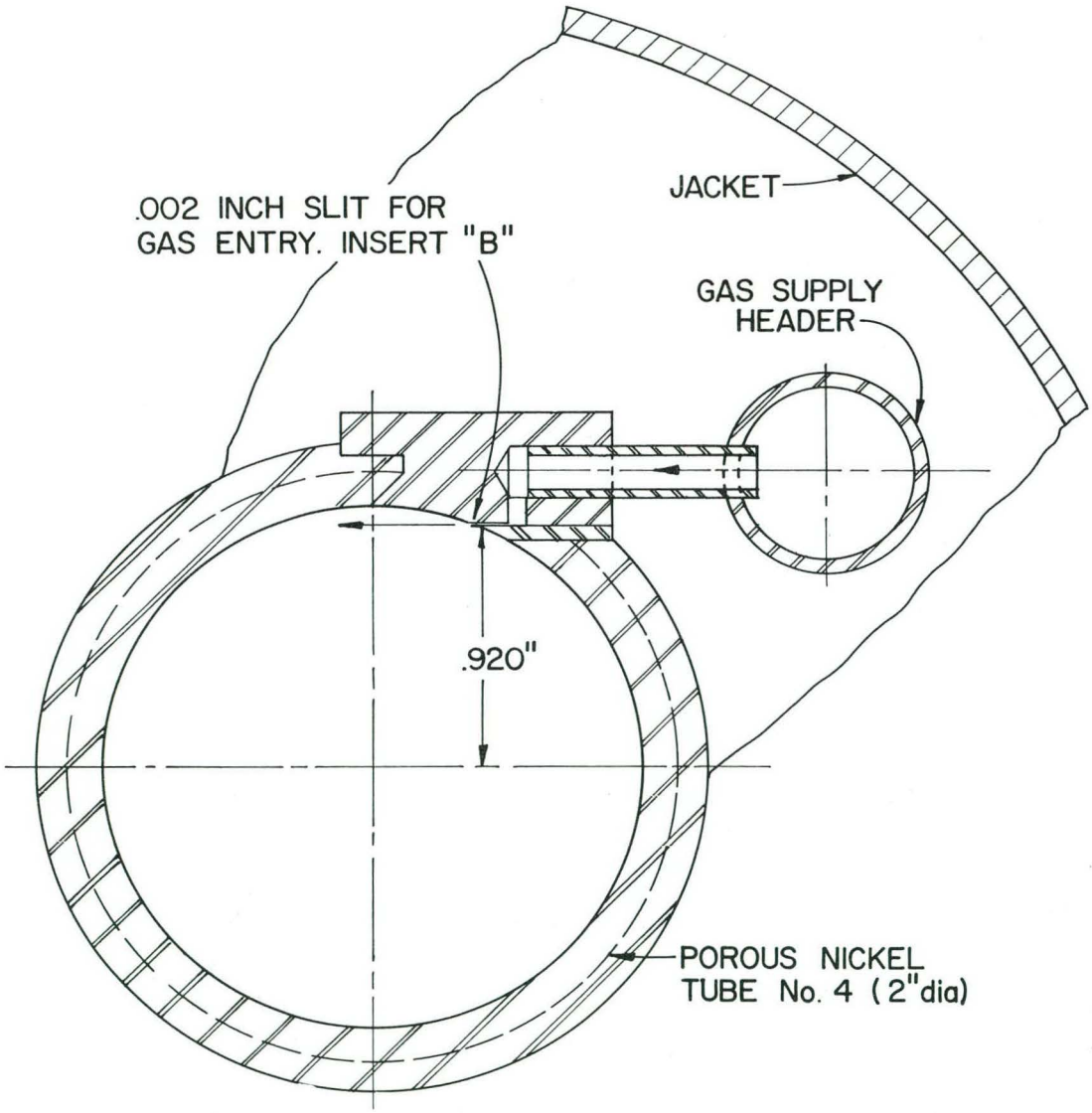

Fig. 10. Cross-Sectional Diagram at Vortex Tube No. 4 – Wall Insert Slit B.

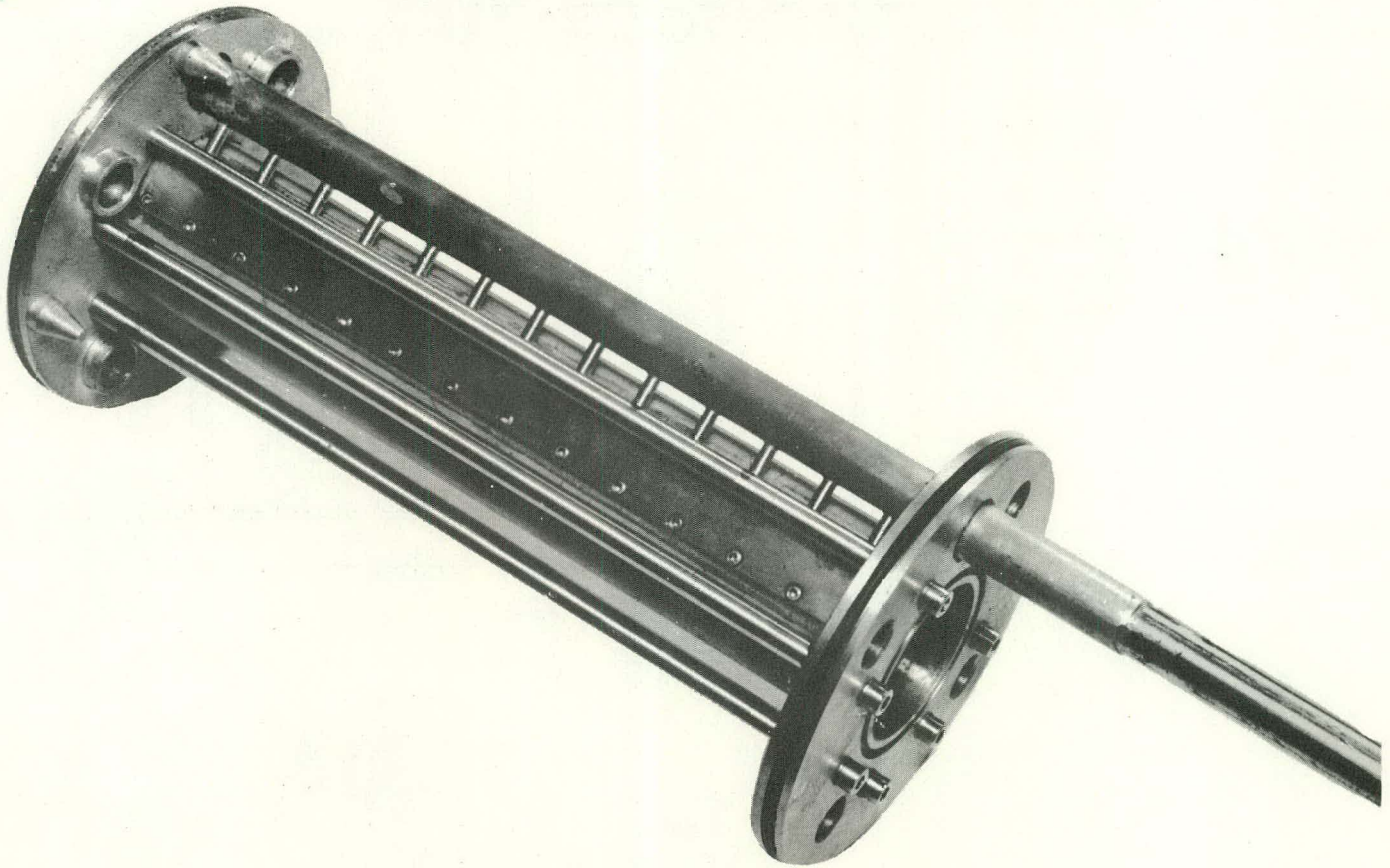

Fig. 11. Vortex Tube No. 4 – Wall Insert Slit B.

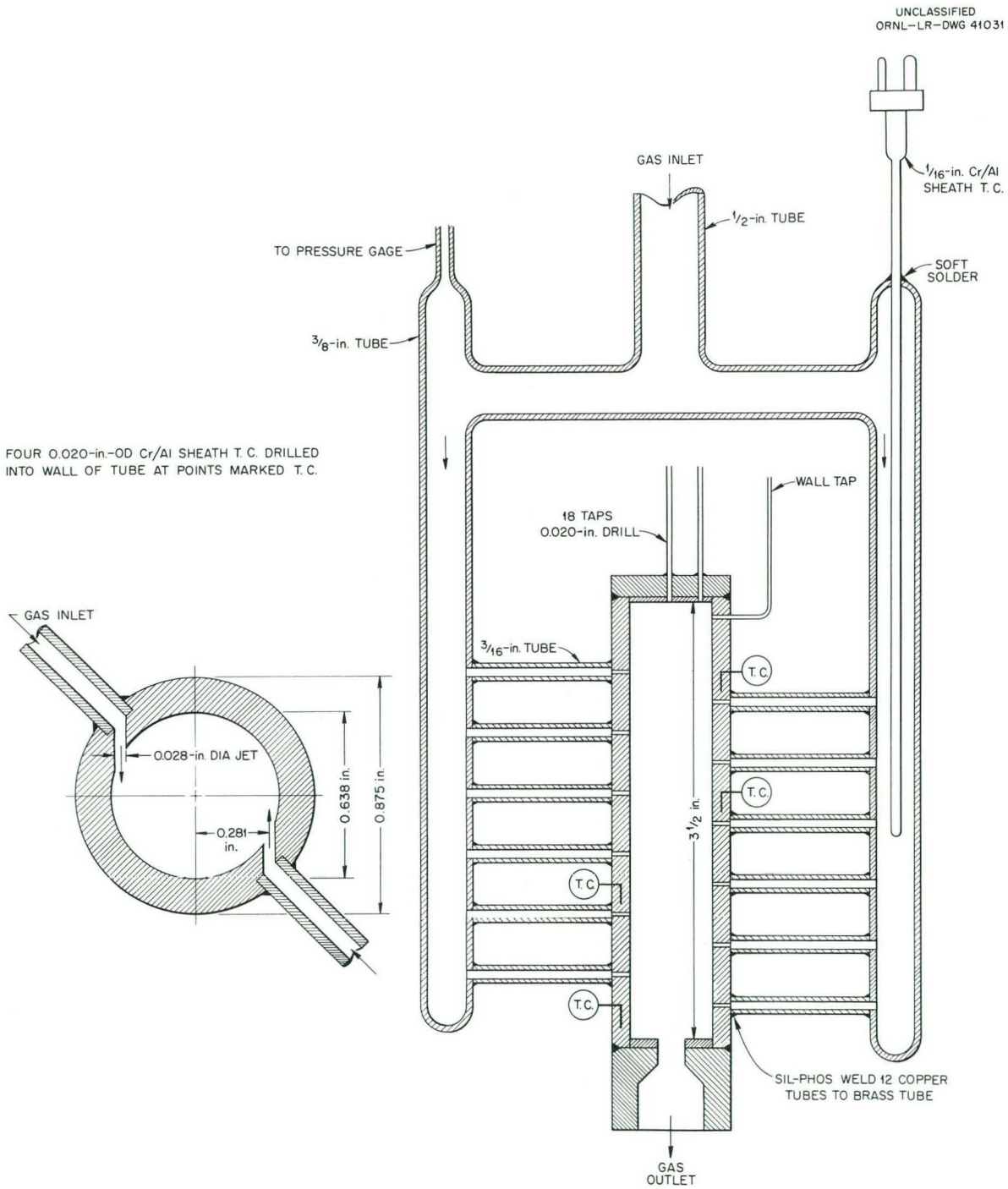

Fig. 12. Vortex Tube No. 5.

(0.020-in. drill) located in the end plug. Into these were brazed small diameter tubes connected to the manometer board. Gas was discharged from the vortex tube through a thick orifice drilled in the end seal. Thermocouples were provided for measurement of inlet gas, outside wall, and exit gas temperature. Figure 13 is a photograph of this vortex tube. For operation with wall cooling, the tube was immersed horizontally in a container of liquid nitrogen. Feed tubes were insulated to minimize precooling of the inlet gas stream.

II. Gas Analysis

The separation measurements necessitated determination of the concentration of small quantities of C_8F_{16} (perfluorodimethylcyclohexane) in helium. C_8F_{16} was chosen because of its stability, inertness, volatility (35 mm Hg at 75°F), and molecular weight (400). Infrared analysis of the material used in the experiments showed it to be of high purity. A very fine radial probe was used to sample the gas mixture in the tube. Figure 14 is a sketch of the probe and manipulator showing the geometry of the telescoping segments, the smallest of which was 0.008-in. OD, 0.004-in. ID; the largest tube in contact with the vortex field near the wall was 0.017-in. OD. Introduction of the probe caused some reduction in vortex strength due to the additional turbulence which it generated. In comparing the experimentally determined mole-fraction peak position with theory, however, the probe was inserted to the position of peak reading for the experimental determination of M_m. Deflection of the probe by the high-velocity flow was measured by a cathetometer, so that the true position of the probe tip was known for each separation run.

The C_8F_{16}-He mixtures were analyzed by measuring the thermal conductivity. Figure 15 is a schematic of the analytical apparatus, consisting of

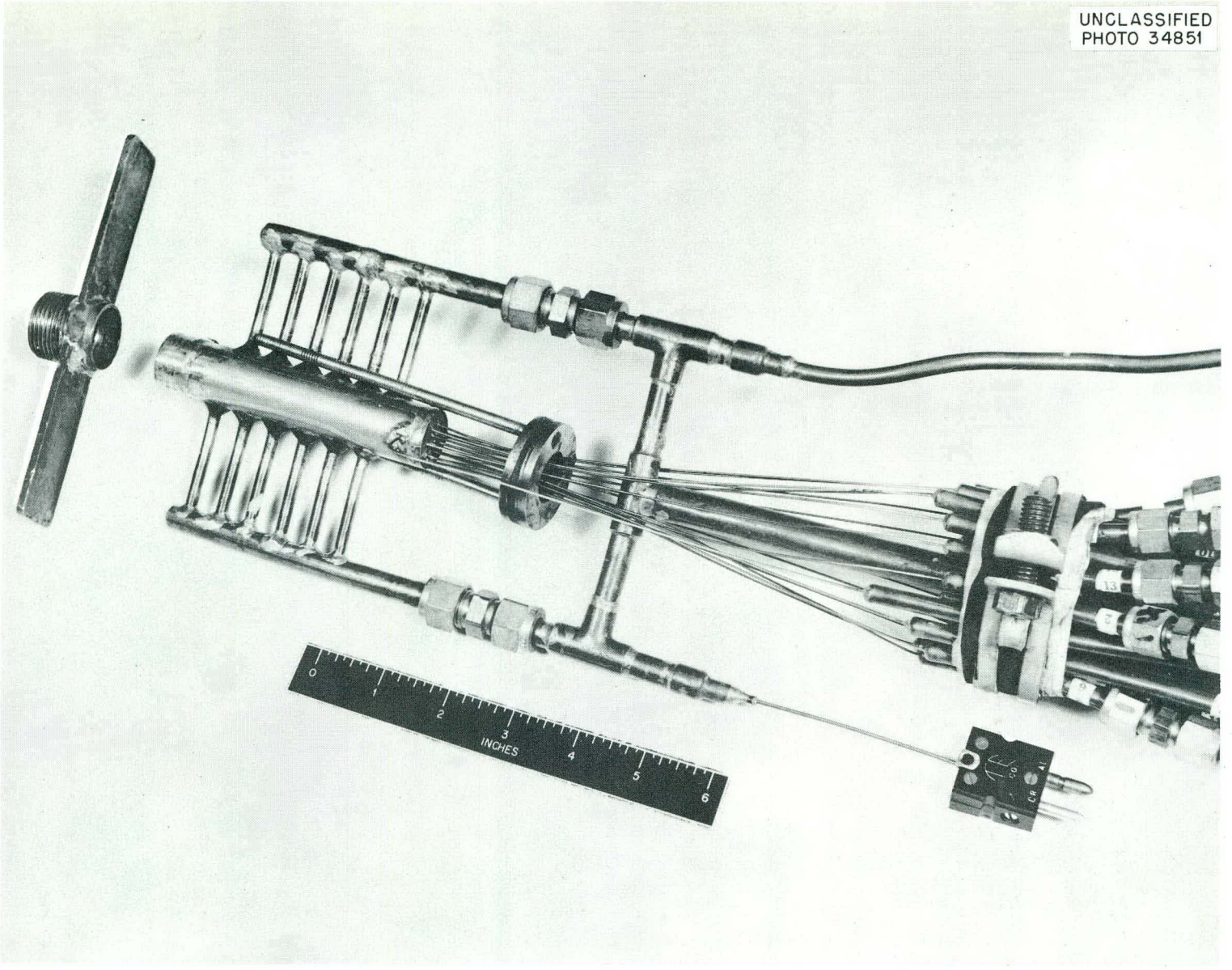

Fig. 13. Vortex Tube No. 5.

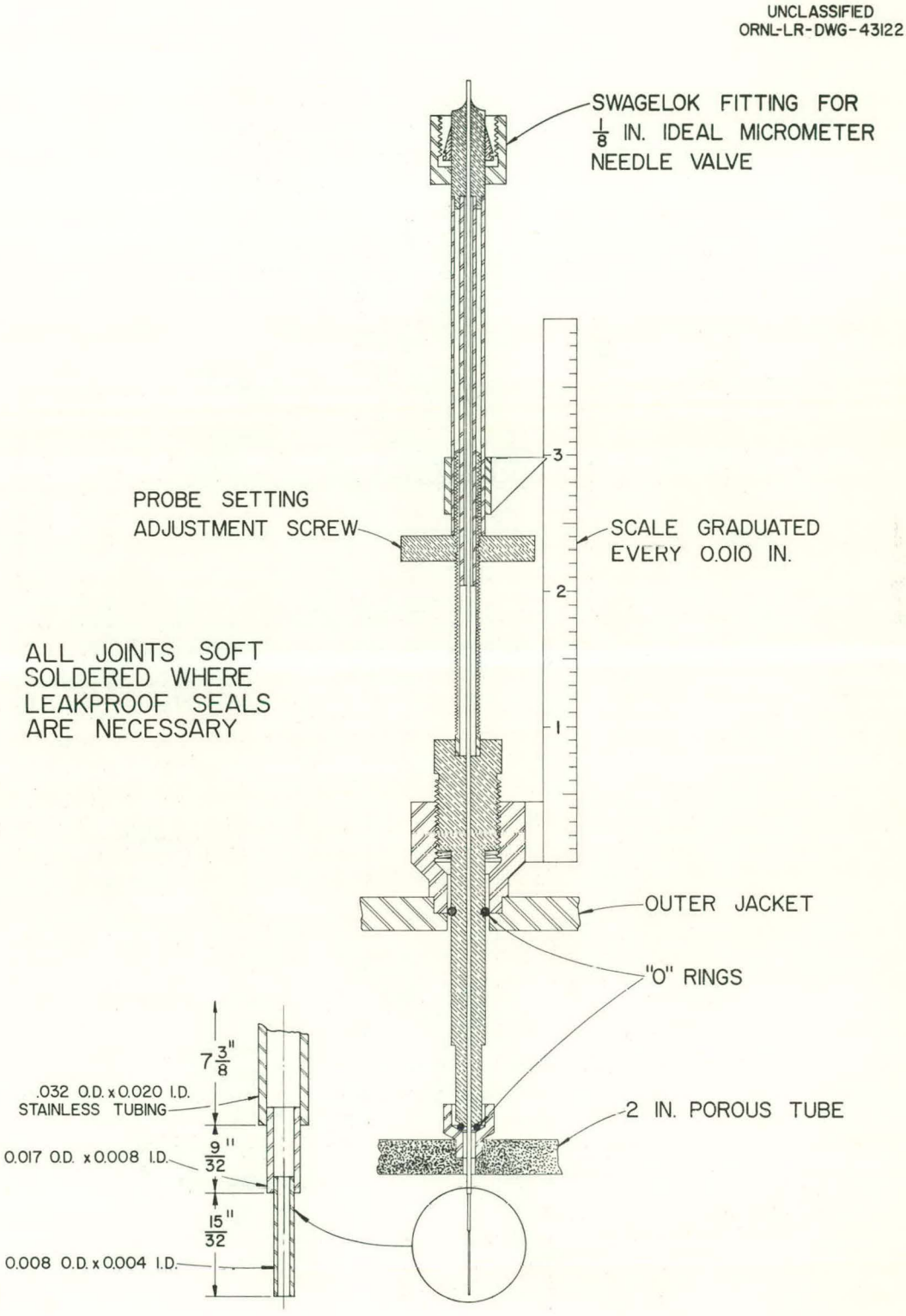

Fig. 14. Detail of Gas Sampling Probe for Vortex Tube Assembly No. 3.

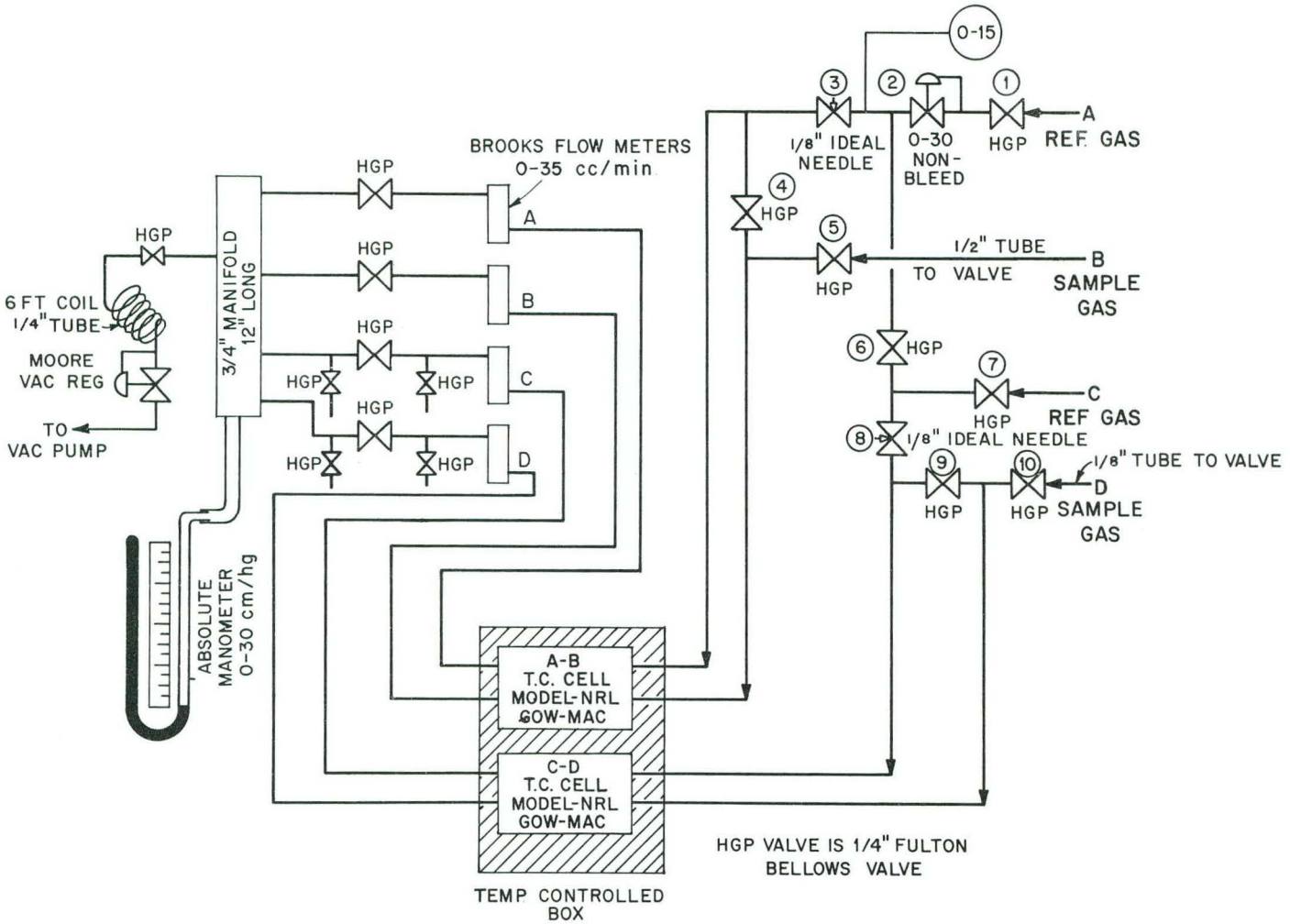

Fig. 15. Schematic Layout of Gas Control System - Thermal Conductivity Gas Analyzer.

two Gow-Mac Instrument Corporation Model NRL thermal conductivity cells. An electronic thermoregulator was used to maintain the cell temperature constant to within ±0.1°F. The cells were operated at 10 cm Hg abs in order to hold the response time to 30 sec or less for the small sample flows of 5 cm^3/min, and for improved stability. The calibration of the thermal conductivity cells at 150 ma total cell current was found to be linear for C_8F_{16} concentrations from 0.0 to 0.5%, with a slope of 10 mv/% C_8F_{16}. This system was sensitive to a variation in concentration of ±2 ppm of the heavy gas, using a Leeds and Northrup type K-3 potentiometer with a Minneapolis-Honeywell null indicator as the read-out device. Thus, concentrations as low as 20 ppm would be measured with accuracy of ±10%.

THE EXPERIMENTAL RESULTS

I. Review of Previously Published Experimental Work

Preliminary experimental results in 2-in.-dia plastic tubes Nos. 1 and 2 (see Table I) were reported in ref 3. Figures 16 and 17 illustrate the variation in the peripheral-to-isentropic jet Mach number ratio, M_p/M_j^*, with mass flow rate per unit of tube length, $\mathcal{M}$, for three values of the wall pressure, p_p. Note that M_p/M_j^* increased with $\mathcal{M}$ due to the increase in driving torque. The analytical method (discussed on page 14) was used in determining M_p. M_j^* was calculated from the ideal gas relationship:

$$M_j^* = \left[\frac{\left(\frac{p_o}{p_p} \right)^{\frac{\gamma - 1}{\gamma}} - 1}{\frac{\gamma - 1}{2}} \right]^{1/2} .$$

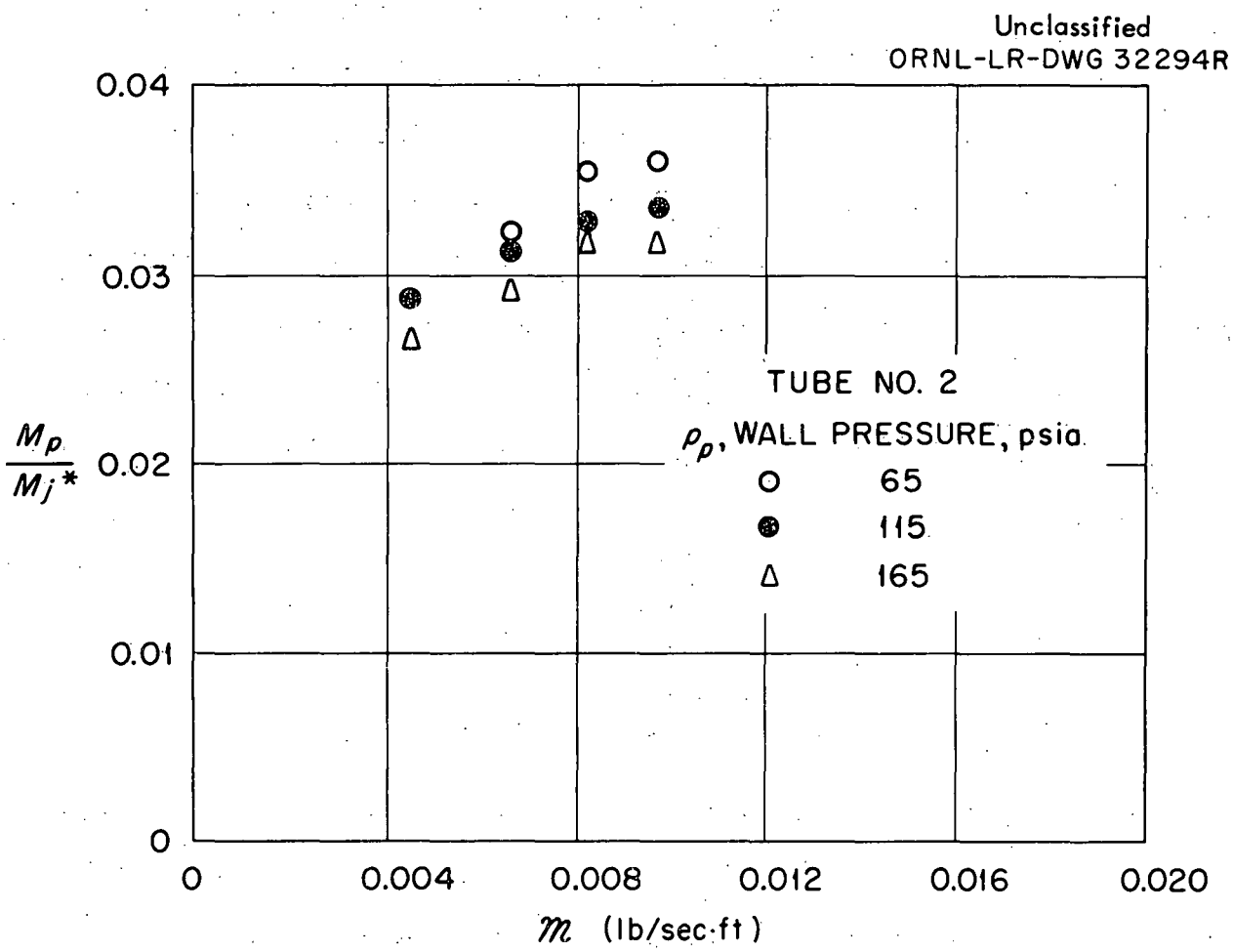

Fig. 16. Variation of Ratio of Vortex Tangential Mach Number and Jet Exit Mach Number Mass Flow Rate per Unit of Tube Length and Tube Pressure, for Tube No. 2.

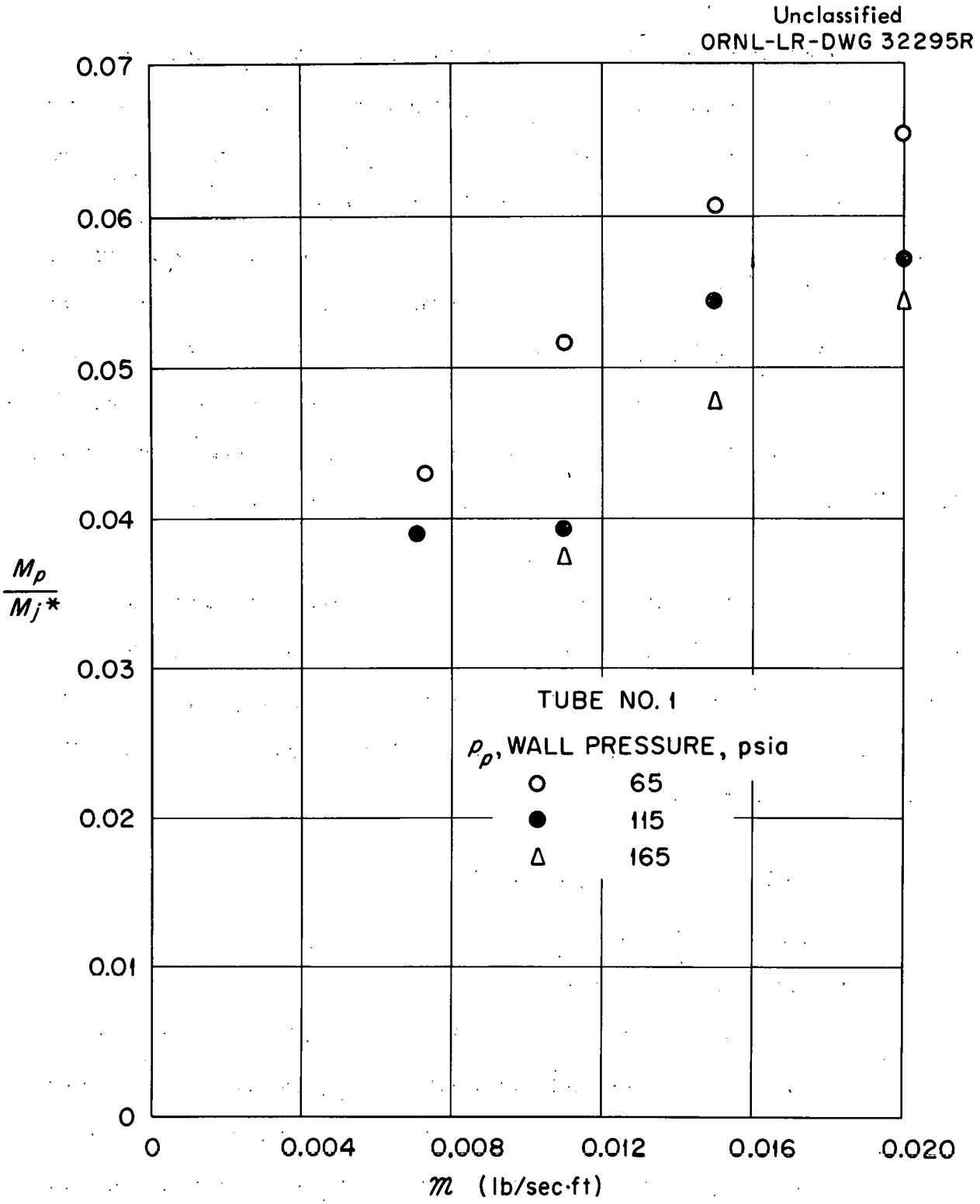

Fig. 17. Variation of Ratio of Vortex Tangential Mach Number and Jet Exit Mach Number with Mass Flow Rate per Unit of Tube Length, and Tube Pressure, for Tube No. 1.

Since the nozzles converged and the pressure ratio, p_o/p_p, across the nozzles exceeded the critical value, the true jet Mach number had to be less than M_j^*. The true jet effectiveness ratio, M_p/M_j, was therefore somewhat greater than the value M_p/M_j^* as plotted. The maximum value of M_j^* was about 2; since M_j cannot be less than 1.0, the true effectiveness ratio for the maximum point in Fig. 16 must lie between 0.056 and 0.13. From theory (1, 2), M_p/M_j should be of the order of 0.95 if the flow field were laminar, $\mu^*/\mu = 1$. The order of magnitude discrepancy between the observed and theoretical (laminar) vortex strength is best explained by postulating a turbulent flow field with $\mu^*/\mu >> 1$. Experimental determination of μ^*/μ is described on pages 70-74.

Figures 18 and 19 show the variation of the exponent ϵ in Eq. 3 with mass flow rate and tube wall pressure for vortex tubes 1 and 2. Note that ϵ was much closer to the value 1.0 for a potential (free) vortex than to the value -1.0 for solid-body rotation, and that ϵ increased with $\mathcal{M}$, up to $\mathcal{M} \cong 0.01$ lb/sec ft.

II. Experiments Aimed at Boundary-Layer Stabilization

A. Uniform Wall Bleed

1. Supersonic Injection

It was estimated in ref 2 that stabilization of the boundary layer might be possible with bleed ratios, R_B, as low as unity, where R_B is defined as the ratio of mass flow bled-off to that which exhausts radially at the tube center. The first experimental attempts at stabilization by uniform wall bleed were performed using vortex tube assembly No. 3, illustrated in Fig. 3 and described in Table I.

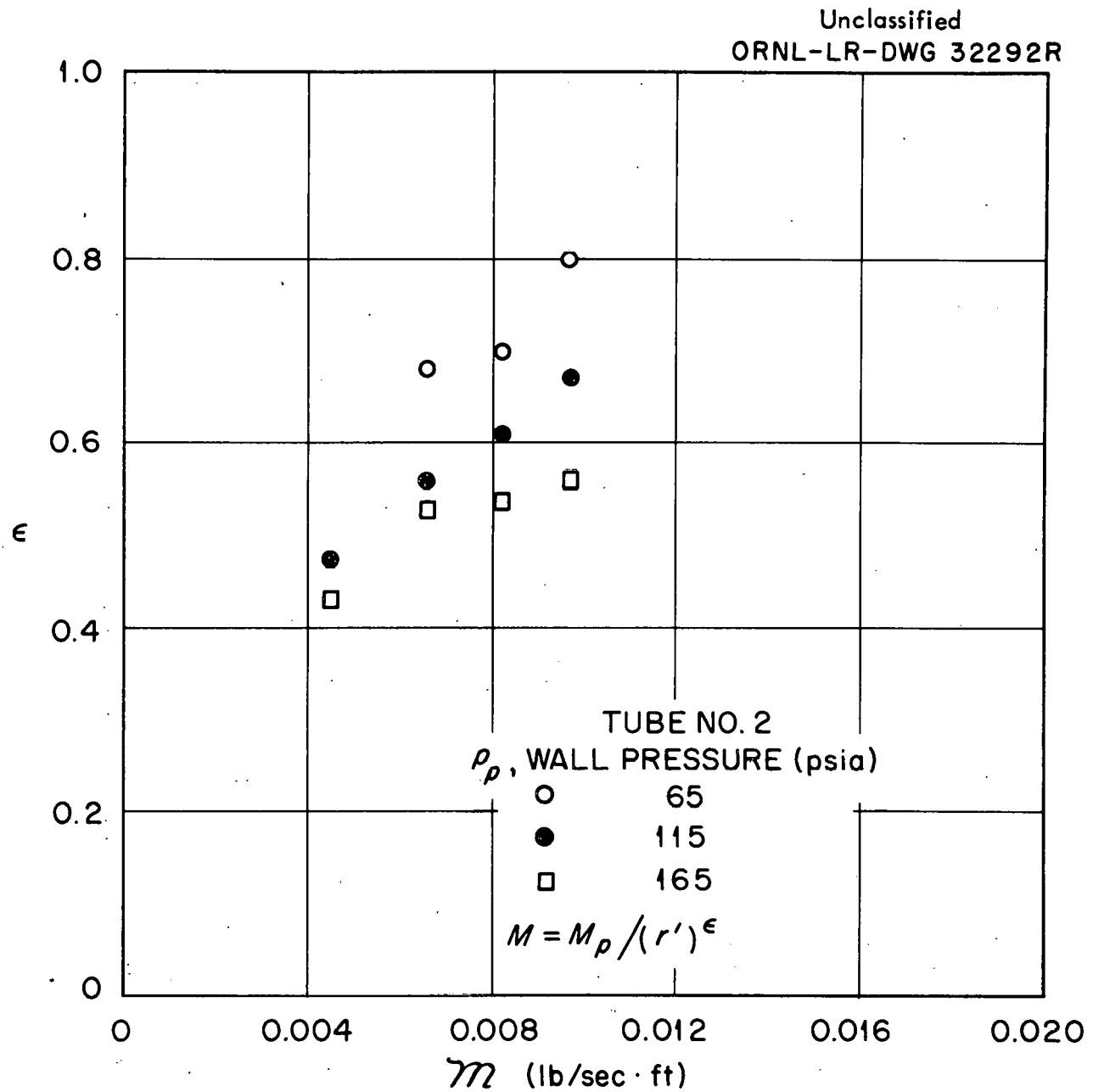

Fig. 18. Variation of ϵ with Mass Flow Rate per Unit of Tube Length, and Tube Pressure, for Tube No. 2.

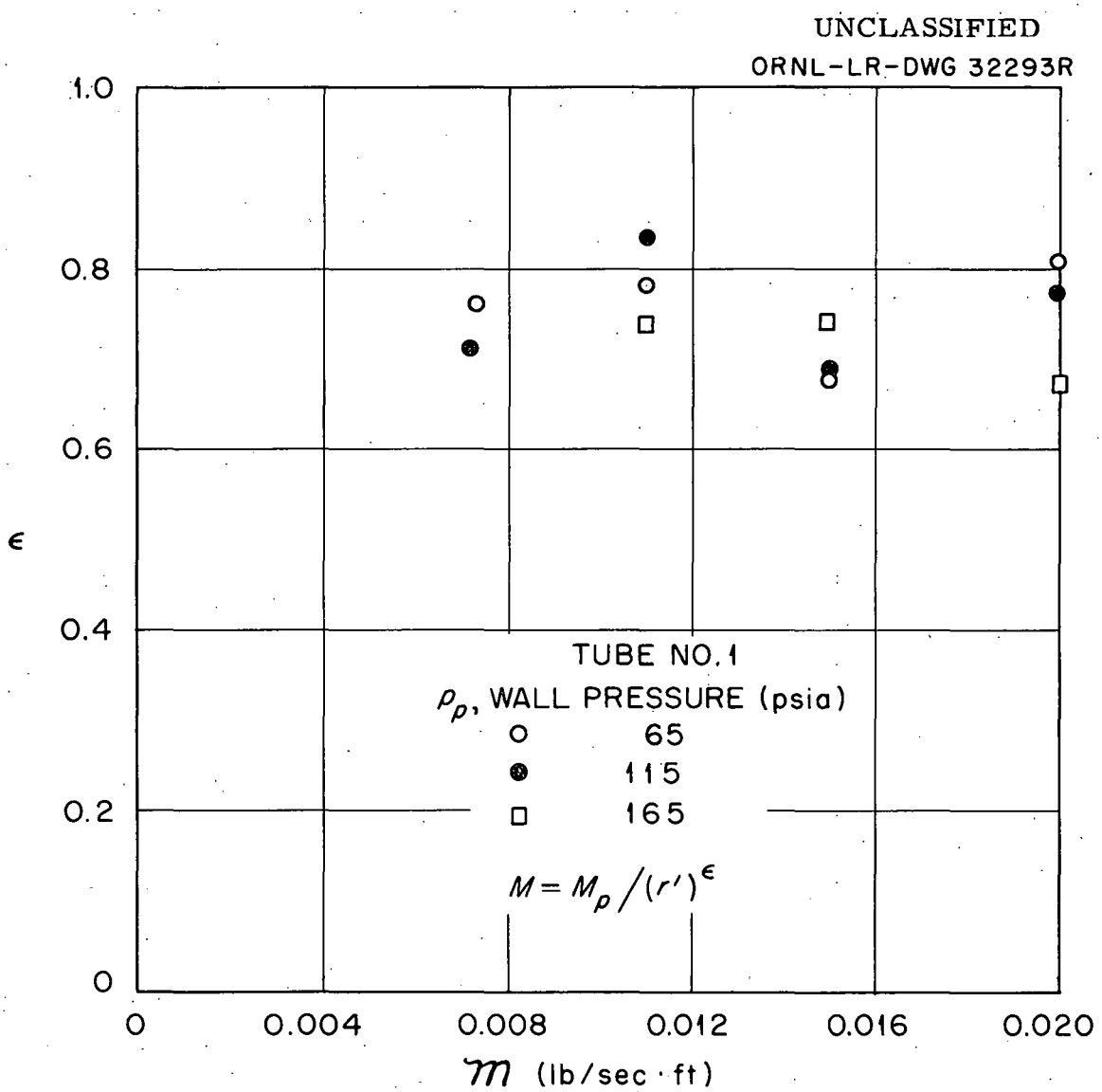

Fig. 19. Variation of ϵ with Mass Flow Rate per Unit of Tube Length, and Tube Pressure, for Tube No. 2.

The results are summarized in Figs. 20 and 21. In these and in the figures to follow, M_p was determined from the radial pressure distribution by the graphical slope method discussed on page 13. Nitrogen gas was employed except where indicated. In Fig. 20 the ratio, M_p/M_j^*, observed with uniform wall bleed to that observed under similar pressure and inlet mass flow conditions but with no wall bleed is plotted against R_B, for R_B from 0.6 to 2.9. M_j^* varied from 1.8 to 2.1 in these runs. Injection Reynolds numbers were in the highly turbulent region. Note that, with the exception of the point at 96 psia, wall bleed resulted in decrease of the Mach number ratio, although the decrease was less than 8% for $R_B \leq 3$.

In illustrating the effect of a particular variable on the velocity variation with radius, the ratio of tangential Mach number at $r' = 0.5$ to that at the periphery is used henceforth, in the form $0.5\ M_{r'=0.5}/M_p$; the choice of $r' = 0.5$ is arbitrary. This quantity is nearly 1.0 for a potential vortex, so that fractional values indicate deviation from ideality. Use of $0.5\ M_{r'=0.5}/M_p$ in place of ϵ to characterize the vortex velocity distribution is based on data which indicate that Eq. 3, which defines ϵ as a constant, is not always valid. Figure 21 illustrates the effect of wall bleed on the Mach number ratio under discussion, normalized by comparison with zero wall bleed conditions. Note that increasing the bleed ratio caused significantly increasing deviation from potential vortex flow.

2. Subsonic Injection

Failure to achieve laminarization in the first series of experiments with supersonic nozzle injection may have been due, it was

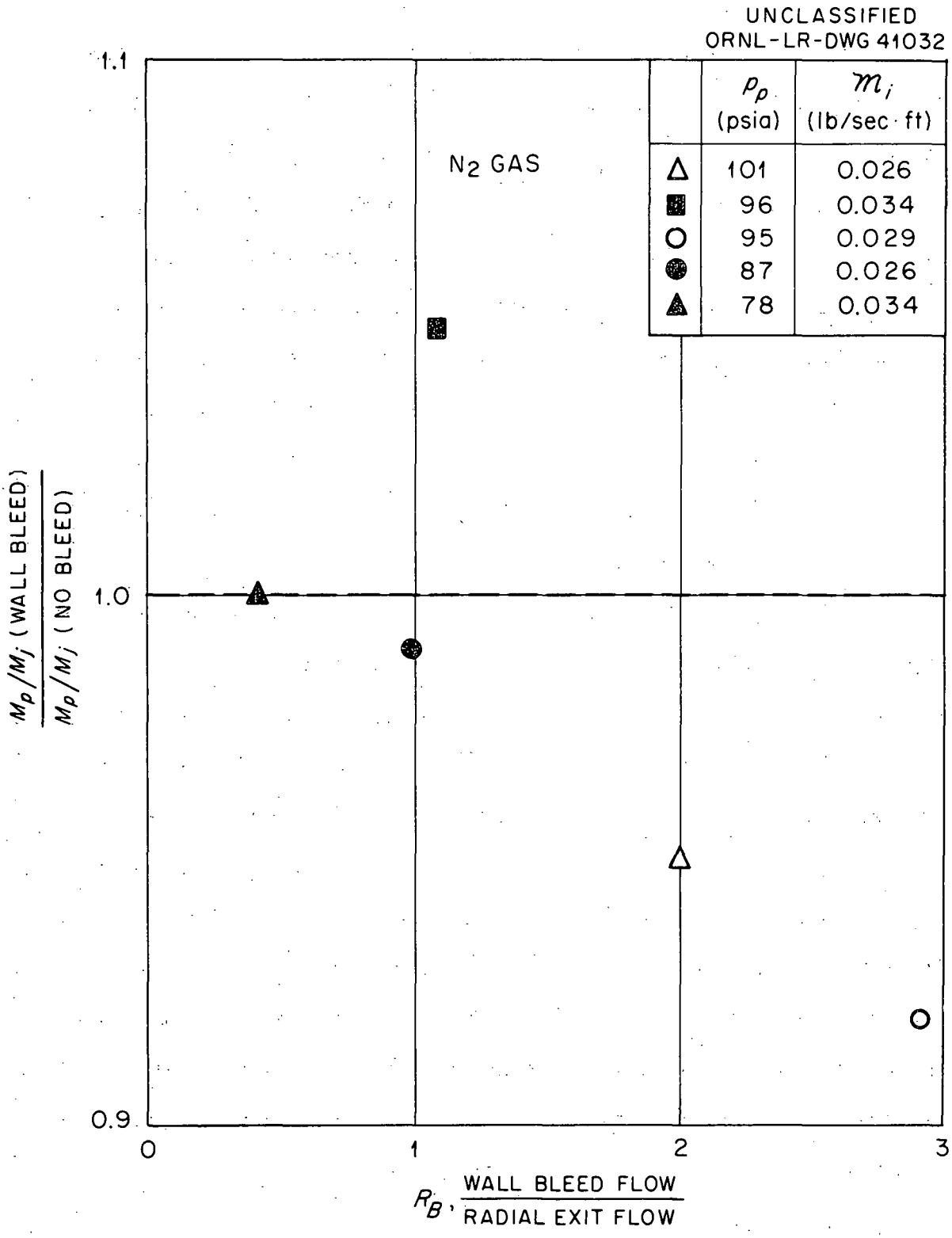

Fig. 20. Effect of Uniform Wall Bleed on Peripheral to Jet Mach Number Ratio, in 2-in. Dia Vortex Tube No. 3 with Nozzle Injection, $M_i^* > 1$.

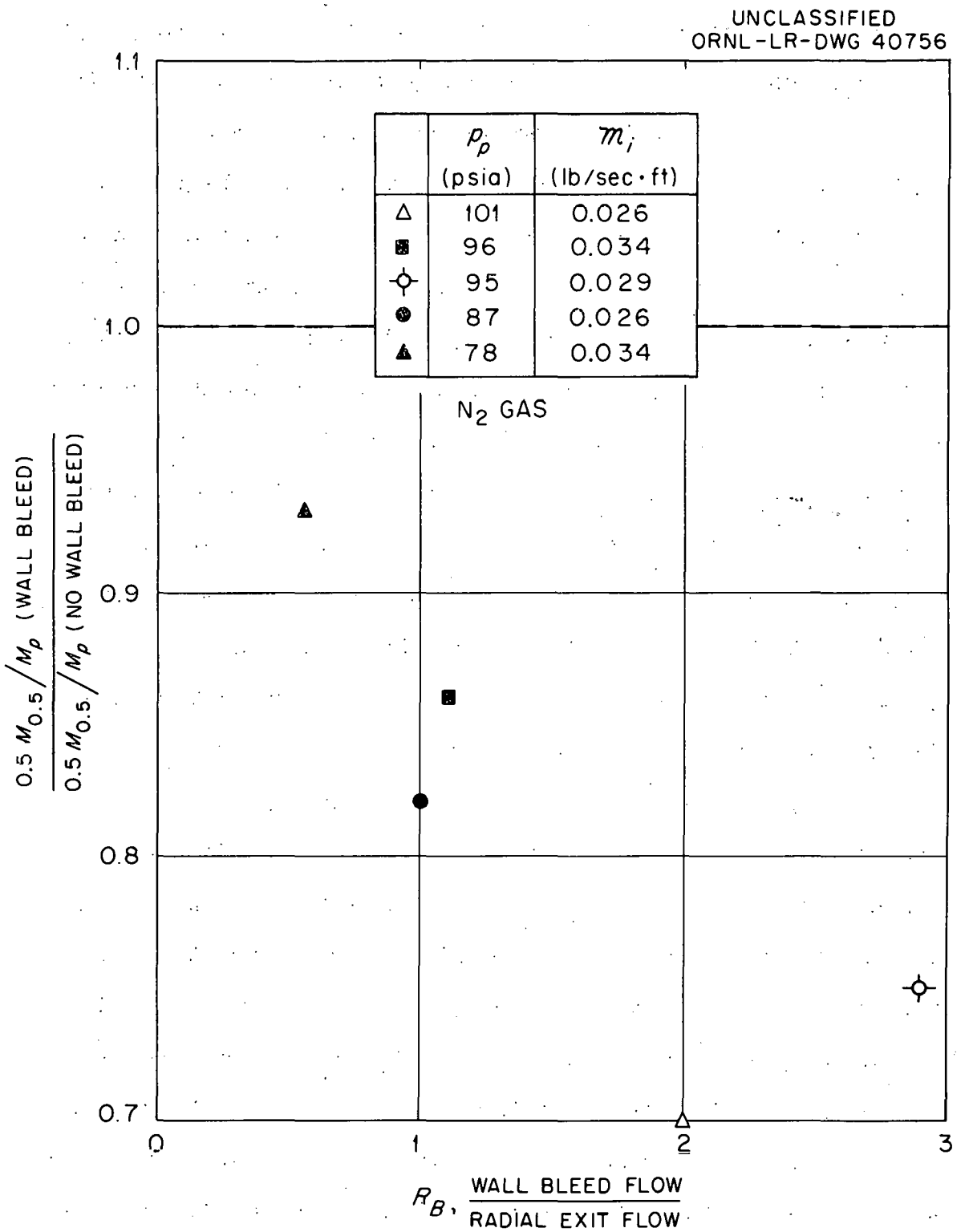

Fig. 21. Effect of Uniform Wall Bleed on Mach No. Ratio, $0.5\,M_{r'=0.5}/M_{p'}$, in 2-in. Dia Vortex Tube No. 3 with Nozzle Injection, $M_i^* > 1$.

thought, to a high degree of turbulence induced in the boundary layer by oblique impingement of the jets of supersonic turbulent gas. In order to test this hypothesis, vortex tube No. 4 was fabricated with a single 0.002-in.-wide continuous slit for injecting the gas subsonically and at low Reynolds number. Insert slit A provided tangential injection at $r_a' = 1.0$, directly into the boundary layer; slit B was moved away from the tube wall to provide injection at $r_a' = 0.92$, outside of the boundary layer. Figures 9 and 10 illustrate these two geometries. Figure 22 indicates that wall bleed may increase the peripherial Mach number, M_p, slightly for slit A, whereas there appears to be a slight decrease in M_p with wall bleed for slit B. On the other hand, Fig. 23 indicates a smaller decrease in the Mach number ratio, $0.5\, M_{0.5}/M_p$, with wall bleed for slit B than for slit A. Injection Reynolds numbers in both figures ranged from 4,500 to 10,000. For slit B, it is seen that, with R_B of 1.5, the value of M_p was decreased by at most 9% as compared to no-bleed conditions, and the ratio $0.5\, M_{0.5}/M_p$ was also decreased by at most 9%. This means that a reduction in exit mass flow by a factor of 2.5 is possible utilizing uniform wall bleed, with little loss in local vorticity. With boundary-layer injection, slit A, decrease in exit mass flow by 2.5 increased M_p slightly, but the ratio $0.5\, M_{0.5}/M_p$ was decreased by perhaps 35%. With supersonic injection, $R_B = 1.5$ (Figs. 20 and 21), little change in M_p was observed, but the Mach number ratio decreased by perhaps 25%. Certainly no significant degree of stabilization was achieved with uniform wall bleed, but, if it is desired to reduce the radial velocity to improve separation, bleed off through the wall may

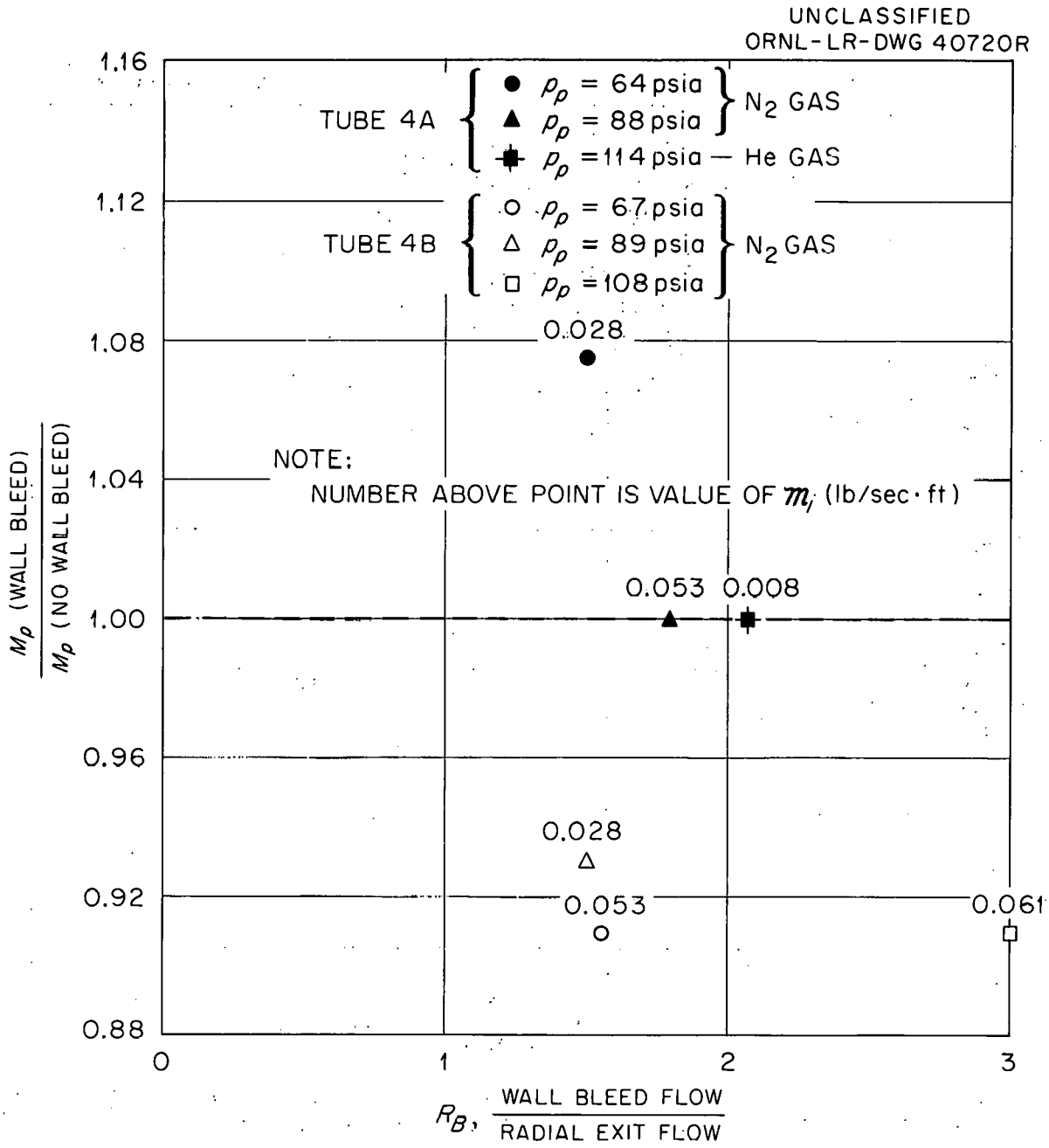

Fig. 22. Effect of Uniform Wall Bleed on Peripheral Mach No. in 2-in. Dia Vortex Tube No. 4 with Slit Injection, $M_i < 1.0$.

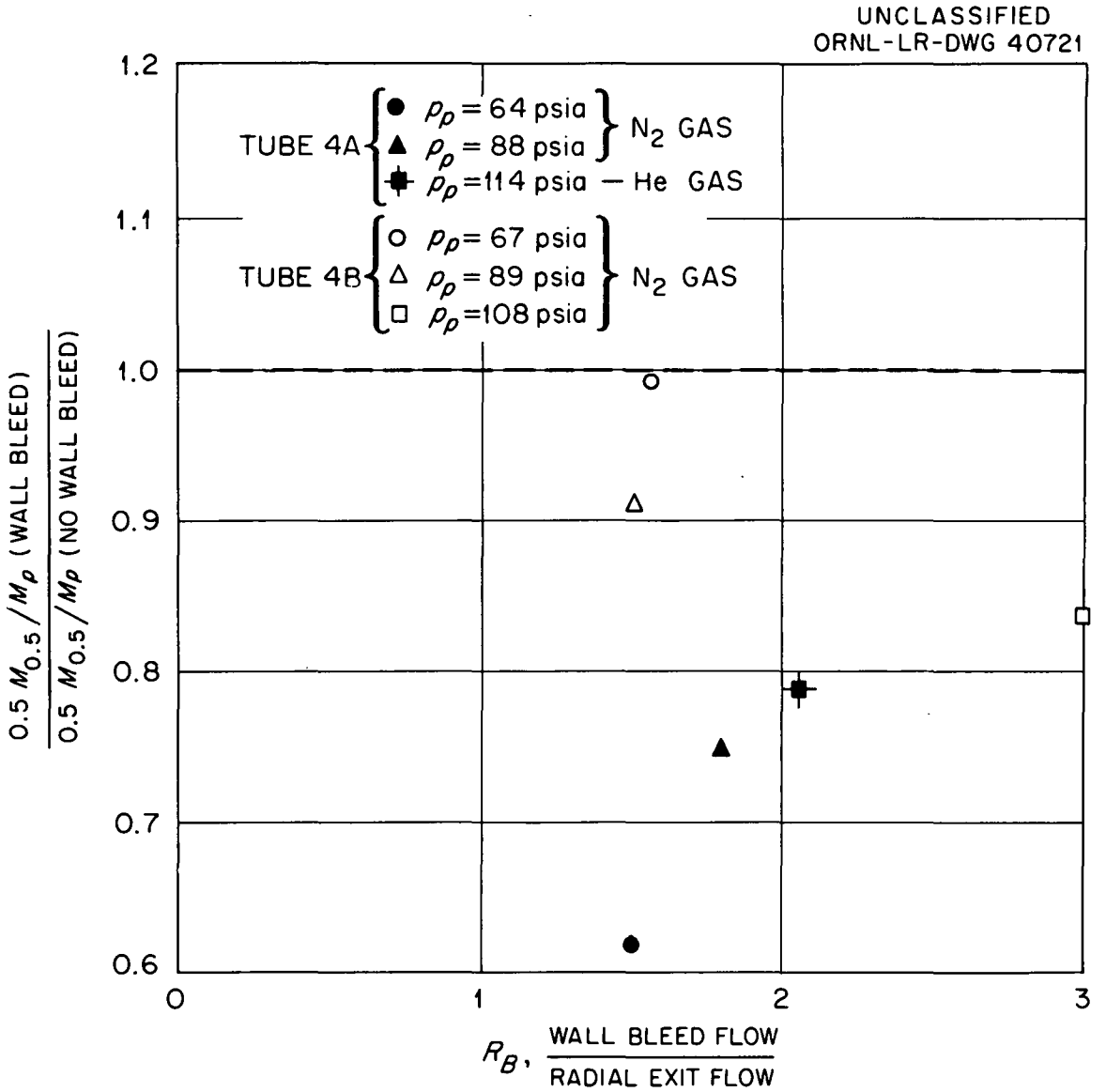

Fig. 23. Effect of Uniform Wall Bleed on Mach No. Ratio, 0.5 $M_{r=0.5}/M_p$, in 2-in. Dia Vortex Tube No. 4 with slit Injection, $M_i < 1.0$.

make it possible to effect a significant reduction in exit mass flow with little decrease in local vorticity when the gas is injected subsonically at $r_a' < 1.0$ at low Reynolds numbers.*

Figure 24 summarizes the effect of exit mass flow rate, $\dot{m}_e$, on the ratio $0.5\ M_{0.5}/M_p$, for the wall bleed data of Figs. 22 and 23. Note that the velocity distribution approached that of a potential vortex as $\dot{m}_e$ increased, in agreement with the necessity that, in a viscous vortex, angular momentum must be transported by radial convection to the inner layers of fluid to produce tangential acceleration.

B. Heavy Gas Injection

A second attempt to stabilize the boundary layer involved injection of Freon-12 (CCl_2F_2), molecular weight 121, uniformly into the boundary layer through the porous wall of vortex tube No. 4-B. As discussed on page 10, a concentration gradient of heavy gas toward the wall is in the direction to produce a favorable density gradient in the boundary layer for suppression of turbulence. Furthermore, since the absolute viscosity of Freon-12 is about 50% less than that of nitrogen at room temperature, the viscosity gradient is also favorable. The purpose of this experiment was, therefore, to determine whether reduction in turbulence and hence increased vorticity would result.

---

*Roughness on the inside wall of the porous tubes (estimated to be 50 to 75 μin.) may have been sufficiently great to have influenced adversely the stabilization attempt.

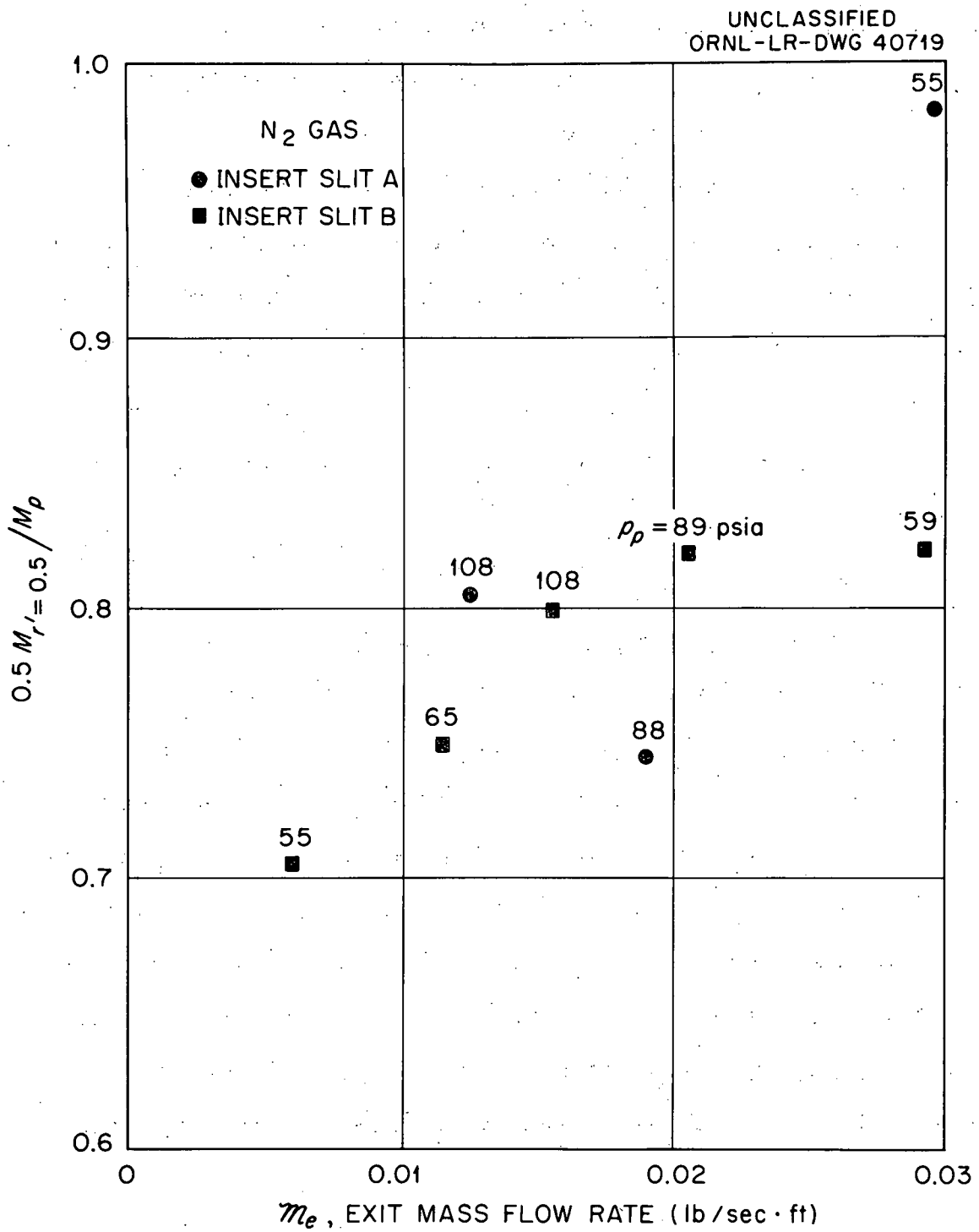

Fig. 24. Mach Number Ratio, $0.5\,M_{r'=0.5}/M_p$ vs. Exit Mass Flow Rate; 2.0-in. Dia Tube, Uniform Wall Bleed, $M_i < 1.0$, Tube No. 4.

Figure 25 illustrates the effect for a typical run with an injection mass flow rate of Freon equal to twice that of nitrogen which was supplied to generate the vortex. The upper curve is the measured Mach number profile for Freon injection, under the conditions indicated. The lower curve is for uniform wall injection of nitrogen at a wall pressure, p_p, such that the tangential Reynolds number at the tube periphery, as defined on page 10, is the same as for the case of Freon injection. In order to correct for the fact that the effective jet input power was lower for nitrogen injection, the basis of plotting for comparison purposes is M/M_j. M_j, incidentally, was calculated from the measured inlet flow rate, the measured wall pressure, the estimated gas temperature leaving the injection slit,* and the known slit area.

It is apparent from the figure that, when compared at equal tangential Reynolds numbers, heavy gas injection caused an increase in the value of M_p/M_j by about 35%, but the ratio $0.5\ M_{0.5}/M_p$ decreased by approximately 15%. Thus, some reduction in turbulent shear at the wall, where the density and viscosity gradient are favorable, may have been produced.

C. Wall Cooling

Density and viscosity gradients in the boundary layer which are favorable for stabilization can be produced by cooling the wall relative to the gas. Based on available information (16), it is estimated that the ratio of the adiabatic wall temperature, T_w, to that of the gas near the wall, T_p, should be less than 0.7 for a significant effect. Such temperature ratios were achieved in an experiment which employed

*Assuming isentropic expansion; for $M_j \leq 1.0$, the temperature correction is less than 10%.

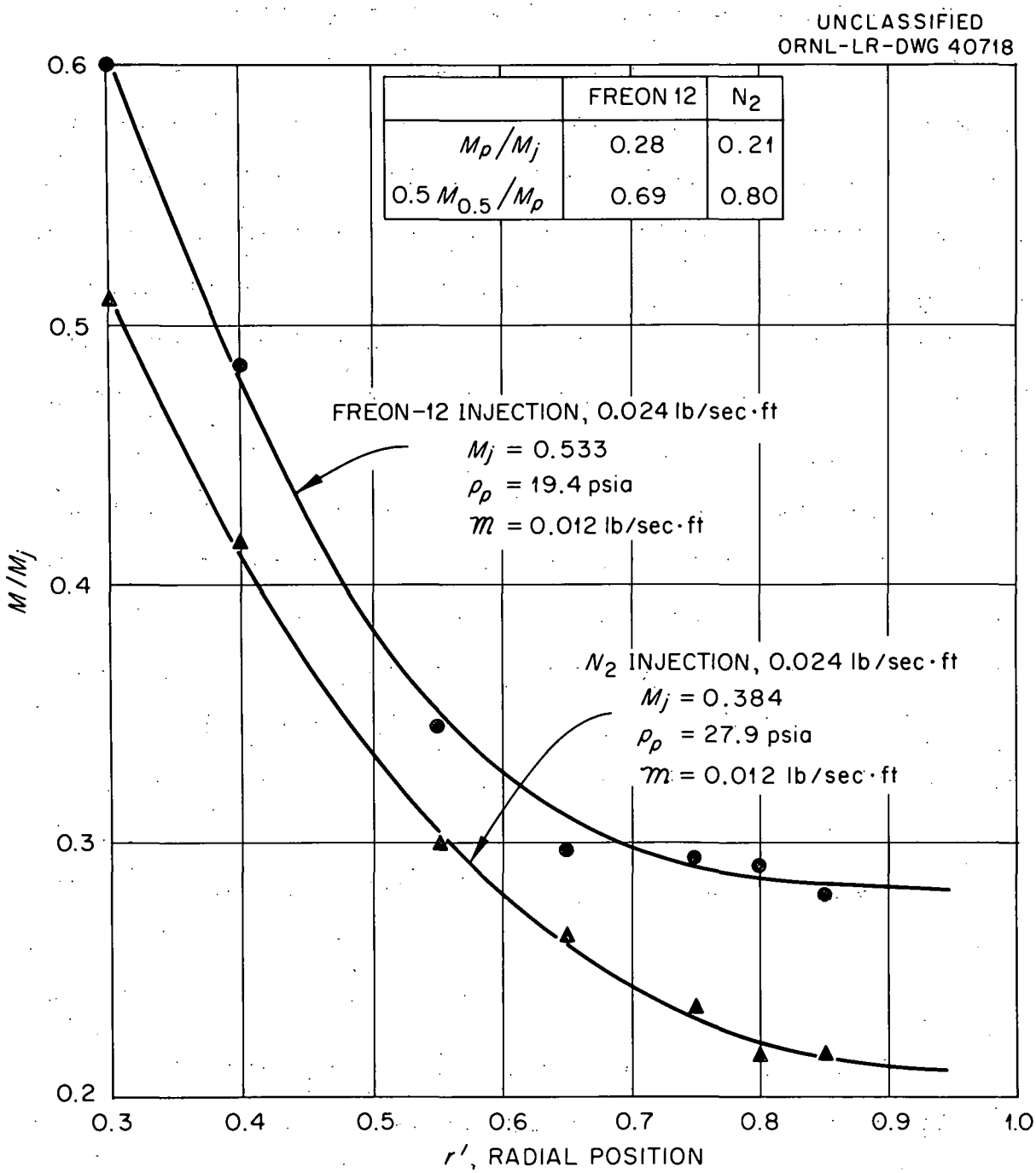

Fig. 25. Effect of Uniform Wall Injection on Mach Number Profile: Basis of Comparison, Equal Tangential Reynolds Numbers; 2-in. Dia Tube No. 4 B.

liquid nitrogen under nucleate boiling conditions (atmospheric pressure) to cool the wall of 0.64-in.-dia vortex tube No. 5. Nitrogen gas was introduced into the tube at about 10°F, and the gas leaving the tube was at a total temperature of -245°F. Measurements without cooling showed a 10°F drop in total temperature from the outer wall to the center of the tube. Assuming this value to obtain also with cooling, the temperature of the gas near the wall was estimated to vary from +10°F at the points of gas injection of -235°F elsewhere. The inside wall temperature was approximately -300°F. Thus the ratio T_w/T_p was estimated to vary between 0.34 and 0.71, depending on the circumferential position.

The upper curve in Fig. 26 is the Mach number profile obtained with wall cooling under the conditions described. The lower curve was obtained with no cooling, and at a pressure such as to give the same tangential Reynolds number at the tube periphery. The jet input power was the same for both runs; consequently, no correction for the differences in M_j was required. Note that wall cooling produced an increase in M_p of about 40%, with a decrease in the ratio $0.5\ M_{0.5}/M_p$ of only 4%. Apparently some reduction in wall shear was effected as was observed also with heavy gas injection.

III. Experiments with Axial Bleed-Off

An alternate method of removing the excess mass flow so that the allowable radial exit flow is not exceeded consisted in bleeding gas off axially at a radial position between the tube center and periphery. This was conveniently done by means of an annular ring of orifice holes drilled

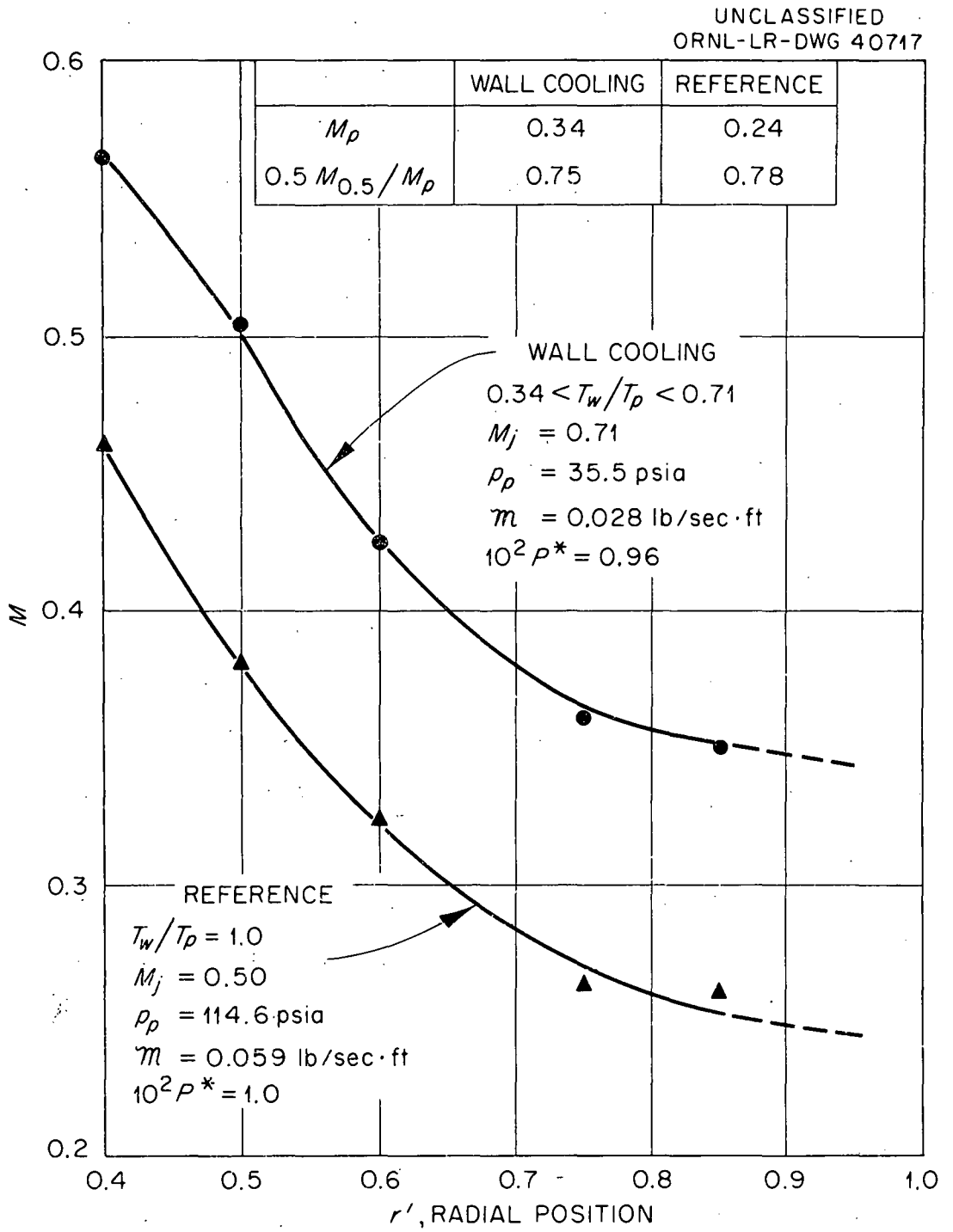

Fig. 26. Effect of Uniform Wall Cooling on Mach Number Profile: Basis of Comparison, Equal Tangential Reynolds Number; 0.64-in. Dia Tube No. 5.

in the exit end plate. Figure 27 compares two Mach number profiles in 1.0-in.-dia vortex tube No. 3-A operating with supersonic injection, $M_j^* = 2$. The solid curve applies to a run wherein gas was bled off axially at radial positions, $r' = 0.5$ and $r' = 0.8$, as indicated. The net bleed ratio was 13.5. The dashed curve was obtained with no bleed-off and at a lower inlet mass flow rate.

Figure 28 is a comparison of axial bleed-off and uniform wall suction, obtained with 2-in.-dia tube No. 4-A, $M_j \leq 1.0$. Mach number profiles are plotted for axial bleed-off at $r' = 0.6$, $R_B = 4.2$, and at $r' = 0.975$, $R_B = 1.6$. Also shown is a profile obtained with uniform wall bleed, $R_B = 1.5$, and a reference profile obtained without bleed-off.

The axial bleed data are summarized in Table II. Note that in the 1.0-in.-dia tube with supersonic injection, bleeding axially resulted in a decrease in $0.5\ M_{0.5}/M_p$ of 15% for a decrease in $\mathcal{M}_e$ by 7.5. In the 2.0-in.-dia tube with sonic injection, the maximum decrease in the ratio is 7% for a decrease in $\mathcal{M}_e$ by 2.3. The value of M_p/M_j was not appreciably affected by axial bleed-off when compared at equal values of $\mathcal{M}_i$ and p_p. It is concluded that axial bleed-off and uniform wall bleed may both be effective means for removing the excess mass flow in vortex reactor application.

IV. Geometrical Effects

A. Tube Diameter

Experiments were performed with 0.64-, 1.0-, and 2.0-in.-dia vortex tubes. Figure 29 summarizes the diameter effect for effective jet input power, $10^2\ P^*$, of 1.0 and 3.1 lb/sec·ft, and for wall pressures, p_p, of 89 and 108 psia. The plotted values of M_p have been adjusted slightly

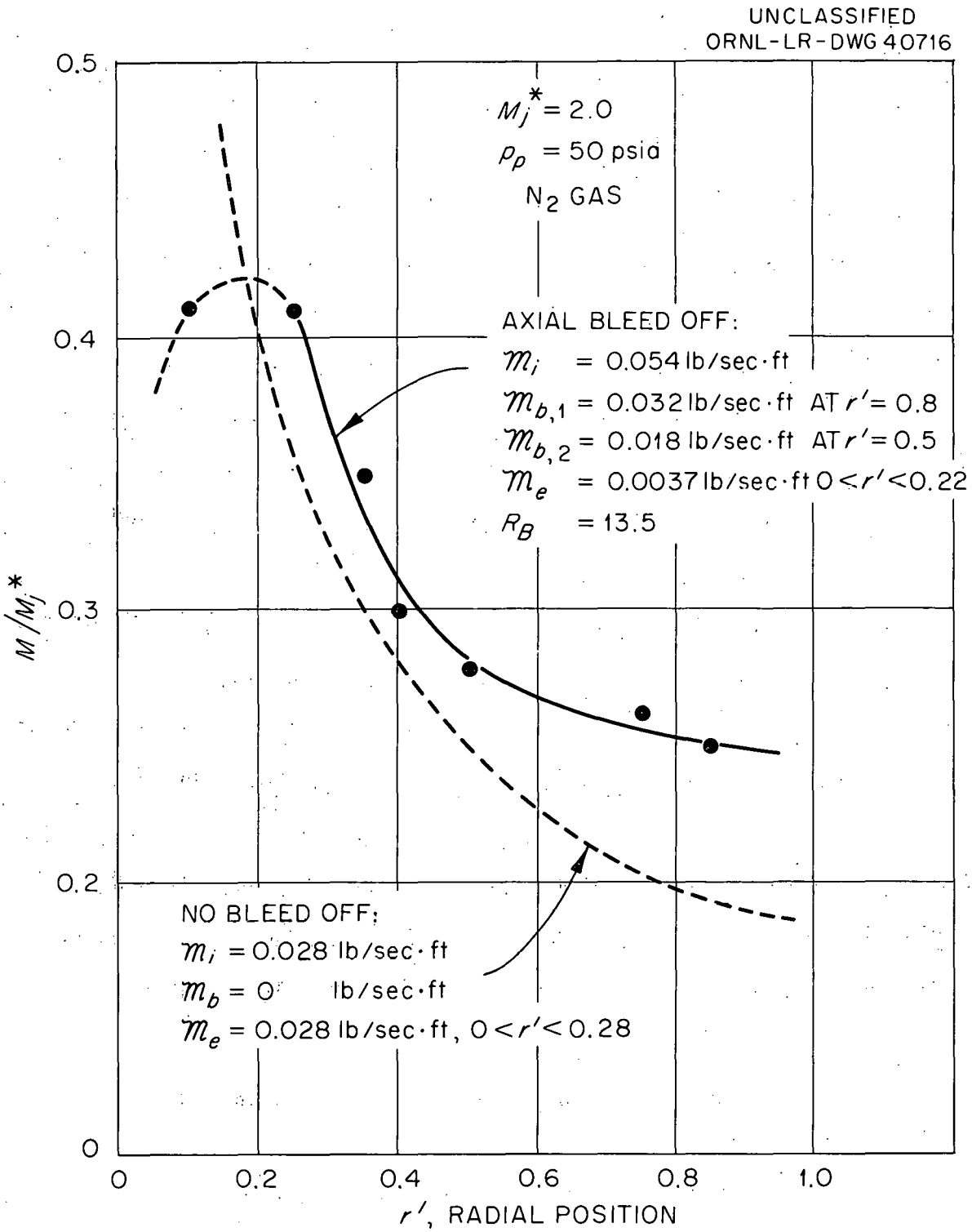

Fig. 27. Effect of Axial Bleed-off on Mach Number Profile for 1-in. Dia Vortex Tube No. 3 A.

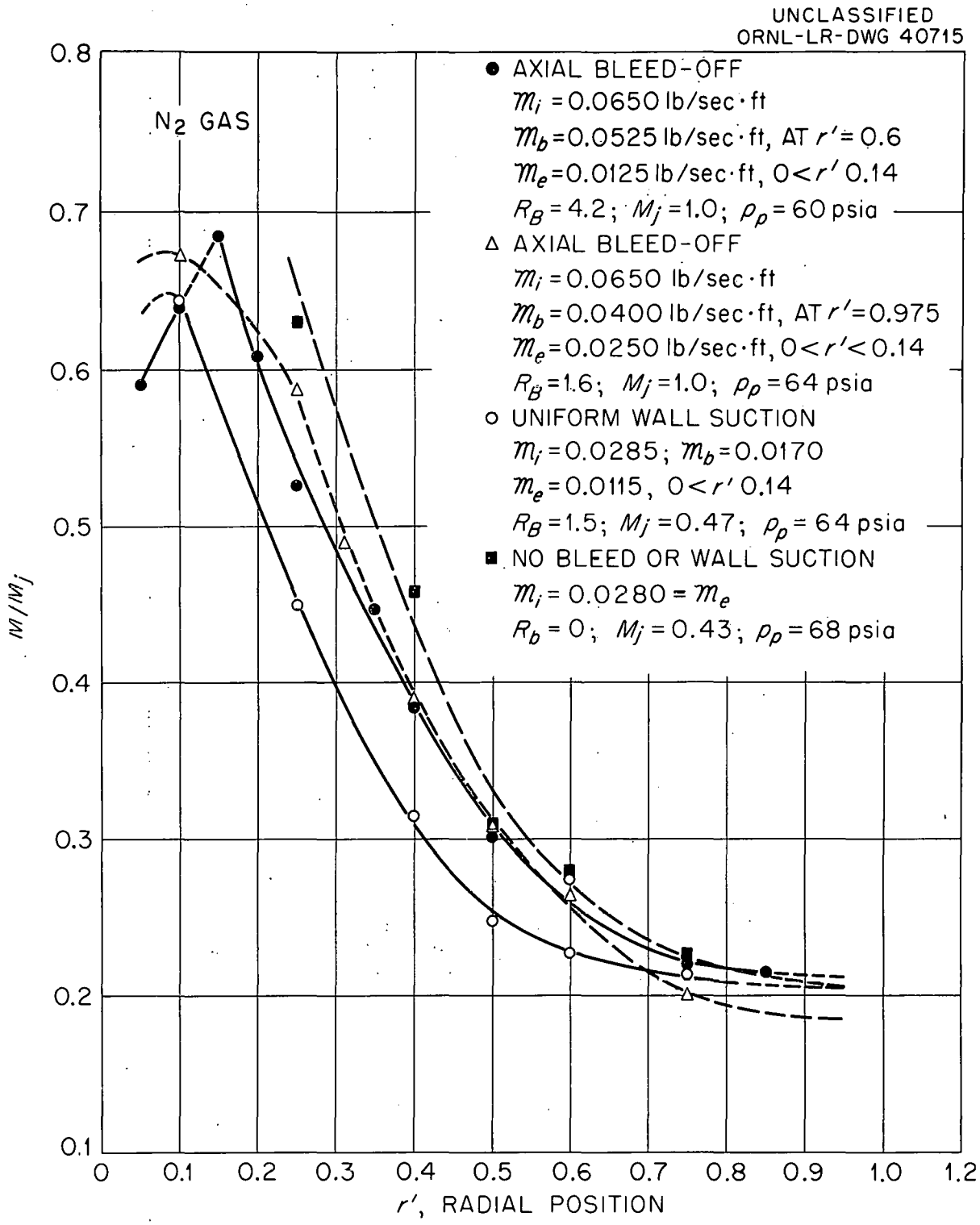

Fig. 28. Effect of Bleed-off on Mach Number Profile for a 2-in. Dia Vortex Tube; Comparison of Axial Bleed-off and Uniform Wall Suction; Tube No. 4 A.

TABLE II. SUMMARY OF AXIAL BLEED-OFF DATA

Tube No.	Tube Diameter, (in.)	$\dot{m}_i$ (lb/sec ft)	$\dot{m}_e$ (lb/sec ft)	Bleed Position, r'	R_B	M_j'/M_j^*	p_p (psia)	$M_p/M_j'/M_p/M_j^*$	$\frac{0.5\, M'_{r=0.5}}{M_p}$
3A	1.0	0.0540	0.0037	0.800, 0.500	13.5	2.0	50	0.25	0.57
4A	2.0	0.0650	0.0125	0.600	4.2	1.0	60	0.21	0.74
4A	2.0	0.0650	0.0250	0.975	1.6	1.0	64	0.18	0.84
3A	1.0	0.0280	0.0280	No Bleed (Reference)	0	2.0	67	0.185	0.67
4A	2.0	0.0285	0.0285	No Bleed (Reference)	0	0.43	50	0.20	0.80

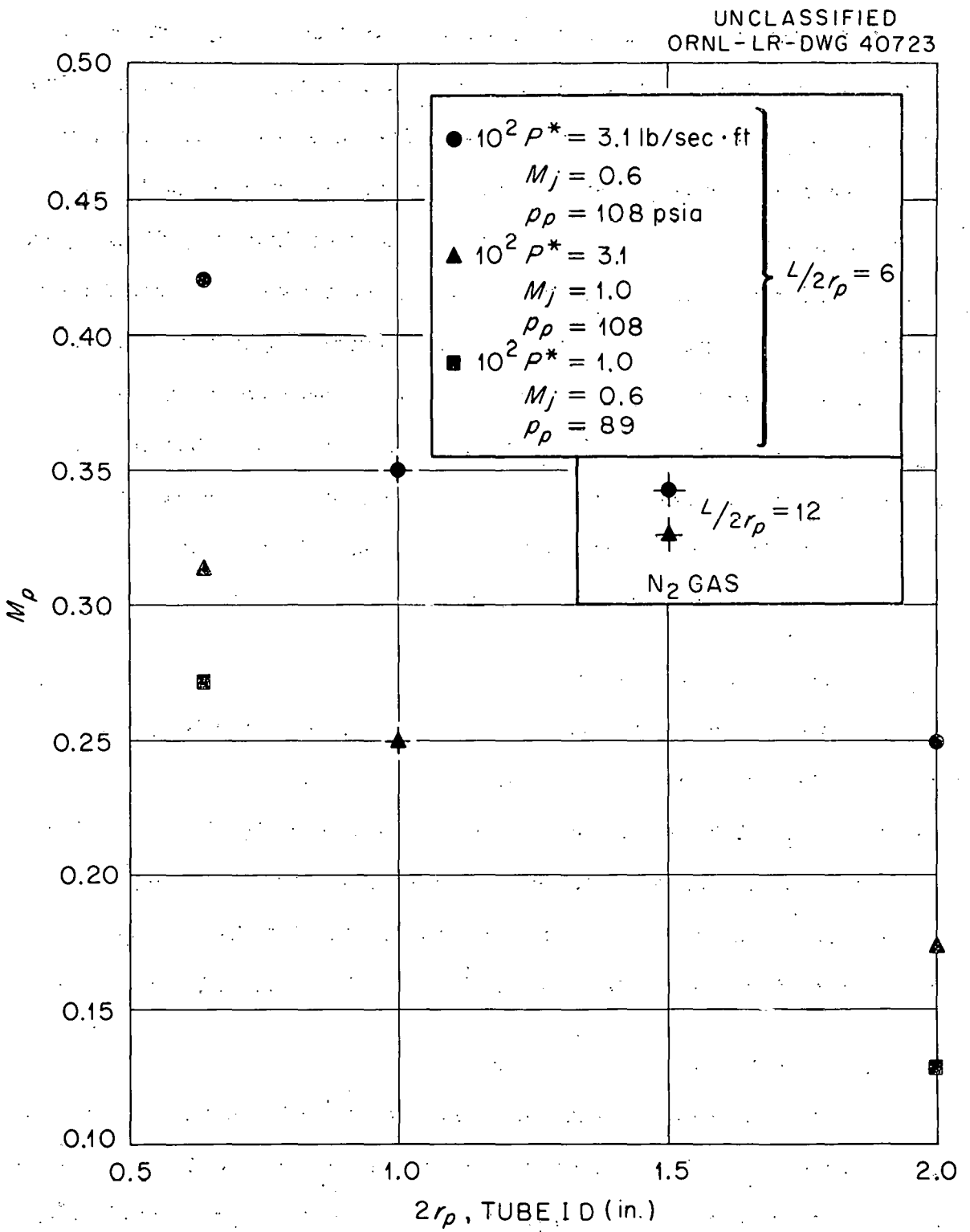

Fig. 29. Dependence of Peripheral Mach Number on Tube Diameter; Data Adjusted to Constant M_j.

from the experimental values to allow for variation in M_j from point to point. The two reference values of M_j chosen are 0.6 and 1.0. Note that the value of $\ell/2\ r_p$ for the 1.0-in.-dia tube was twice that for the other tubes; however, as indicated in Fig. 30, the length/diameter effect appears to be very small. It is concluded from Fig. 29 that, at a given effective input power and pressure, decreasing the tube diameter results in a significant increase in Mach number. Specifically, reduction in tube diameter from 2.0 in. to 0.64 in. produced an increase in M_p by a factor of 1.7 to 2.1. This occurred most likely because of decrease in tangential Reynolds number with resulting decrease in turbulent viscosity. The effect of tube diameter will also be evident in several of the data plots to be discussed in later sections.

B. Length-to-Diameter Ratio

The measurements of this effect were obtained using 0.63-in.-dia tube No. 3-B, and are shown in Fig. 30, where the value of M_p is corrected to $M_j = 0.6$ as discussed in connection with Fig. 29. No effect of length on the corrected M_p value was evident, over the range of $\ell/2\ r_p$ from 5 to 18. This is an indication that the flow is essentially two dimensional, as is assumed in the theorectical derivations.

C. Radial Position of Gas Injection

The best comparative data are those for tube No. 4 with continuous injection at $r_a' = 1.0$ (insert slit A) and at $r_a' = 0.92$ (insert slit B). As Fig. 31 indicates, slit B produced values of M_p/M_j about 45% higher than slit A. A similar result was found for nozzle injection, from which it is concluded that the injection radius ratio, r_a', should not

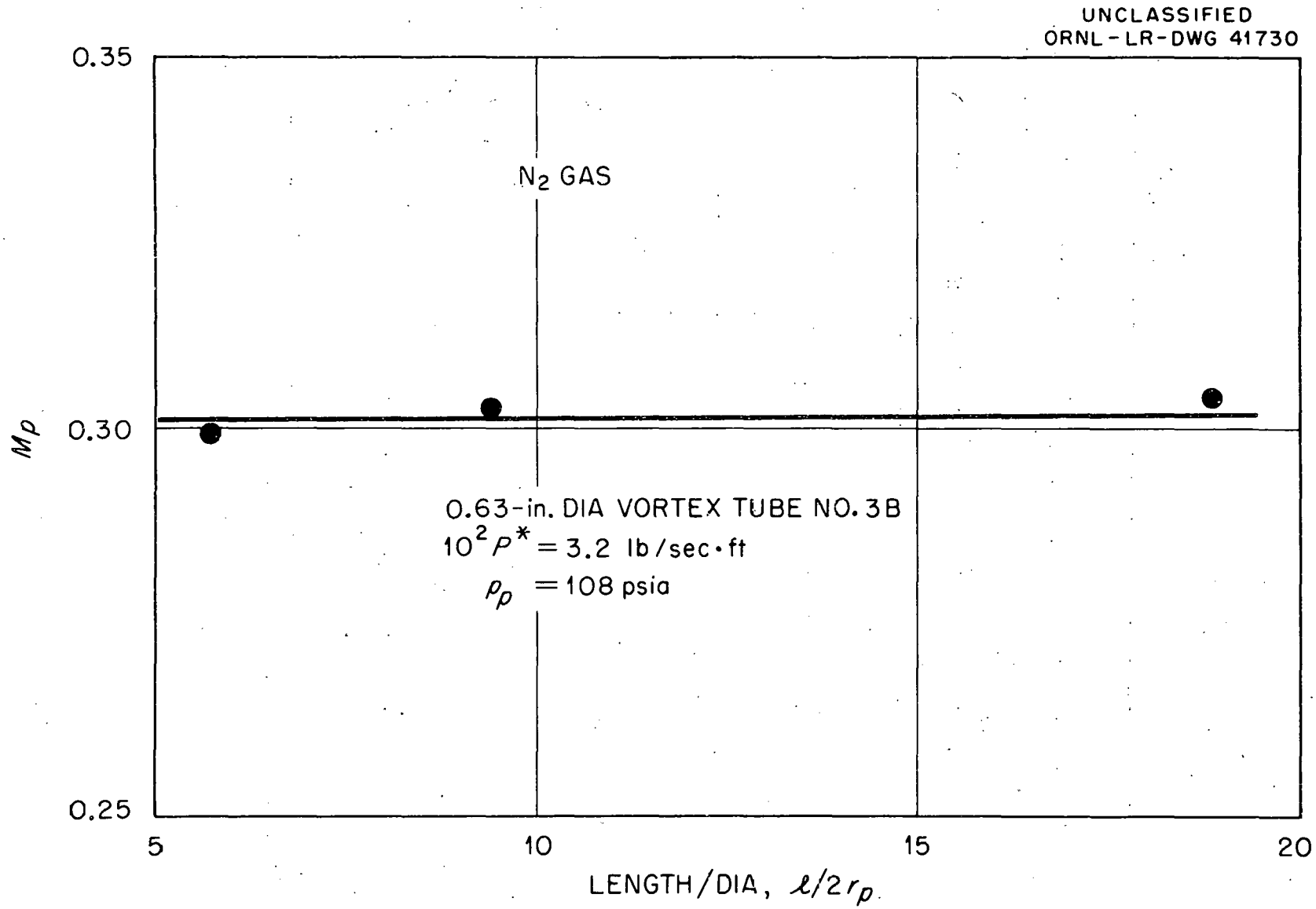

Fig. 30. Dependence of Peripheral Mach Number on Length/Dia. Ratio-Corrected to $M_i = 0.6$.

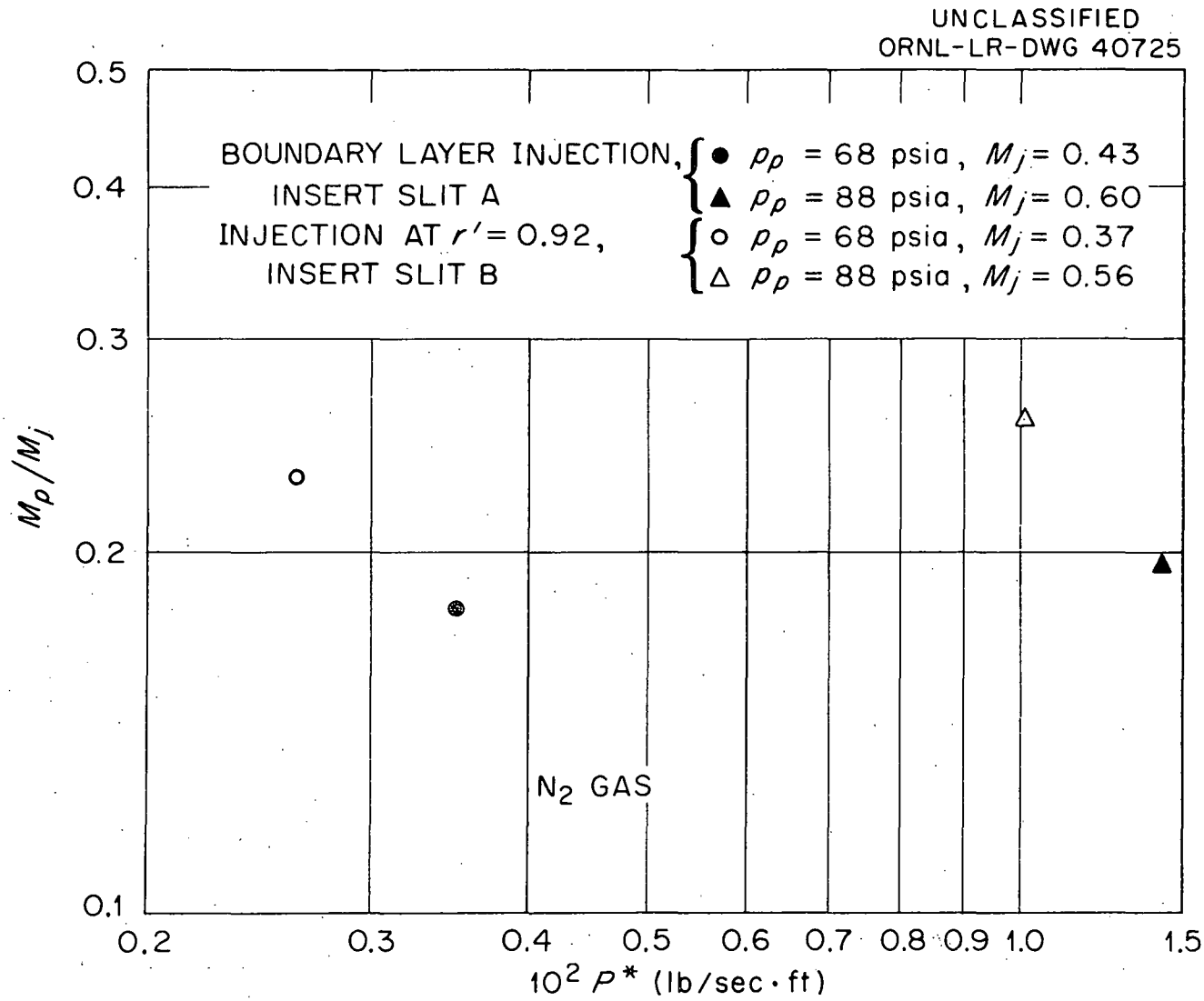

Fig. 31. Comparison of Peripheral to Jet Mach Number Ratio for Two Injection Slit Positions: Tube No. 4.

exceed 0.95; data obtained with $r_a' < 0.85$ also showed inferior performance. r_a' values of 0.90 to 0.92 appear to be near optimum.*

V. Experimental Investigation of the Effects of Important Flow and System Variables

A. Mass Flow Rate per Unit Tube Length

From a comparison of data for sub- and supersonic injection, the following observations can be made:

1. Jet effectiveness ratios M_p/M_j and M_p/M_j^* increased with mass flow rate at constant tube wall pressure.
2. Jet effectiveness ratios were greater by a factor of about two for 0.6-in. tubes as compared with 2.0-in. tubes at equal $\dot{m}$ and p_p, for both sub- and supersonic injection.
3. The ratios for subsonic injection were from two to three times greater than for supersonic injection, for a given tube diameter, mass flow rate, and pressure.
4. With subsonic injection, values of the ratio as high as 0.60 were observed.

Values of the Mach number ratio $0.5\ M_{0.5}/M_p$ which characterizes the deviation from a potential velocity distribution scattered more or less randomly when plotted against mass flow rate; the actual values of the ratio ranged from 0.66 to 0.98. Consequently, the velocity distributions in the vortices generated were closer to that of a free vortex than to

*From shadow observations of Freon-12 injection, it was found that the jet of gas entering the vortex tube was deflected 12 to 20 deg from the axis of the nozzle, due to the angular contour of the nozzle exit. This results in an effective reduction in inlet jet radius.

that of solid body rotation, as was concluded also in ref 3.

B. Jet Injection Velocity

The effect of injection Mach number is illustrated in Fig. 32 which shows that the ratio decreases monotonically with increasing jet velocity for constant tube diameter, effective jet input power, and wall pressure.* It is concluded from these data that the more closely the jet velocity matches the tangential velocity at the point of jet entry, the more effective is the utilization of the jet energy in producing rotation, since less of the energy is dissipated in slowing down the jet.

C. Effective Jet Input Power

This quantity, defined by Eq. 1, appears to correlate the combined effect of mass flow rate and injection velocity. M_p is plotted against P^* in Fig. 33 for three tube diameters. The lines drawn for 0.6-in. and 2.0-in.-dia tubes connect points of constant wall pressure. These data indicate that M_p increases with P^* to approximately the 0.42 power when no correction is made for variation in M_j; if there were complete conversion of the inlet jet kinetic energy to tangential kinetic energy, M_p would vary with P^* to the 0.5 power. A peripheral Mach number of 0.49 was measured in 0.64-in.-dia tube No. 5 at a wall pressure 83 psia, $M_j = 0.9$, and an effective power input of 4.4×10^{-2} lb/sec·ft. The data also indicate that to achieve the same M_p in a 2.0-in.-dia tube at the same wall pressure requires increase in P^* by a factor of about 3.5.

*Constant jet input power with increasing M_j is obtained by decreasing $\dot{m}$.

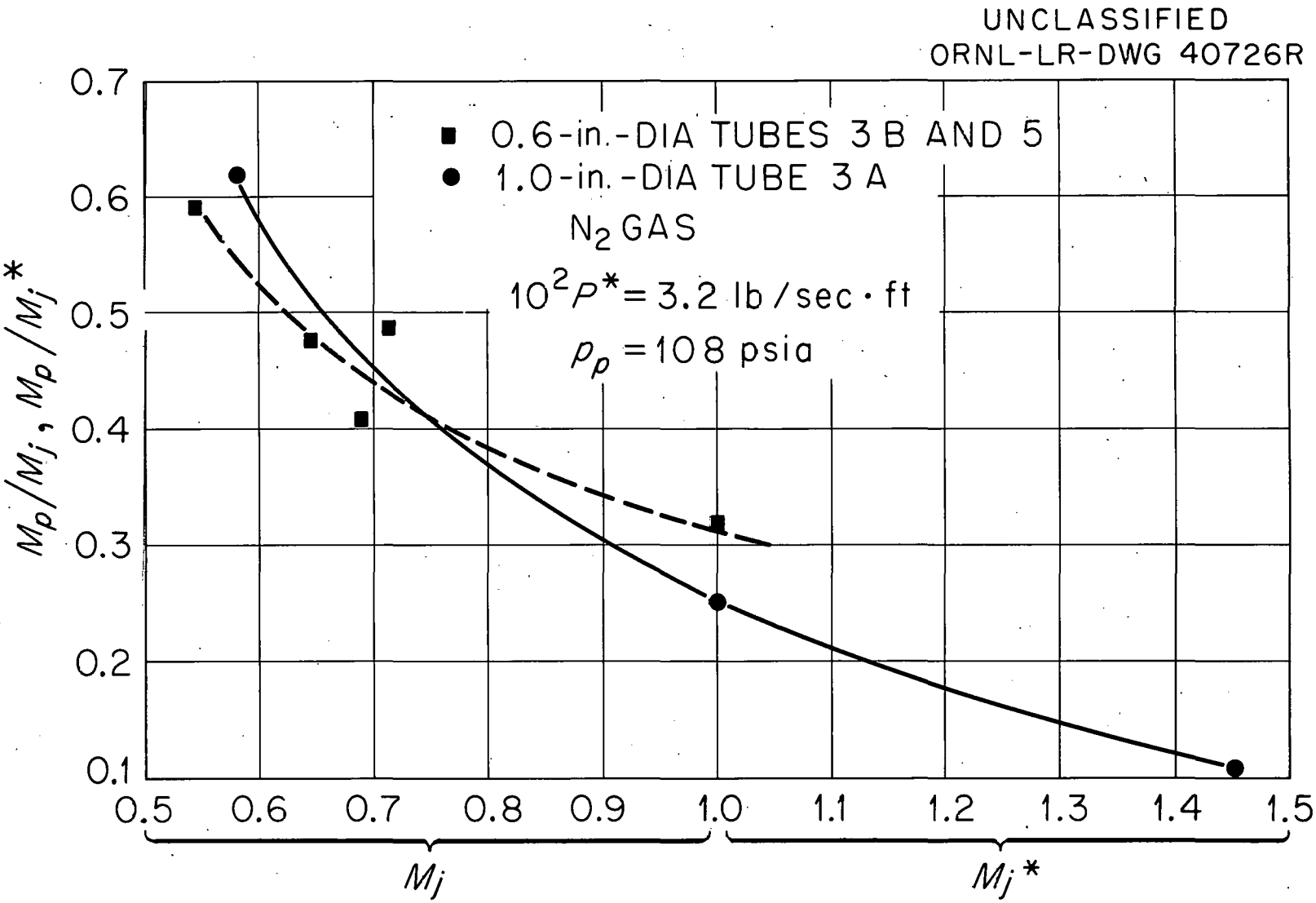

Fig. 32. Variation of Ratio of Tangential to Jet Mach Number with Jet Mach Number.

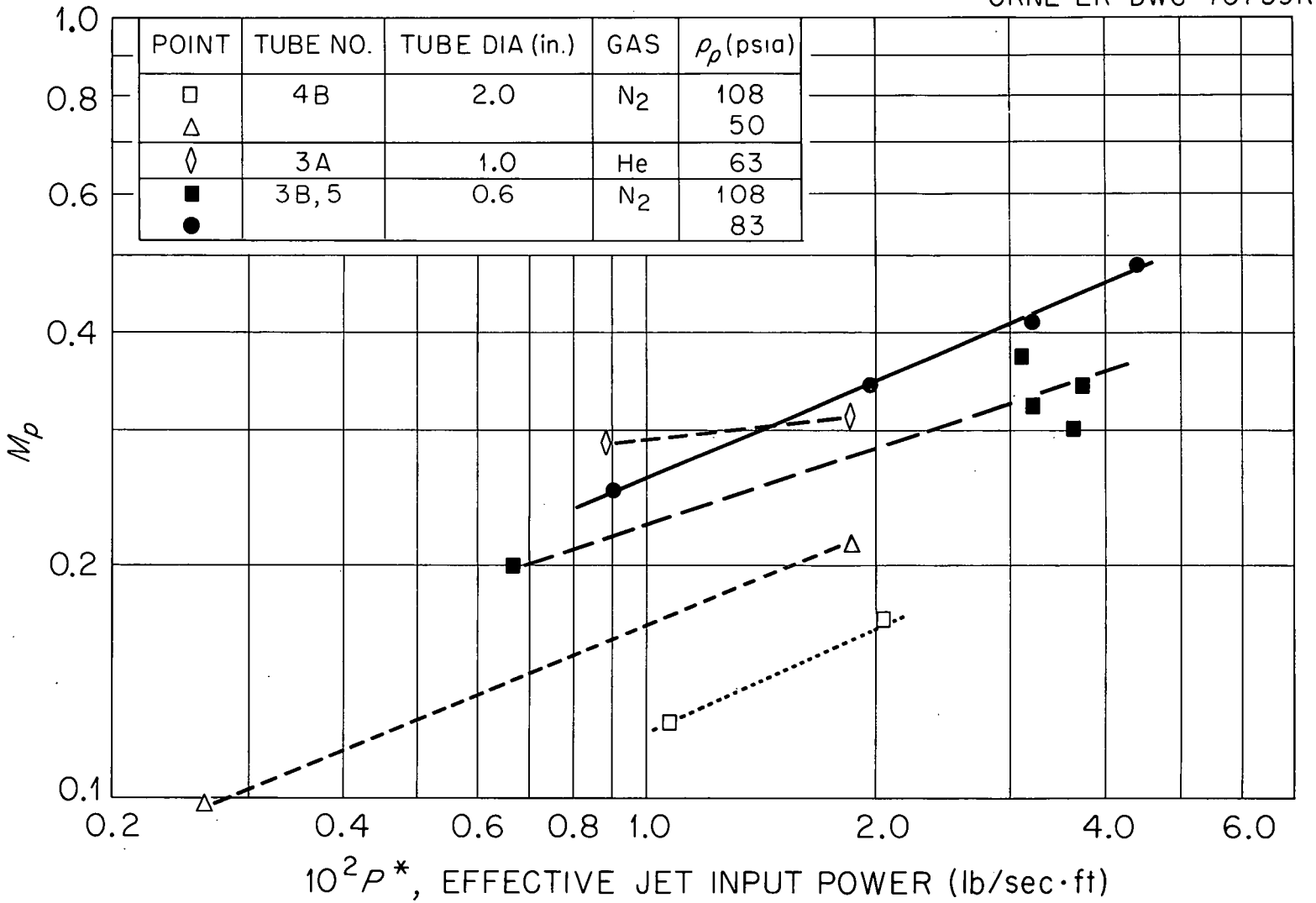

Fig. 33. Dependence of Peripheral Mach Number on Jet Input Power for 0.6, 1.0 and 2-in. Dia Tubes; N_2 and He Gas; Subsonic Injection.

D. Wall Pressure

Increasing the wall pressure, p_p, increases the tangential Reynolds number and, as will be shown, the virtual viscosity increases. Thus, it is not unexpected that the peripheral Mach number decreased with increasing p_p, as illustrated in Fig. 33. A value of $M_p = 0.5$ was obtained in a 0.6-in.-dia tube a $p_p = 20$ psia, $10^2 P^* = 2.1$. To obtain the same Mach number at 83 psia, for example, required an increase in the effective jet input power by approximately a factor of two. This is also illustrated in Fig. 34 which is a plot of P^* versus p_p for 0.6-in.-dia tubes at several fixed values of M_p.

E. Peripheral Tangential Reynolds Number

This parameter is defined as the product of tube diameter, tangential velocity at the tube periphery, and density at the tube periphery, divided by absolute viscosity:

$$N_{Re_{t,p}} = \frac{2 r_p v_{t,p} p_p m_1}{\mu_p R T_p} .$$

Peebles and Garber (17) found this definition to be valid for vortex flow in a sphere, and the Reynolds number so defined should be an important similitude parameter. To test this hypothesis, a summary performance chart was constructed with the effective jet input power as a function of Reynolds number for data of 64 runs, including tube diameters of 0.6, 1.0, and 2.0 in., nitrogen and helium gas. Figure 35 is such a chart. The observed range in M_p of from 0.11 to 0.50 is divided into seven subranges for convenience. The lines fanning out from the origin represent linear approximations to the data for each

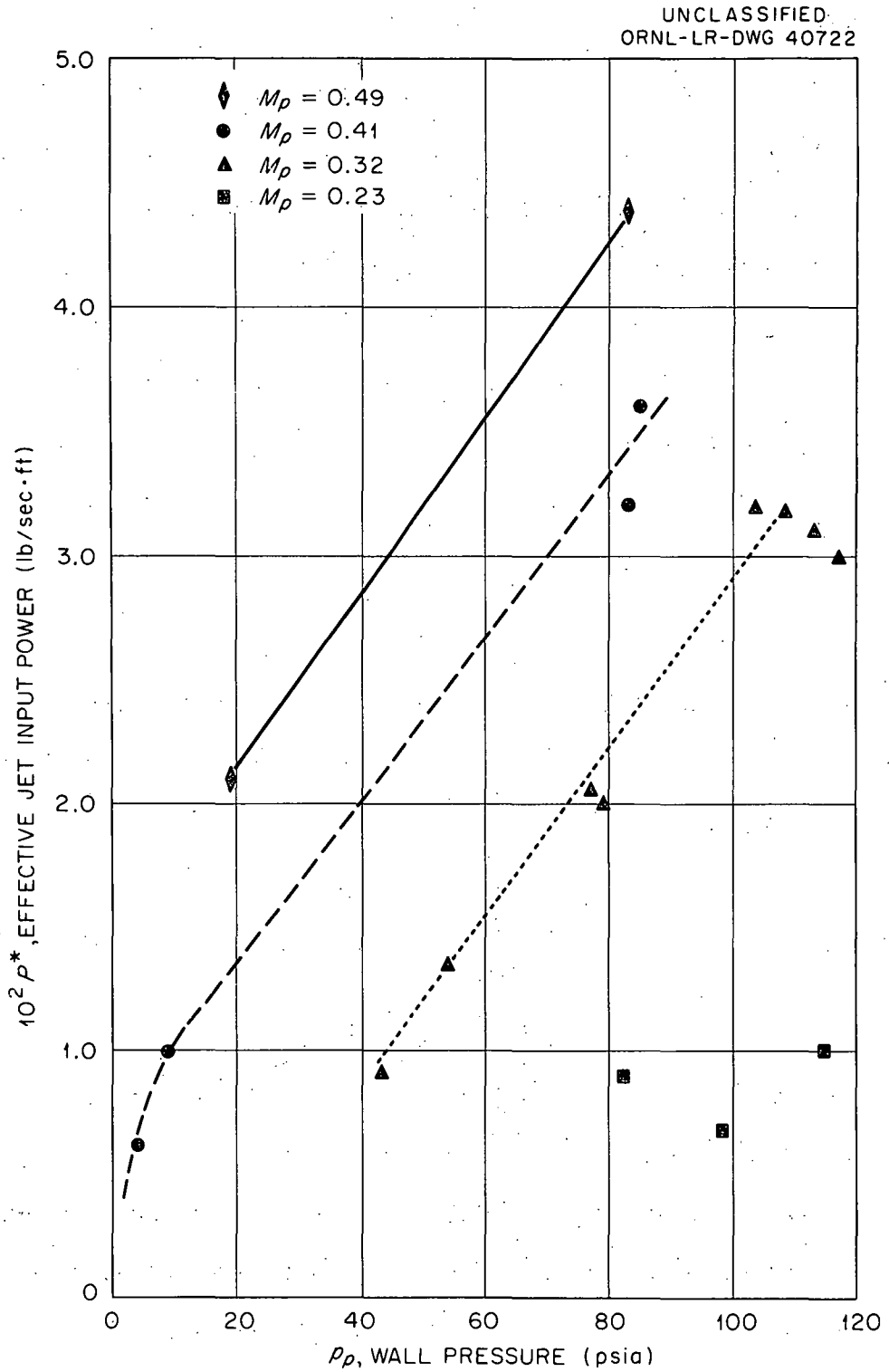

Fig. 34. Performance Characteristics of 0.6-in. Dia Vortex Tubes Jet Input Power vs. Wall Pressure.

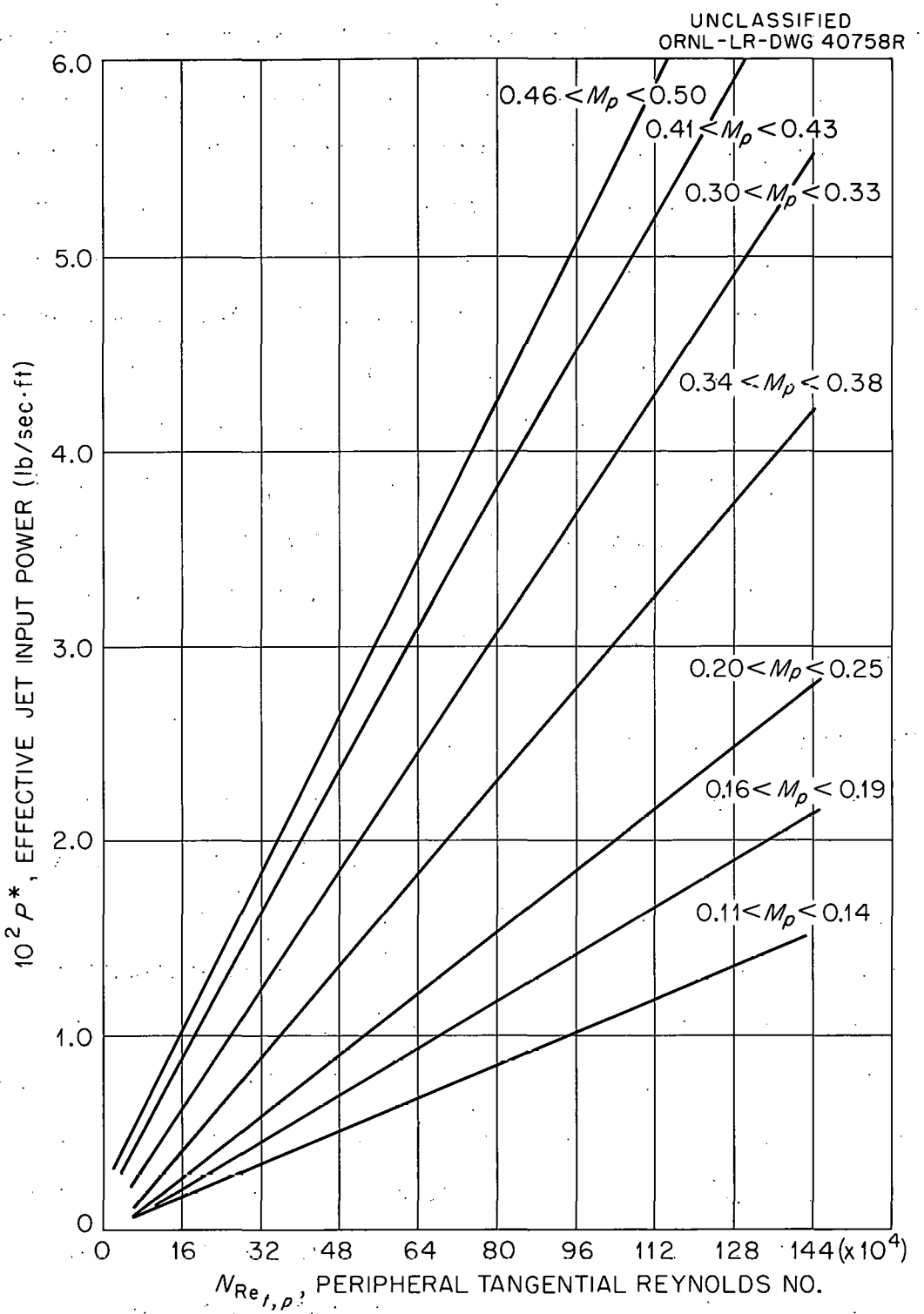

Fig. 35. Vortex Tube Performance Characteristics Summary Plot: Peripheral Tangential Reynolds No. vs. Jet Input Power. Linear Fit to Data for 0.6, 1.0 and 2-in. Dia Tubes; N_2 and He Gas.

Mach number range; the data cover Reynolds numbers from 4×10^4 to 1.6×10^6. It is inferred from the chart that to maintain constant tangential Mach number with increase in Reynolds number requires an approximately proportionate increase in input power. A discrepancy in the results is apparent for $0.30 < M_p < 0.38$, since at constant $N_{Re_{t,p}}$, increasing P^* causes a decrease in the observed M_p, whereas outside this range the expected increase with P^* is found. More precise measurements are needed to resolve this discrepancy. Nevertheless, it may be generally concluded from the chart that to achieve high tangential Mach numbers at Reynolds numbers of practical interest, say $N_{Re_{t,p}} \geq 1.0 \times 10^6$, will require large input power unless some means can be found for effective suppression of turbulence.

VI. Determination of Virtual Viscosity

It has been suggested that failure to achieve higher vortex strengths is due to turbulence which increases the effective viscosity and thus the shear drag. From velocity data obtained in two-dimensional vortex flow, estimates of the virtual viscosity, μ^*, can be made by application of Eq. 6, which relates the ratio $r' v_t/v_{t,p}$ to $A = \mathcal{M}/2\pi\mu^*$ and the exit radius, r_e'. This equation is plotted as Fig. 42 in the Appendix. Sixty-four runs were analyzed by determining A and hence μ^* from the observed ratio $0.5\ v_{t,r'=0.5}/v_{t,p}$.* Three tube diameters (0.6, 1.0, and 2.0 in.) and two gases (nitrogen and helium) were represented. Mass flow rates covered by the data ranged from 0.012 to 0.13 lb/sec·ft, jet Mach numbers from 0.2 to 1.0, tube wall pressures from 2.5 to 120 psia, and effective jet input powers

*The value of μ^* so determined actually represents an average value over the range $0.5 < r' < 1.0$.

from 0.2×10^{-2} lb/sec·ft to 5.0×10^{-2} lb/sec·ft. No runs involving bleed-off, injection, or wall cooling were included, however, nor were any data included for supersonic injection.

The combined results for all three tube sizes are summarized in Fig. 36 with the ratio of virtual viscosity to molecular viscosity plotted against peripheral tangential Reynolds number. The least-squares line is also shown. Note that at the lowest Reynolds number, 4×10^4, the experimental virtual viscosity is already thirty times the molecular viscosity, and at the highest Reynolds number, 1.6×10^6, the ratio is increased to nearly 700. Thus, the conclusion that the flow is turbulent appears well founded. The data of Peebles (17) indicates similarly high values of μ^* for aqueous vortices.

Table III is a summary of the results of linear regression analyses* of all data combined, as plotted in Fig. 36, and also of the data for the 0.6-, 1.0-, and 2.0-in.-dia tubes separately. Note from the last two columns that only the 1.0-in.-dia data fails to correlate significantly at the 95% confidence level. The equations for the least-squares lines show variation in the Reynolds number exponent from 0.66 to 0.86, omitting the 1.0-in.-dia data from consideration. The value of 0.86 for the combined data is consistent with results of the Martinelli analogy (18) for turbulent pipe flow which predicts a variation in eddy thermal diffusivity with N_{Re} to the 0.9 power. The diffusivity in pipe flow is not constant with radius, however, as assumed in ref 6 for vortex flow.

Scatter of the points on the μ^*/μ versus $N_{Re_{t,p}}$ plot is shown by the wide 95% confidence bands calculated for the coefficients and exponents of the least-squares equations. The least scatter and highest degree of

*Linearized by plotting on log-log paper.

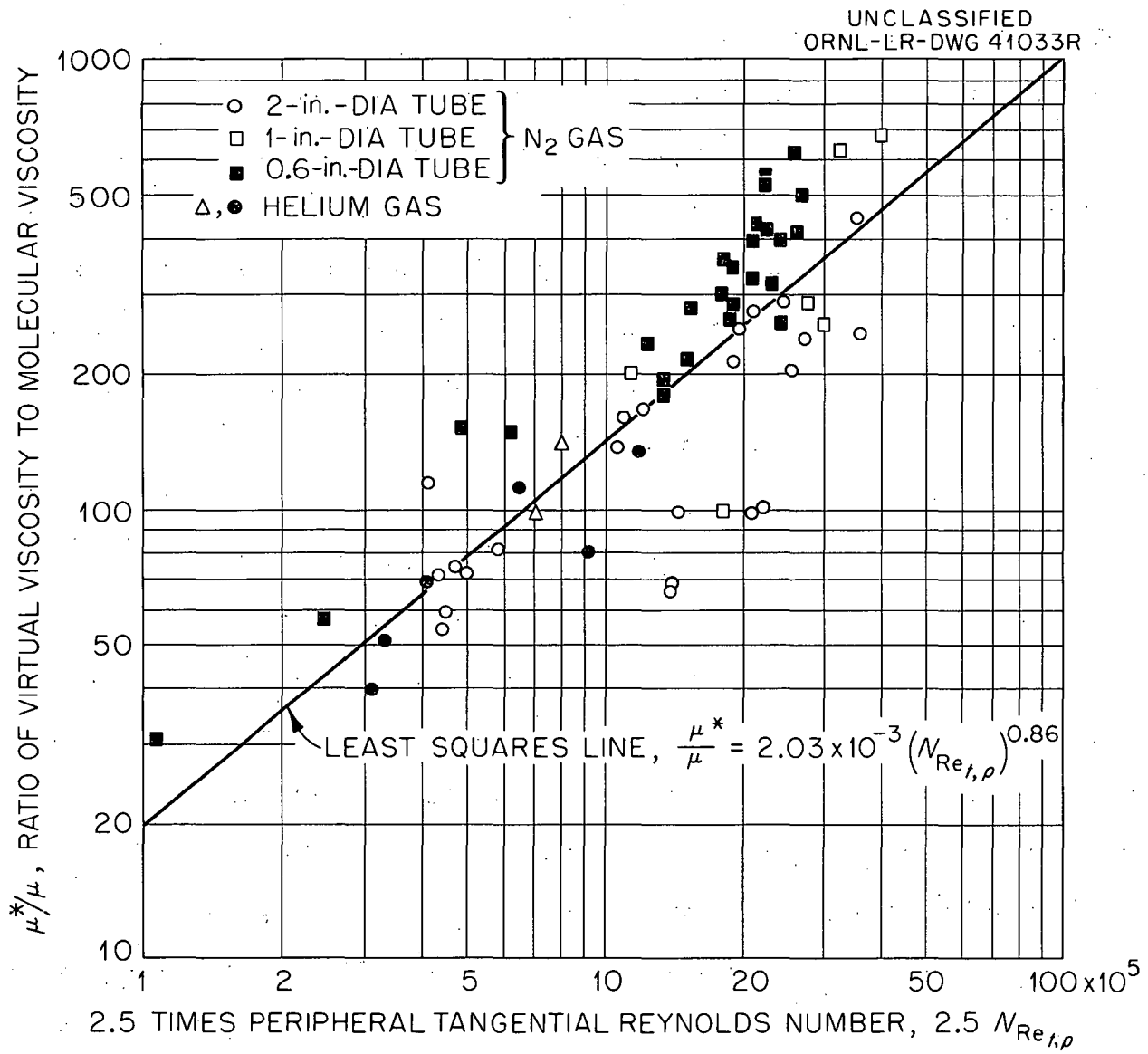

Fig. 36. Variation of Ratio of Virtual Viscosity to Molecular Viscosity with Peripheral Tangential Reynolds Number; 0.6, 1.0 and 2-in. Dia Tubes; N_2 and He Gas.

Table III. Summary of Regression Analysis

(μ^*/μ vs $N_{Re_{t,p}}$; Nitrogen and Helium Gas)

Description	Number of Observations	Equation of Least-Squares Line[a]	95% C. I. – Coefficient	95% C. I. – Exponent	Extrapolated Estimate of $(N_{Re_{t,p}})_{crit.}$	Correlation Coefficient of Data	Correlation Coefficient at 95% C. L.
0.6-, 1.0-, & 2.0-in.-dia tubes	64	$\mu^*/\mu = 2.03 \times 10^{-3} \left(N_{Re_{t,p}}\right)^{0.86}$	$+1.02 \times 10^{-3}$ -0.70×10^{-3}	±0.16	1300	0.81	0.25
0.6-in.-dia tubes only	26	$\mu^*/\mu = 5.25 \times 10^{-3} \left(N_{Re_{t,p}}\right)^{0.82}$	$+1.70 \times 10^{-3}$ -1.27×10^{-3}	±0.10	630	0.96	0.39
1.0-in. dia tubes only	8	$\mu^*/\mu = 1.2 \times 10^{-3} \left(N_{Re_{t,p}}\right)^{0.90}$	very large	very large	---	0.12	0.71
2.0-in.-dia tubes only	30	$\mu^*/\mu = 22 \times 10^{-3} \left(N_{Re_{t,p}}\right)^{0.66}$	$+16 \times 10^{-3}$ -9×10^{-3}	±0.23	340	0.74	0.36

[a]Linearized by log-log plot.

correlation were observed for the 0.6-in. tube diameter data.

The estimates of critical Reynolds number listed in the sixth column of the table were obtained by linear extrapolation of the least-squares lines (log-log plot) to a value $\mu^*/\mu = 1$. Because of the wide 95% confidence bands and the long extrapolation involved, little significance should be attached to the actual numerical values of the estimates; the general conclusion that the critical Reynolds number in vortex flow is quite low is probably valid, however. As a matter of fact, Peebles, from a theoretical analysis of boundary layer flow, found that the Reynolds number as defined in this report is the proper one to characterize vortex flow and, furthermore, postulated that the critical Reynolds number may be approximately 2,000. The results of this study lend support to Peebles' postulate.

VII. Separation Experiments

Preliminary separation studies reported in ref 3 were inconclusive, due in part to the possibility of condensation of the heavy trace gas which was injected through the nozzles along with the helium under conditions conducive to droplet formation. In order to eliminate such condensation, several runs were made with the heavy gas, C_8F_{16} ($m_2 = 400$), injected as a very dilute mixture with helium uniformily into the periphery of the vortex tube through a porous wall. Two-in.-dia tube No. 3 was employed. Descriptions of the sampling technique and gas analysis system are given on pages 33 – 37. The sample probe was introduced at the mid-point of the tube. To reduce the possibility of condensation due to the radial cooling effect, the mole-fraction of heavy gas at the concentration peak was limited to a value below saturation at the temperature which the gas would attain by isentropic expansion from

conditions at the periphery. Based on vapor pressure data for C_8F_{16} (19), the peak mole-fraction was maintained below 1 x 10^{-4} (100 ppm).

From an examination of Eq. 7, it is seen that the Mach number, M_m, at the radius of maximum mole-fraction varies directly as the square root of the exit mass flow, and inversely as the square root of the molecular diffusivity. In view of the small magnitude of the diffusivity of C_8F_{16} in helium near room temperature, Eq. 7 can be satisfied for values of M_m which are experimentally feasible only if the exit mass flow is low. Thus, it was necessary to resort to a system for bleeding off the excess flow. In four of the experiments reported here, bleed-off was axial; in one, a 0.017-in.-wide slit in the tube wall, extending the length of the tube, served for bleed-off.

Table IV summarizes the operating conditions and results for five typical separation runs. Note the large bleed ratios employed, and that injection was supersonic. Figure 37 illustrates separation profiles for runs 3 and 4, with the ratio of mole-fraction C_8F_{16} at r' to that at the tube wall plotted against the radial position, r', of the sample probe. Run 3 shows a distinct peak at $r_m' = 0.15$, with rapid drop off at lower radii, for axial bleed-off at $r' = 0.25$ and 0.40, $R_B = 15.6$. With bleed-off at $r' = 0.4$ and $R_B = 4.8$, run 4 shows a weaker peak at $r_m' = 0.17$. Increasing the bleed ratio to 17.5 resulted in slight outward shift of the peak position to $r_m' = 0.21$, as seen in Fig. 38. It must be understood that the observed intensities of peak formation may be appreciably weakened by the local influence of the probe itself, although the peak position may be only slightly altered.

UNCLASSIFIED
ORNL-LR-DWG. 40727

TABLE IV. SUMMARY OF OPERATING CONDITIONS AND RESULTS FOR SOME $He\text{-}C_8F_{16}$ SEPARATION EXPERIMENTS IN 2-in.-dia VORTEX TUBE No. 3

Parameter	Experiment Number				
	1	2	3	4	5
Inlet He Mass Flow Rate, $\mathfrak{m}_{1_i}$ (lb/sec ft)	0.028	0.030	0.023	0.013	0.030
Bleed Ratio, R_B	11.3	17.5	15.6	4.8	9.4
Inlet Jet Mach Number (Isentropic), M_j*	2.0	2.1	1.9	2.3	2.2
Exit Diameter, $2r_e$ (in.)	0.250	0.250	0.221	0.221	0.250
Bleed-Off Position, r'	0.40 (axial)	0.40 (axial)	0.25, 0.40 (axial)	0.40 (axial)	1.00 (wall slit)
Wall Pressure, p_p (psia)	55.6	53.0	56.3	40.8	40.8
Observed Mole-Fraction Peak Position, r_m'	0.15	0.21	0.15	0.17	0.11
Observed Mach Number at r_m', M_m	0.64	0.55	0.70	0.48	0.70
Observed Ratio of Exit Mole-Fraction to that at r_m', x_e/x_m			0.5		0.67
Calculated M_m (Eq. 10)			0.58		0.81
Ratio of Observed M_m to Calculated M_m			1.2		0.87

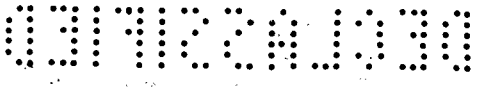

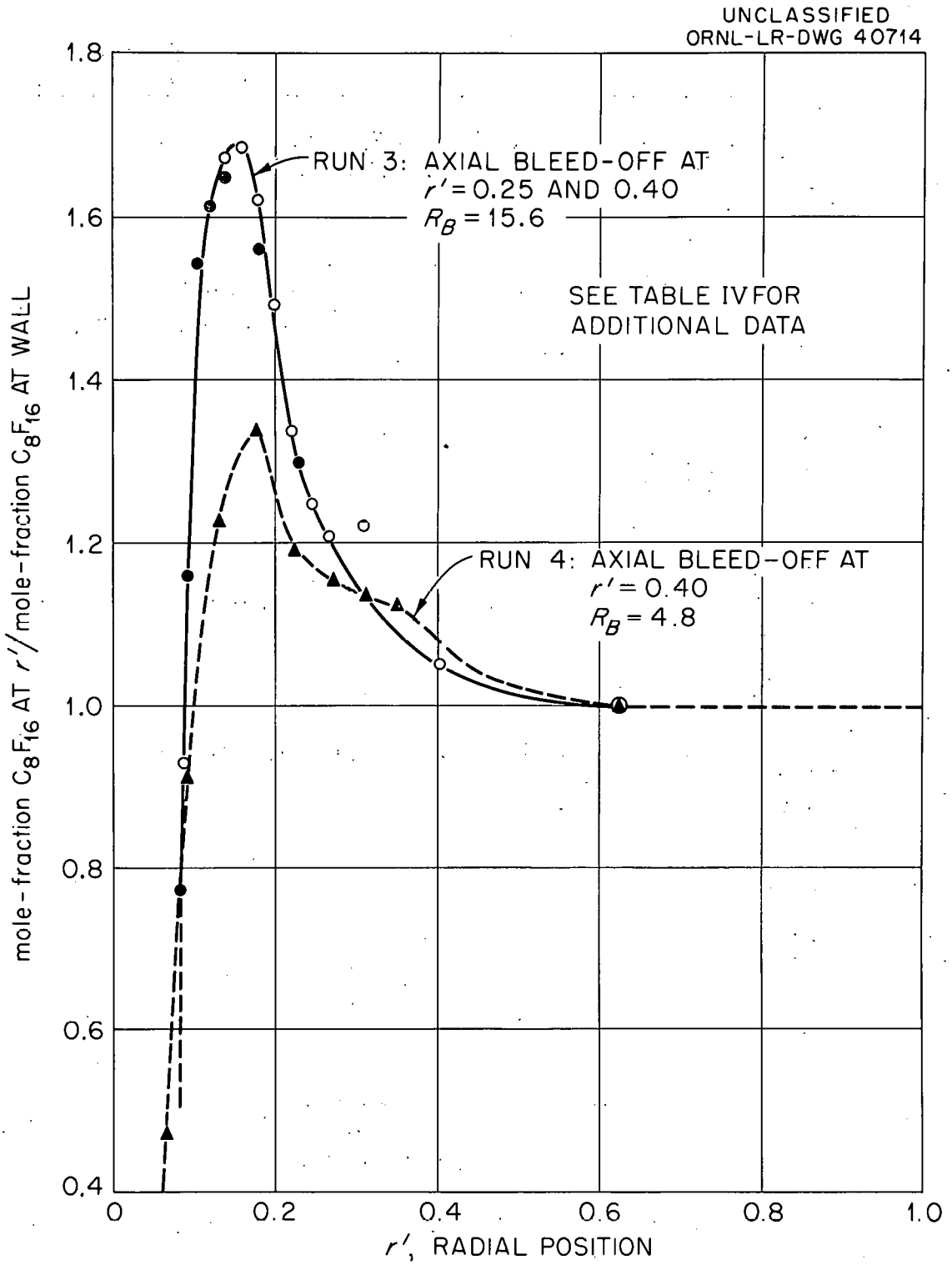

Fig. 37. Separation Profiles for He-C_8F_{16} Mixture in 2-in. Dia Vortex Tube No. 3; Uniform Wall Injection of C_8F_{16}.

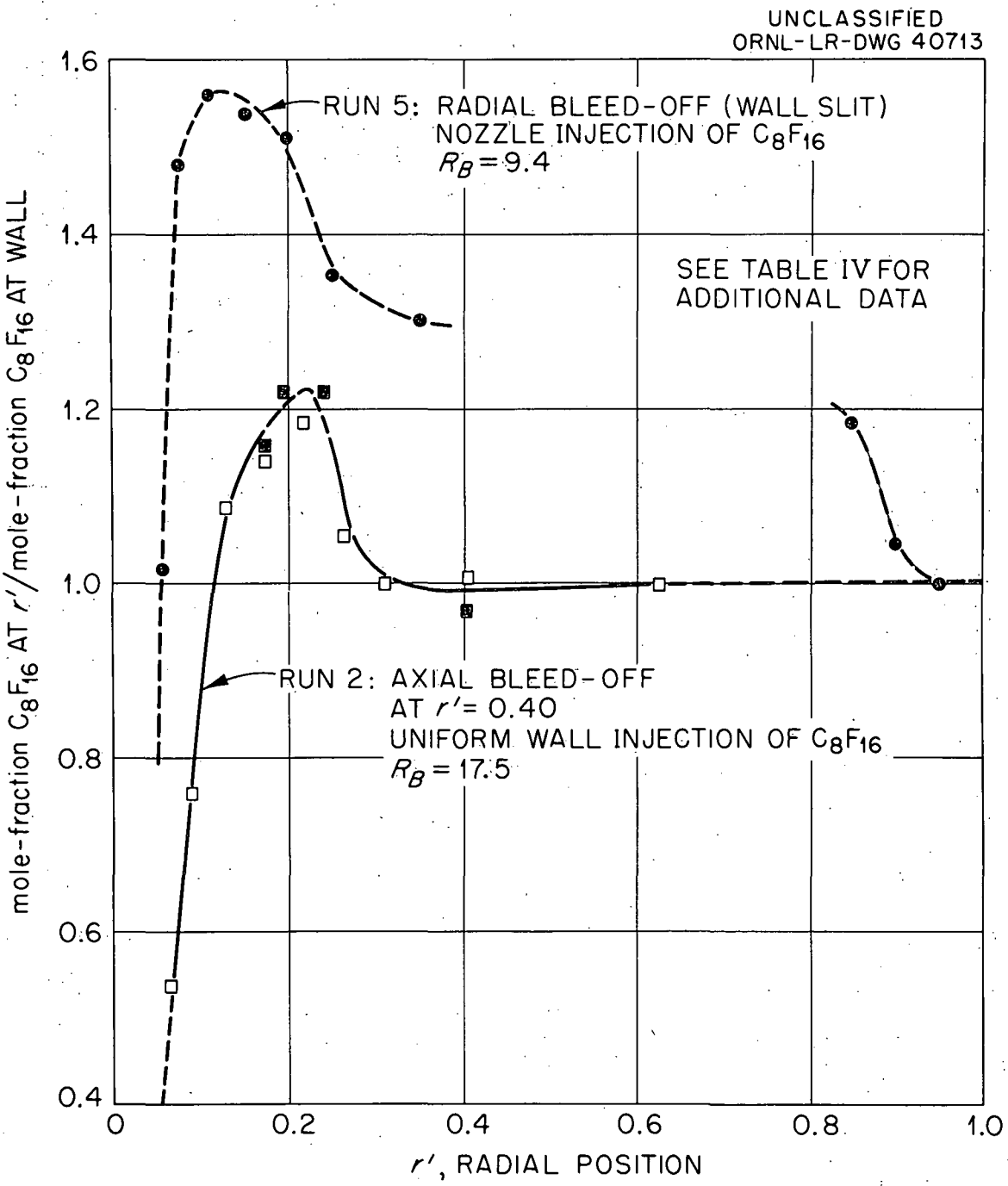

Fig. 38. Separation Profiles for He-C_8F_{16} Mixture in 2-in. Dia Vortex Tube No. 3.

In run 5 bleed-off was radially outward through a single continuous wall slit, and the heavy gas was injected through three of the twelve nozzles. Droplet formation may have occurred, therefore, causing uncertainty in the profile in the region between $r' = 0.4$ and the wall.

In run 1, depicted in Fig. 39, the heavy gas was introduced axially through four of the pressure taps at the closed end of the tube, at radial positions between $r' = 0.2$ and $r' = 0.32$. Bleed-off was axial at $r' = 0.4$. Note that the gas was swept inward toward a peak at $r' = 0.15$, with little back diffusion. A similar result is reported in ref 3. The dashed curve is the corresponding Mach number profile obtained with the sample probe inserted to $r_m' = 0.15$.

Table IV compares observed values of M_m obtained with the sample probe inserted to r_m' with values calculated from Eq. 7 for runs 3 and 5 in which experimental measurements of the exit mole-fraction, x_e, were made. An experimental value of molecular diffusivity, D_{12}, for C_8F_{16} in helium of 0.247 $\pm$ 0.050 cm^2/sec at 80°F, 1 atmosphere was obtained. This value was corrected by assuming an isentropic temperature drop between $r' = 1.0$ and $r' = r_m'$, using the relation $D_{12} \sim T^{1.75}$. Note that the observed and calculated values of M_m agree sufficiently well to support the applicability of the equation. Apparently, considerable suppression of turbulence occurred near the tube center, otherwise the molecular diffusivity would not be expected to apply.

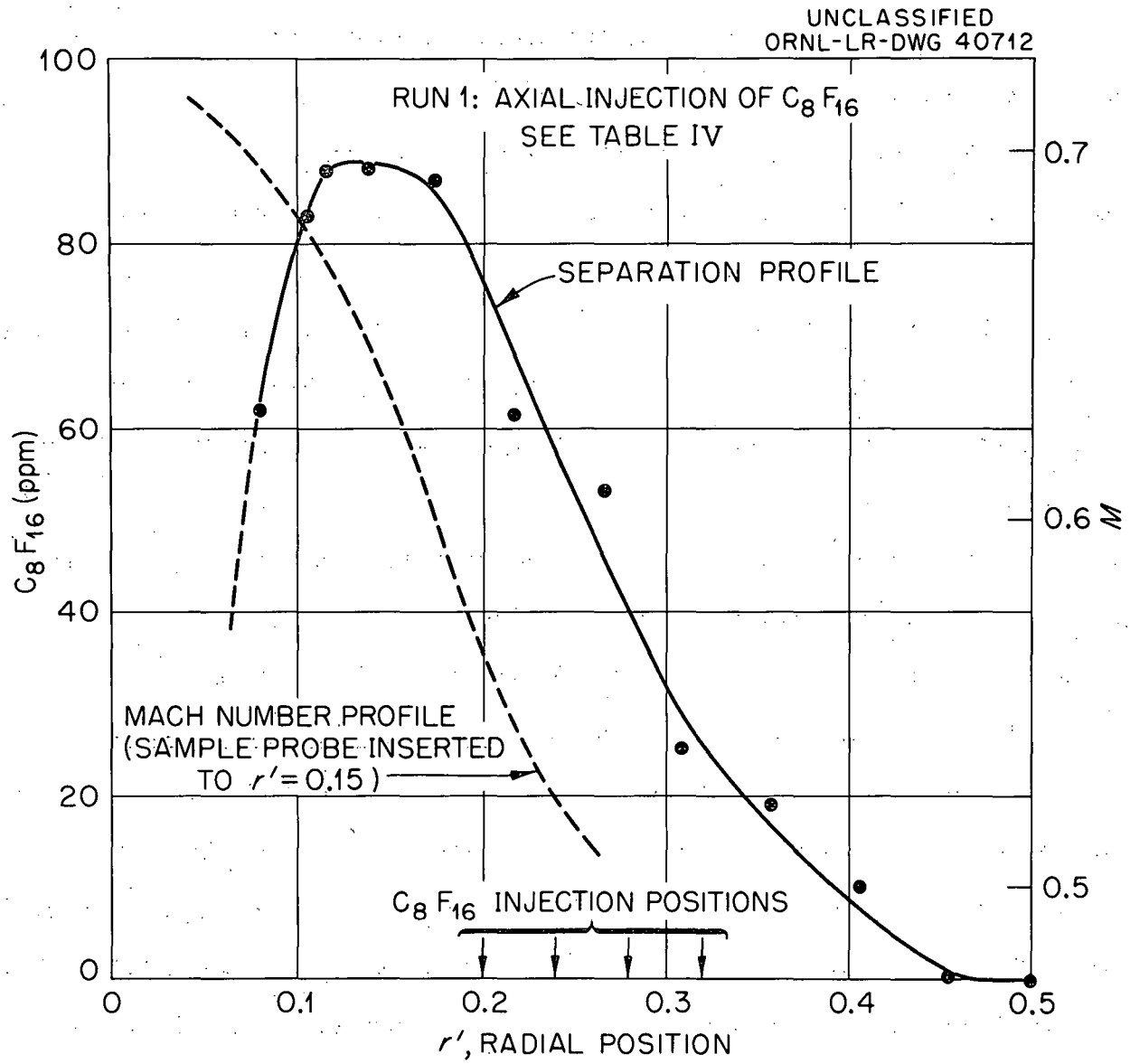

Fig. 39. Separation Profile for He-C_8F_{16} Mixture in 2-in. Dia Vortex Tube No. 3 and Corresponding Mach Number Profile.

ERROR ANALYSIS

Static pressure was the basic quantity measured; from the radial static pressure gradient, tangential Mach numbers were obtained by graphical differentiation:

$$M^2 = \frac{r'}{\gamma\, p'} \frac{dp'}{dr'} \qquad (2)$$

This equation neglects radial and axial velocity components, but it is doubtful that the error thus introduced amounts to more than a few per cent.

The relative radius r' at which a particular static pressure tap was located was known to within ±0.5%. Differential pressure measurements were accurate to better than ±1% of the measured Δp, and the absolute tube wall pressure was known to ±0.5%. Thus the p' ratios are known to ±1.5% or better. The largest errors associated with the application of Eq. 2 involve those of fitting the correct curve to the p'-r' data, and interpreting the slope of the curve graphically as a function of r'. It is estimated very approximately that errors in measurement of dp'/dr' of up to ±15% are possible. Thus the observed value of M may be in error by ±8.5% if the errors accumulate.

An additional error results from extrapolation of the velocity profile to $r' = r_a'$ to obtain the peripheral Mach number, M_p. This error is generally small for the 2.0-in.-dia tube data, say ±5%, but may be as large as ±10% for the 1.0- and 0.6-in.-dia tube data due to increased scatter in the p' values near the wall. Thus the values of M_p reported might be in error by as much as ±13% for 2.0-in.-dia tubes, and by as much as ±18% for 1.0- and 0.6-in.-dia tubes. The corresponding maximum errors in the ratio $0.5\, M_{0.5}/M_p$ are ±21%, and ±26%, respectively. Of course, the expected errors are less than these maximum values.

Errors in measurement of mass flow rate were probably of the order of ±2%. M_j can be determined to within ±8%. Thus the effective jet input power, $\frac{\gamma \dot{m}}{2} M_j^2$, may be in error by as much as 18%. The tangential peripheral Reynolds number, $2 r_p v_{t,p} \rho_p / \mu_p$, may be in error by at most ±15% and ±20% for 2.0- and 0.6-in.-dia tubes, respectively.

In view of the magnitude of possible errors, the degree of scatter of the data is not surprising. Specifically, the wide spread of the data in Fig. 36, in which the virtual to molecular viscosity ratio is plotted as a function of $N_{Re_{t,p}}$, may be explained by consideration of errors in determination of the velocity ratio, $0.5\ v_{t,0.5}/v_{t,p}$, which is derived from $0.5\ M_{0.5}/M_p$. Because of the nature of the relationship between the virtual viscosity and the velocity ratio, Fig. 42 (Appendix), errors in the latter quantity of say ±25% are multiplied to represent errors of forty to as much as several hundred per cent in the estimated value of μ^*; the more nearly the velocity distribution approaches that of a potential vortex, the larger is the uncertainty in μ^*. It is for this reason that the values of critical Reynolds number listed in Table III are order-of-magnitude estimates at best.

CONCLUSIONS AND RECOMMENDATIONS

The principle aim of this investigation was to ascertain the nature of flow in a jet-driven vortex tube with emphasis on the measurement of vortex strengths at low mass flow rates. A secondary aim was the study of separation of a light and a heavy gas. The following conclusions summarize the experimental results pertinent to these aims:

1. The flow field in the outer region of the vortex tube ($r' > 0.5$) was highly turbulent for all conditions of this study. It is estimated that laminar flow in a 0.6-in.-dia near-sonic-jet-driven tube operating at room temperature would not exist at mass flow rates of interest for pressures in excess of a few tenths psia. It is further estimated that, at conditions of practical interest for reactor application, the tangential Reynolds number may be as much as 10^3 times the critical value.

2. Reduction in the turbulent wall shear drag was effected by heavy gas injection and by wall cooling.

3. Turbulent vortices of strength adequate for cavity reactor application will require jet input powers appreciably greater than the minimum value required with laminar flow. Because of the high inlet mass flow rate required, some method for removal and recirculation of the excess flow is necessary. Uniform wall and axial bleed-off techniques show promise in this regard.

4. The significant independent variables which affect the vortex strength are: tube diameter, jet Mach number, mass flow per unit tube length, and wall pressure. Combinations of variables which appear to correlate the data include $\gamma \dot{m}_i M_j^2/2$, the effective jet input power, and $2 r_p v_{t,p} \rho_p/\mu_p$, the tangential peripheral Reynolds number.

5. Subsonic injection was more effective in generating vorticity than was supersonic injection for a given jet input power.

6. Agreement of the observed concentration peak position for separation of C_8F_{16}-He mixtures with theory for laminar flow is good. This fact suggests that, near the center of the vortex tube where the peak developed, the radial density (pressure) gradient may have been sufficiently strong to suppress turbulence.

Since the results of this experimental study have shown that the vortex flow field at conditions of interest for reactor application probably will be turbulent and since the original analysis assumed laminar flow, it is apparent that the influence of turbulence on reactor feasibility must be evaluated. This will require a study of the effect of turbulence on separation. Specifically, it is recommended that separation studies be carried out first at a sufficiently low pressure and high temperature to insure laminar flow; as the pressure is raised and turbulent transition takes place, any effect on separation should be readily detected.

Re-examination of cavity reactor performance should also be carried out analytically, taking into account turbulence and the energy required for recirculation of the excess mass flow.

It must be emphasized that the conclusions reached here are based primarily on the experiments at room temperature with no internal heat generation and with internal density gradients as produced by the vortex motion alone. The possibility is suggested in ref 1 that internal heat generation combined with the proper concentration profile might produce a sufficiently strong internal density gradient to stabilize the flow. There is experimental evidence that strong density gradients in the boundary layer produce some

stablilizing effect. There is also evidence that stabilization may occur near the center of the vortex tube where the static pressure gradient is high.

ACKNOWLEDGMENTS

This experimental program was suggested by Dr. R. V. Meghreblian. Dr. J. L. Kerrebrock made valuable suggestions regarding a method of driving the vortex and of pressure measurement. The authors wish to acknowledge also the contributions of Mr. F. F. Morris for the detailed design of the vortex tubes, Mr. J. W. Krewson for instrumentation design, and Mr. J. Lones for assistance during certain phases of the experimental work. The thermal conductivity gas analyzer was based on a circuit developed by Mr. H. S. McKown (Oak Ridge Gaseous Diffusion Plant). Messrs. R. J. Elbert, C. J. King, H. E. Trammell, and T. E. Zava of ORGDP contributed technical assistance with regard to porous media.

REFERENCES

(1). J. L. Kerrebrock and R. V. Meghreblian, An Analysis of Vortex Tubes for Combined Gas-Phase Fission-Heating and Separation of the Fissionable Material, ORNL CF-57-11-3 (April 11, 1958).

(2). J. L. Kerrebrock and P. G. Lafyatis, Analytical Study of Some Aspects of Vortex Tubes for Gas-Phase Fission Heating, ORNL CF-58-7-4 (July 21, 1958).

(3). J. L. Kerrebrock and J. J. Keyes, Jr., A Preliminary Experimental Study of Vortex Tubes for Gas-Phase Fission Heating, ORNL-2660 (Feb. 6, 1959).

(4). E. R. G. Eckert and J. P. Hartnett, Experimental Study of the Velocity and Temperature Distribution in a High Velocity Vortex Type Flow, Technical Report No. 6, University of Minnesota Institute of Technology (September 1955).

(5). R. G. Deissler and M. Perlmutter, "An Analysis of the Energy Separation in Laminar and Turbulent Compressible Vortex Flows," Heat Transfer and Fluid Mechanics Institute, p 40, Stanford University Press, Stanford, Calif., 1958.

(6). H. A. Einstein and H. Li, "Steady Vortex Flow in a Real Fluid," Heat Transfer and Fluid Mechanics Institute, p 33, Stanford University Press, Stanford, Calif., 1951.

(7). C. D. Pengelley, "Flow in a Viscous Vortex," J. of Appl. Phys. 28, No. 1, p 86 (January 1957).

(8). R. Kassner and E. Knoernschild, Friction Laws and Energy Transfer in Circular Flow, Report No. F-TR-2198ND, GS USAF Wright-Patterson AFB No. 78 (1948).

(9). K. Rietema and H. J. Krajenbrink, "Theoretical Derivation of Tangential Velocity Profiles in a Flat Vortex Chamber – Influence of Turbulence and Wall Friction," Appl. Sci. Research, Sec. A, Vol. 8, p 177 (1958).

(10). R. H. Wilson, The Effect of Viscosity upon the Pressure Distribution for Swirling Flow Through a Right Circular Cylinder, ORNL-1958

(11). C. B. Shepherd and C. E. Lapple, "Flow Pattern and Pressure Drop in Cyclone Dust Collectors," Ind. Eng. Chem. 31, 972 (1932).

(12). C. B. Shepherd and C. E. Lapple, "Flow Pattern and Pressure Drop in Cyclone Dust Collectors," Ind. Eng. Chem. 32, 1246 (1940).

(13). G. I. Taylor, "Stability of a Viscous Liquid Contained Between Two Rotating Cylinders," Phil. Trans. Roy. Soc. London, A, 223-289 (1923).

(14). H. Goertler, "Uber eine Dreidimensionale Instabilitat Laminare Grenzchichten an Konkaven Wanden," Nachr. Akad. Wiss. Gottingen, Math.-physik. Kl. 2, No. 1 (1940).

(15). Hsuan Yeh, "Boundary Layer Along Annular Walls in a Swirling Flow," Trans. Am. Soc. Mech. Engrs. 80, 767 (May 1958).

(16). H. Schlichting, Boundary Layer Theory, p 355, Pergamon Press, London, 1955.

(17). F. N. Peebles and H. J. Garber, Studies on the Swirling Motion of Water Within a Spherical Vessel, PhD Dissertation, Depart. of Chem. Eng., University of Tennessee (1956).

(18). W. H. McAdams, Heat Transmission, 3d ed., p 210, McGraw-Hill, New York, 1954.

(19). J. L. Gabbard et al., Fluorocarbons and Fluorocarbon Compounds, Section I, K-220(1) (August 1948).

THIS PAGE

WAS INTENTIONALLY

LEFT BLANK

APPENDIX

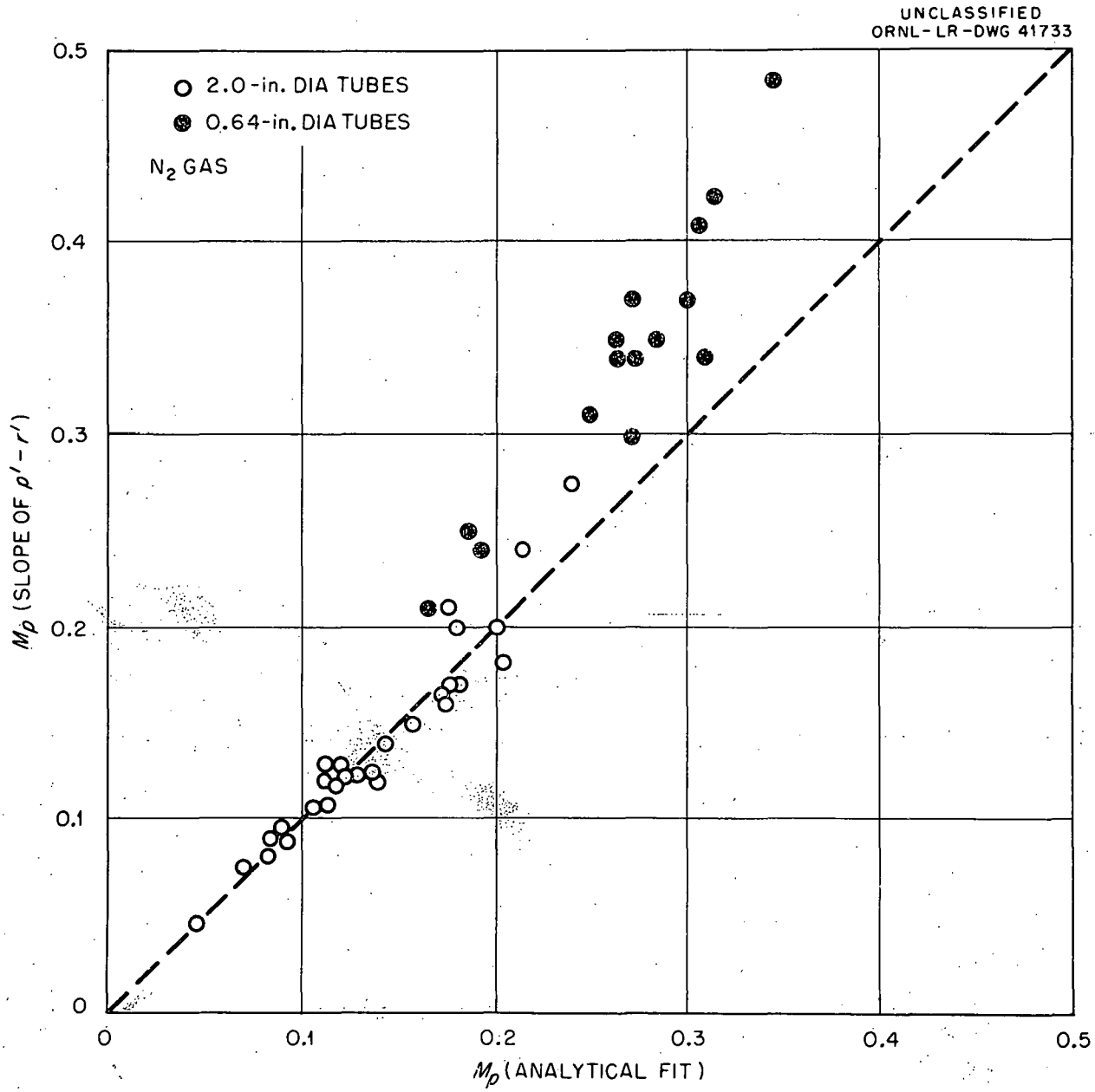

Fig. 40. Comparison of Graphical Slope Method for M_p with Analytical Fit, M_p/r'^{ϵ}.

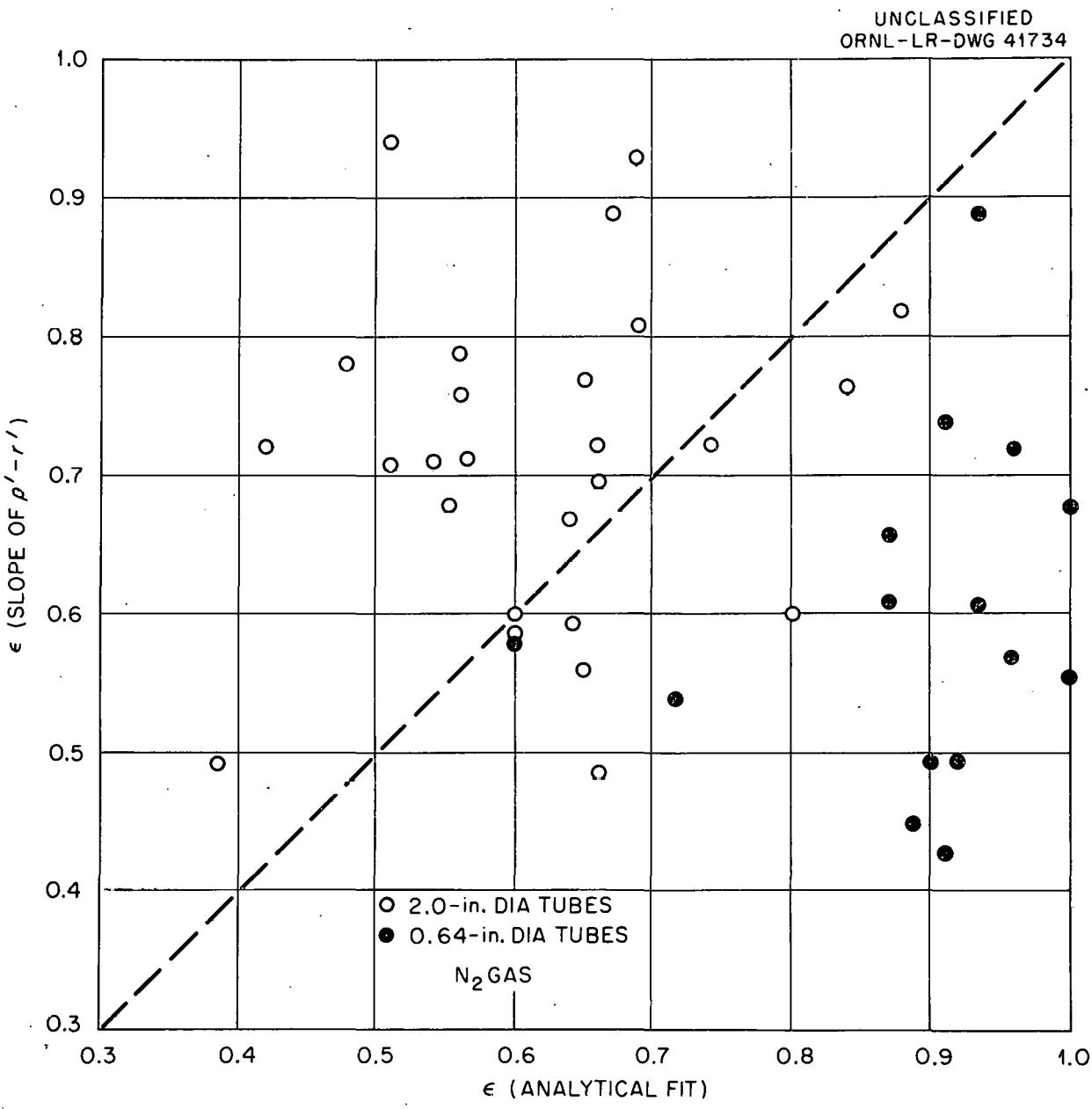

Fig. 41. Comparison of Graphical Slope Method for ϵ with Analytical Fit, M_p/r'^{ϵ}.

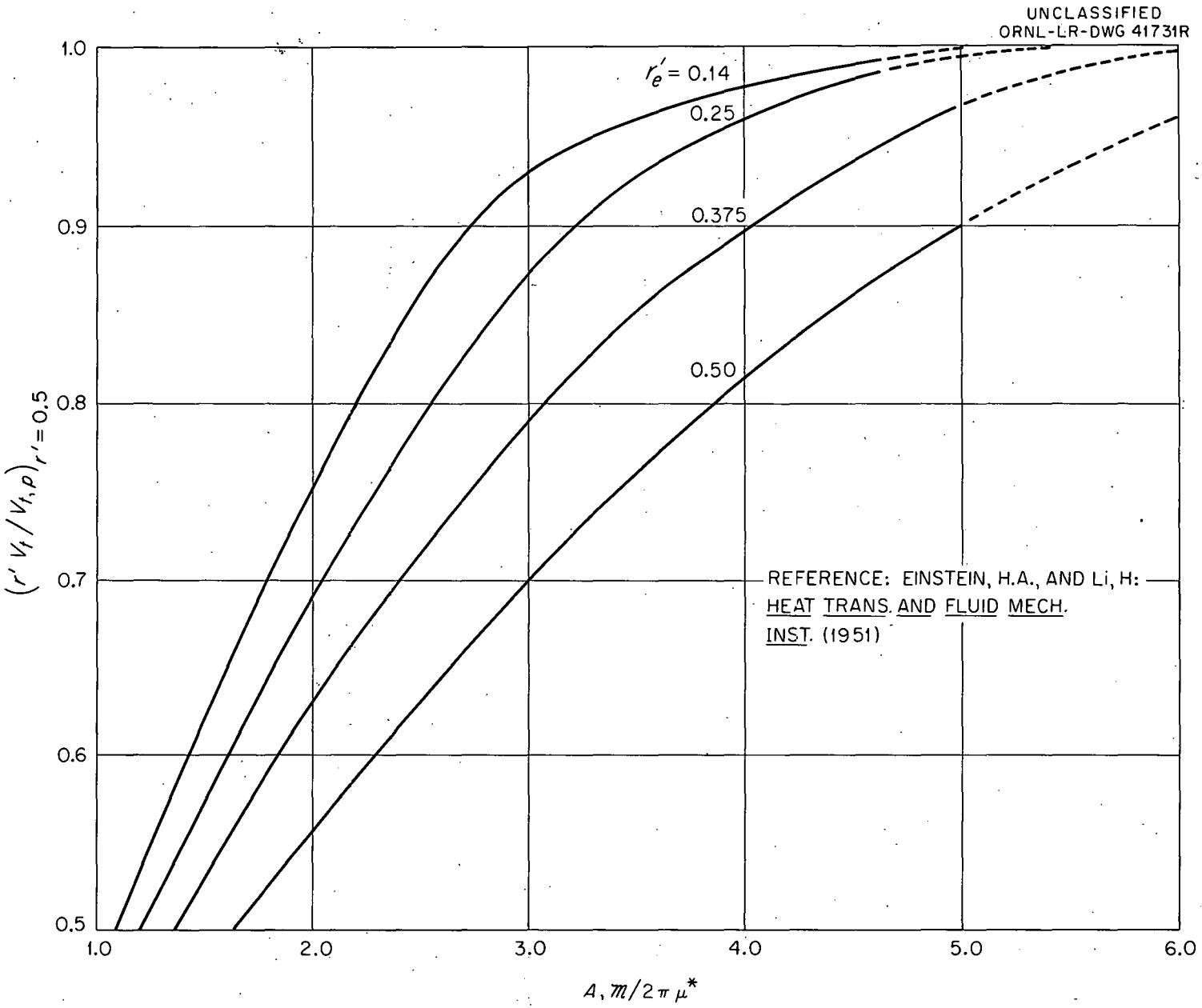

Fig. 42. Variation of Velocity Ratio $(r' V_t / V_{t,\rho})_{r'=0.5}$ with Turbulent Radial Reynolds Number, $m/2\pi\mu^*$.

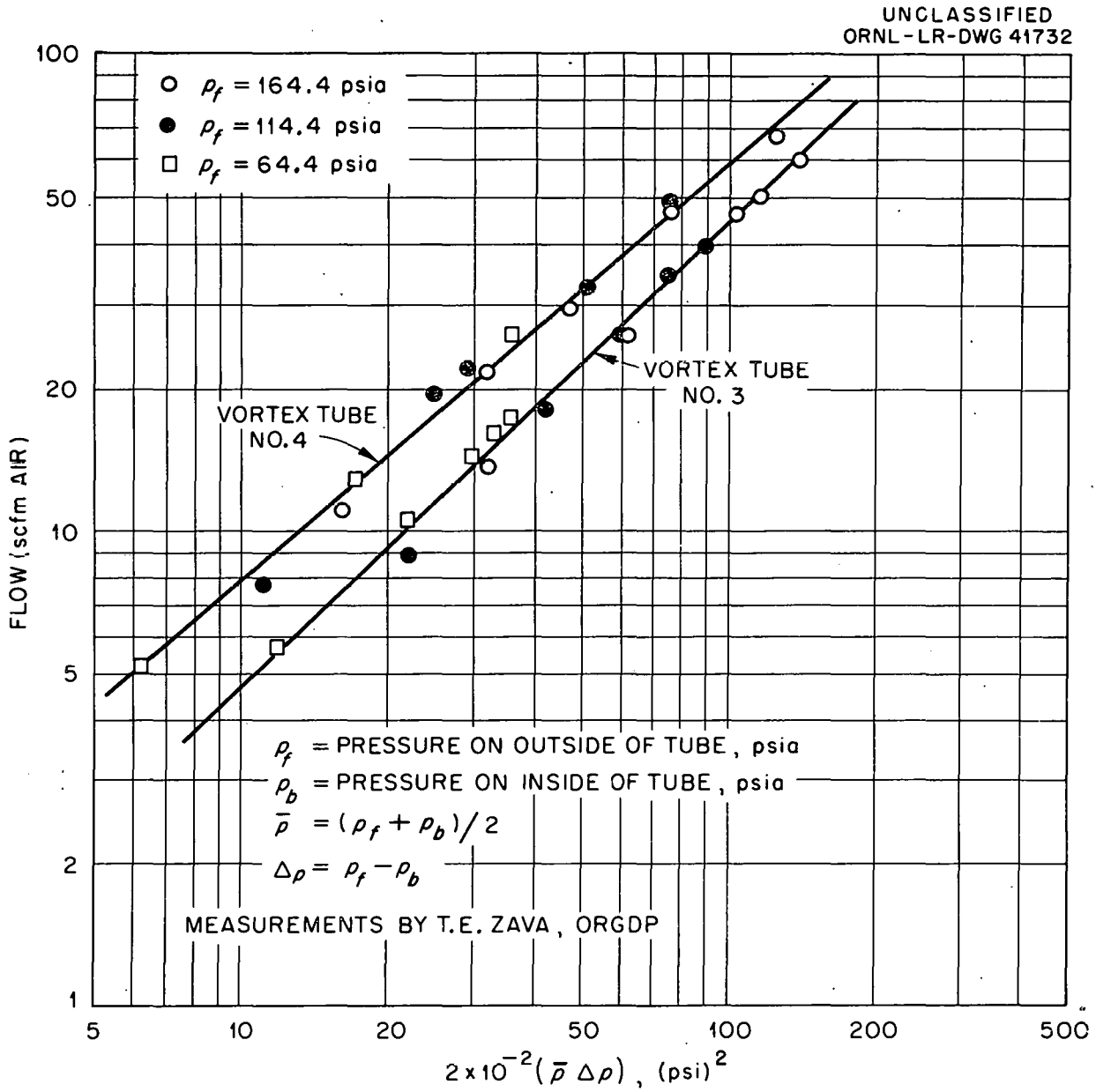

Fig. 43. Permeability Characteristics of Porous Ni ("Cormet") Tubes; Air Flow.

THIS PAGE

WAS INTENTIONALLY

LEFT BLANK

ORNL-2837
C-86 Nuclear Rocket and
Ram-Jet Engines
M-3679 (24th ed.)

INTERNAL DISTRIBUTION

1. F. F. Blankenship
2. E. P. Blizard
3. R. B. Briggs
4. R. A. Charpie
5. J. W. Cooke
6. R. E. Dial
7. W. K. Ergen
8. A. P. Fraas
9. J. H. Frye, Jr.
10. W. R. Gambill
11. B. L. Greenstreet
12. W. R. Grimes
13. H. W. Hoffman
14. W. H. Jordan
15-16. J. J. Keyes, Jr.
17. A. I. Krakoviak
18. J. W. Krewson
19. P. G. Lafyatis
20. F. E. Lynch
21. R. N. Lyon
22. W. D. Manly
23. A. J. Miller
24. R. F. Newton
25. F. N. Peebles
26. M. J. Skinner
27. W. J. Stelzman
28. J. A. Swartout
29. A. M. Weinberg
30. E. P. Wigner (consultant)
31-55. Laboratory Records Dept.
56. Laboratory Records, ORNL R.C.

EXTERNAL DISTRIBUTION

57. Division of Research and Development, AEC, ORO
58-165. Given distribution as shown in M-3679 (24th ed.) under Nuclear Rocket and Ram-Jet Engines category